

NBS
Publi-
cations

NATL INST. OF STAND & TECH



A11106 978926

NBSIR 84-1699

EXPERIMENTAL RESULTS FOR FITNESS-FOR-SERVICE ASSESSMENT OF HY130 WELDMENTS

National Bureau of Standards
U.S. Department of Commerce
Boulder, Colorado 80303

March 1984

QC
100
.U56
84-1699
1984
C. 2

NBSIR 84-1699

EXPERIMENTAL RESULTS FOR FITNESS-FOR-SERVICE ASSESSMENT OF HY130 WELDMENTS

STANDARDS
LIBRARY
: circ-NBS
QC
100
.U57
No. 84-1699
1984
C. 2

D. T. Read

Fracture and Deformation Division
National Bureau of Standards
Boulder, Colorado 80303

March 1984

Sponsored by:
Naval Sea Systems Command (SEA O5R25)



U.S. DEPARTMENT OF COMMERCE, Malcolm Baldrige, Secretary

NATIONAL BUREAU OF STANDARDS, Ernest Ambler, Director

Contents

	Page
1. Introduction	1
2. Materials	3
3. Techniques	3
4. Results and Discussion	6
4.1 Uncracked Weldment	6
4.2 Through Cracks	8
4.3 Surface Cracks	11
5. Conclusions	13
6. Acknowledgments	14
7. References	14

D. T. Read

National Bureau of Standards, Boulder, Colorado

Applied J-integral values for through and surface cracks in HY130 weldments and for surface cracks in HY130 base metal have been measured using a previously developed technique. The applied J-integral is taken as a measure of the crack driving force. The results confirmed previous conclusions, namely, the strong effect of deformation pattern on applied J-integral values, the utility of the J-integral estimation curve for fitness-for-service assessment in cases of gross section yielding (crack size less than 1 percent of load-bearing cross-section), and the need to consider ligament yielding behind surface cracks. Additional conclusions for surface cracks and for weldments were: surface-crack depth controls crack driving force; overmatching weld metal strength greatly reduces crack driving force for strains above yield; the relationship between crack length and crack driving force for cases of residual stress is similar to that for applied stress; for a crack in a weld transverse to the tensile axis, gross section yielding occurs if the crack intercepts less than 1.5 percent of the load-bearing cross section; the effective crack size for J-integral estimation is 0.75 of the actual crack depth for crack aspect ratios of 12 or less, and is no larger than the crack depth for any crack length; the line J-integral in the plane perpendicular to the surface crack root at the crack center is sufficiently path independent to allow direct experimental measurement of the J-integral.

Key words: design curve; elastic-plastic fracture mechanics; gross section yielding; net section yielding; residual stress; surface crack.

1. Introduction

Indications of the presence of surface flaws can be found by non-destructive inspection of structures during construction and repair. Even if no indications are found, the existence of flaws smaller than the detection threshold must be considered possible, especially in weldments. Structural integrity in the presence of flaws is assured by a combination of sufficiently small flaws, sufficiently tough structural material, and sufficiently low applied stresses and strains. The needed balance among flaw size, material toughness, and applied stress and strain has been obtained by the Navy in the past by accepting only excellent welding workmanship to minimize flaws, by using only the toughest available materials, and by controlling stress and strain levels according to experience, model tests, and engineering judgment. Costs associated with material procurement and weld repair provide incentive for using a more quantitative approach to selection of plate and weld quality, in order to ensure that as much construction as possible is accomplished with the available resources.

This report was prepared as part of the Fracture Control Technology program under the sponsorship of Dr. H. H. Vanderveldt, Naval Sea Systems Command (SEA 05R25). The effort was directed by Mr. John P. Gudas, David Taylor Naval Ship R&D Center, under Program Element 62761N, Task Area SF-61-544-504.

During an investigation of Navy fracture control requirements [1], it was reported that rational procedures are needed to provide answers to several recurring questions, including:

1. How much material toughness is sufficient for a given application?
2. How large a defect can be tolerated in a given structural element, particularly in a weld?

Fitness for service assessment (FFSA) relates actual flaw sizes, fracture mechanics characterization of material toughness, and quantitative levels of applied stress and strain. Therefore, FFSA allows quantitative evaluation of the balance among flaw size, material toughness, and applied stress and strain. This is especially useful for decisions on new materials and applications where experience is lacking. Unfortunately, no fully-developed fitness-for-service assessment method applicable to surface flaws in weldments exists.

This report describes experimental results in support of fitness-for-service assessment of HY130 weldments. It extends previous reports on FFSA for base metals [2, 3] to weldments and describes additional results of experiments on surface flaws in both base metal and weldments.

The present approach uses the J-integral [4-7] as the measure of fracture toughness and of the driving force for fracture. Required toughness can be related to applied strain and flaw size in HY130 through the J-integral estimation curve for gross section yielding (Fig. 1), provided that net section yielding [2, 3] is avoided. The curve of figure 1 lies at the upper bound of experimental results for applied J-integral as a function of strain for gross section yielding for a variety of through flaws in HY130 tensile panels. The curve is expressed algebraically as [3]:

$$j = 2e^2, \quad e \leq 1 \tag{1a}$$

$$j = 4(e-1) + 2, \quad e > 1 \tag{1b}$$

In these equations, j denotes normalized J-integral, given by

$$j = EJ/(\pi a \sigma_y^2) \tag{2a}$$

where E is Young's modulus, J is applied J-integral, a is crack size (taken in the usual fracture mechanics usage as crack length per crack tip for through cracks), and σ_y is material yield strength. The normalized strain, e, is given as

$$e = \epsilon/\epsilon_y \tag{2b}$$

where ϵ is applied tensile strain remote from the crack and $\epsilon_y = \sigma_y/E$. The J-integral estimation curve of eq (1) is at the upper bound of previously published estimation curves [3, 8-10].

Both welds and surface flaws complicate the dependence of required fracture toughness on applied stress and strain and on crack size. Weld metal generally has different tensile properties than base plate; welds can be overmatching (higher strength than base plate) or undermatching. In the HY130 weldments used in the present study the weld metal itself was overmatching, but an undermatching heat-affected-zone (HAZ) occurred beside the welds. Weld over- or undermatching can have a strong effect on the strain pattern in and around the weld. It, therefore, can have a strong effect on required toughness because of the close connection between strain patterns and required fracture toughness. This connection was emphasized in the previous report on HY130 base plate [3]. Overmatched welds tend to require lower toughness; but often less material toughness is available in overmatched weld metal. Residual stresses in weldments can also contribute to the driving force for fracture, and so must be accounted for in FFSA. For surface flaws, the zone of plasticity can spread from the

flaw root through the plate to the back face [3, 11-14], a process referred to as ligament yielding (LY). Ligament yielding is an intermediate process between elastic behavior and full yielding, and requires explicit treatment in FFSA. Furthermore, gross section yielding (GSY) around surface flaws cannot be treated directly using the J-integral estimation curve for through flaws until the effective flaw size for surface flaws for GSY is defined.

Experimental results leading to a method for FFSA for through flaws in weldments and for surface flaws in both base metal and weldments are described in this report.

2. Materials

The materials used in the present study were HY130 base metal and HY130 weldments. The base metal is described in the previous report [3]. The weldments were made using the GMAW process with standard Naval shipyard procedures. A diagram showing the location of the weld passes is shown in Fig. 2a. The chemical composition of the weld metal as obtained from analysis of a specimen cut from a weldment is given as Table 1. The weldment tensile properties are not identical with the base metal. As shown by a test of an uncracked tensile panel with a weldment transverse to the tensile axis, discussed below in the "Results" section, the heat affected zone (HAZ) has a lower yield strength but a higher ultimate strength than the weld metal, and the weld metal itself has higher yield and ultimate strengths than the base metal.

Table 1. Chemical composition by weight percent of HY130 weld metal used in the present study.

<u>Ni</u>	<u>Mn</u>	<u>Mo</u>	<u>Cr</u>	<u>C</u>	<u>Cu</u>	<u>Si</u>
4.8	1.4	1.0	0.68	0.086	0.12	0.34
	<u>P</u>	<u>S</u>	<u>V</u>	<u>Ti</u>	<u>Co</u>	<u>Fe</u>
	0.003	0.004	<0.01	<0.01	<0.01	bal

The toughness of the weld metal used in the present study was tested by the J-R curve technique. Compact tensile specimens of the standard 1T-CT geometry were used. Crack growth was monitored by the compliance technique. The compliance measured crack growth values were rescaled linearly to agree with the actual final crack lengths for presentation in Fig. 2b. The three critical J-integral values were scattered considerably, from 66.5 kN/m (380 lb/in.) to 161 kN/m (922 lb/in). The slopes of the tearing portions of the R-curves were in good agreement, with values all approximately 37 MN/m² (5.3 ksi). The large intervals of crack growth between data points for two of the specimens occurred because the tearing was only marginally stable. The compliance of the loading apparatus used, exclusive of the specimen itself, was approximately 3 x 10⁻⁵ mm/N (5 x 10⁻⁶ in/lb).

3. Techniques

The analytical approach and experimental techniques used in the present study for direct experimental measurement of the contour J-integral were described in detail in the previous report. The J-integral was given as [4]:

$$J = \int_{\Gamma} W dy - \vec{T} \cdot \partial \vec{u} / \partial x ds \quad (3)$$

where W is strain work density, $\int \sigma_{ij} d\epsilon_{ij}$; σ_{ij} and ϵ_{ij} are the stress and strain tensors; \vec{T} is the traction vector across the contour of integration, Γ , \vec{u} is the displacement vector; ds is increment of displacement along the contour of integration and x and y are Cartesian position coordinates, with the crack perpendicular to the y direction propagating in the x direction. The integrand terms of the J -integral were obtained from strain gage and linear variable differential transformer (LVDT) measurements. The J -integral was computed by numerical integration. The analytical approach and experimental techniques used to obtain the J -integral were discussed at length in the previous report [3]. It was concluded that uncertainty in the measured J -integral values themselves was about ± 10 percent, and that material variability could raise this uncertainty in specimen-to-specimen comparisons.

Use of the J -integral and other integrals for three-dimensional flaws has been discussed in the recent literature [15,16]. For surface flaws, the line integral form of J is not in general path independent. The surface integral form of J is surface-independent, but it provides only an average value over the whole crack front. By choosing a special surface enclosing a thin slice of the specimen penetrated by the crack front it can be shown that for contours in two special planes, one in the surface of the plate enclosing the end of the crack and one perpendicular to the surface cutting through the crack front, the line integral form of J is path-independent if an area integral containing terms in σ_{kz} is insignificant [16]. In the area integral, σ_{kz} is a stress tensor component, where k is the x , y , or z direction and the z direction is parallel to the crack front.

The hypothesis that the area integral in question is insignificant is supported by arguments based on: nearness of strain fields near the two special contours to plane-stress or plane-strain fields, smallness of out-of-plane stress-displacement gradient products, similarity of strain fields in the special planes to strain fields in face-cracked or center-cracked specimens, analogy of J -integral to crack-opening-displacement, and numerical evaluations of J -integrals.

The strain field near the side surfaces of a surface-cracked specimen must be nearly a plane-stress field, because no tractions exist at the side surfaces to create stress in the out-of-plane directions. Since J is path-independent under plane-stress conditions, it should be essentially path-independent for line contours in the surface of a surface-cracked specimen. The strain field near the center of a surface-cracked specimen must be nearly plane-strain near the crack, because of constraint provided by the specimen geometry. Away from the crack, plane-stress conditions are expected because of the absence tractions at the specimen sides. But exactly the same conditions exist in specimens widely used for J -integral measurements. Therefore, path independence should pose no more of a problem for surface cracks than it does for more usual specimens used for J -integral measurements.

All terms inside the area integral involve the derivative with respect to the out-of-plane direction (z direction) of the product $\sigma_{kz} u_{k,x}$ (sum on k implied) where z is the crack propagation direction. This product vanishes on both of the two special contours. It includes only out-of-plane stresses, which are not driven directly by applied tractions. Therefore, the quantity $\partial/\partial z \cdot (\sigma_{kz} u_{k,x})$ should be insignificant on the two special planes.

The strain field near the face of a surface-cracked specimen should be similar to the field near the face of a through-cracked specimen with a crack of the same length. Therefore, the J -integral on the special contour in the specimen face should be as path-independent as the J -integral in a center-cracked panel. The strain field in the other special plane, the longitudinal mid-plane perpendicular to the crack root in a surface-cracked specimen, should be similar to the strain field in the same plane in a specimen with a face crack, that is, a full width surface crack. Therefore, the J -integral for integration paths in such a plane should be path-independent, as it is for the face-cracked specimen.

The crack-opening-displacement δ has been used extensively as a measure of the crack driving force for surface cracks [13]. The J -integral obtained using the two special contours is closely related to the crack-opening-displacement. For plastic strain $\Delta J = \bar{\sigma} \cdot \Delta \delta$ where ΔJ is an increment of J , $\Delta \delta$ is an increment of δ , and $\bar{\sigma}$ is material flow strength [3]. Therefore, the J -integral obtained on the two special contours should be as good a measure of the crack driving force as the crack-opening-displacement, and so it should be essentially path independent.

Finite element analysis of model specimens containing surface cracks under elastic-plastic conditions will soon be possible. Evaluation of the J -integral for such models should definitively settle the question of the significance of the area term in the line J -integral in three-dimensional strain fields. Indications of the relative size of the area integral can be found in current studies of through cracks. It was found [15] that \hat{J} , an integral equal to the sum of the line integral plus the area term, was equal to the Merkle-Corten expression for the J -integral for a compact specimen. Since the Merkle-Corten expression was intended to give the line integral part of J , it is indicated that the area term was small for the case considered. If similar results occur for surface cracks, the utility of the line J -integral for surface cracks will have been established.

For the present study it is assumed that the line J -integral for surface flaws is sufficiently path-independent for practical purposes.

The path independence of J in weldments also requires consideration. Figure 3 shows some integration paths in a welded tensile panel with a through crack. The weld boundary remains at the same in-plane position through the whole thickness. One wishes to evaluate the J -integral on the major contour F'E'D'C'B' ABCDEF. Consider three minor contours, F'E'B'ABEF, EBCDE and E'D'C'B'E'. Each of these minor contours is within a homogenous material, therefore, J -integrals on each of these are path-independent. The relationship between the J -integral around contour F'E'B'ABEF, within the weld, around contour EBCDE, within the base metal, around contour E'D'C'B'E', within the base metal, and J , on contour F'E'D'C'B'ABCDEF, is now sought. Let the notation $J(XY)$ indicate the J integral along contour segment XY . Let the notation $J_W(XY)$ indicate that the contour XY is traversed within weld-metal; $J_B(XY)$ indicates the J -integral within the base metal along contour segment XY . Path-independence has been established for the following integrals:

$$J_W = J_W(F'E') + J_W(E'B') + J_W(B'AB) + J_W(BE) + J_W(EF) \quad (4a)$$

$$J_B = J_B(EB) + J_B(BC) + J_B(CD) + J_B(DE) = 0 \quad (4b)$$

$$J_{B'} = J_{B'}(E'D') + J_{B'}(D'C') + J_{B'}(C'B') + J_{B'}(B'E') = 0 \quad (4c)$$

The integrals J_B and $J_{B'}$ are not only path-independent, but are also zero because they enclose no singularities. The sum of these integrals is formed:

$$J_W = J_W + J_B + J_{B'} \quad (5a)$$

$$= J_W(F'E') + J_{B'}(E'D') + J_{B'}(D'C') + J_{B'}(C'B') + J_W(B'AB) + J_B(BC) + J_B(CD) + J_B(DE) + J_W(EF) + [J_W(E'B') + J_{B'}(B'E')] + [J_W(BE) + J_B(EB)] \quad (5b)$$

Consider the bracketed term:

$$J[\] = J_W(BE) + J_B(EB) = 0 \quad (6a)$$

This term is zero by mutual cancellation because segment EB has no extent along the y direction, outward tractions are opposite and displacements are equal along the weld-base metal interface, and the increment of path length ds is positive for both segment integrals.

Similarly,

$$J'_{[]} = J_w (E'B') + J_{B'}(B'E') = 0 \quad (6b)$$

But the resulting expression for J_w , from eq (5b) is just the segment-by-segment expression of J , the J-integral around the major contour:

$$J = J_w \quad (7)$$

It is already well known that the J-integral retains path-independence as long as the material properties are constant along the x direction. The derivation above indicates the correction terms needed if the fusion lines EB and E'B' do not lie along the x direction. This correction term is the difference between the J-integral measured on a remote contour, for instance (F'E'D'C'B'ABCDEF), and J_w . The bracketed terms $J'_{[]}$ and $J'_{[]}$ are the needed correction terms. Because the traction terms always cancel, the following holds:

$$J'_{[]} = \int_B^E (W_w - W_B) dy, \quad (8)$$

where W_w represents strain work density in weld metal and W_B is work density in base metal Figure 3b. A similar expression holds for $J'_{[]}$. It is usual for weld metal to have elastic constants nearly equal to those of the base metal. Therefore, for elastic strains the correction term would vanish. For large plastic strains, the strain in the weld metal, ϵ_w , might be less than the strain in the base metal, ϵ_B , (overmatching weld) for equal stress, σ . In this case

$$J'_{[]} = \int_B^E \sigma(\epsilon_w - \epsilon_B) dy, \quad (\text{large plastic strains}) \quad (9)$$

and similarly for $J'_{[]}$. If the stress and strain along EB were constant, and the strains were large, the correction term, ΔJ , for the J-integral would be given by

$$\Delta J = 2\sigma(\epsilon_B - \epsilon_w)\Delta y, \quad (\text{large plastic strains}) \quad (10)$$

where Δy is the total extent in the y direction of the fusion line, as illustrated in figure 3b.

Returning to the case of a fusion line that does lie along the x direction, the actual form of $J_w(BE)$ would be $J_w(BE) = \int_B^E T_y du_y/dx dx$. If u_y were constant along BE, as would be the case for a very small crack, then $J_w(BE)$ and its complement $J_w(B'E')$ would be negligible and J_w would be given by

$$J_w = J_w(F'E') + J_w(B'AB) + J_w(EF) \quad (11)$$

In the present study no correction terms like eq (10) were used. For through cracks eq (7) was used, and for surface cracks eq (11) was used. In one specimen with a weld along the tensile axis, the flow properties of the weld metal were similar enough to those of the base metal that no corrections to the J-integral were needed. The use of eq (11) for surface-cracked specimens implies that only strains near the crack in the weld metal are considered to contribute to the J-integral. The strains in the HAZ and BM are assumed to be the same on the front and back faces of the specimen, so that their effects on the J-integral mutually cancel. Figure 4 shows the general form of the instrumentation layout used on the surface-cracked specimens. In all cases the strain values from the gages away from the crack supported the use of eq (11).

4. Results and Discussion

Tests on uncracked and through-cracked weldments, surface-cracked base metal tensile panels, and surface-cracked weldments were performed during this study. Table 2 lists the specimen types and dimensions and the crack dimensions used.

4.1 Uncracked Weldment

The first specimen listed in Table 2, a transverse-welded uncracked tensile panel, was instrumented with strain gages, as shown in figure 5, and a photoelastic coating. It was strained to failure with

periodic pauses to record strain gage readings, LVDT readings, and load. Individual strain gage readings representative of longitudinal strain in weld metal (WM), heat-affected-zone (HAZ), and base metal (BM) are plotted against applied stress in Fig. 6. These strain values represent composite weldment behavior, rather than behavior of homogenous specimens of WM, HAZ, or BM. These stress-strain curves show that the WM was overmatched and the HAZ was initially undermatched to the BM.

The photoelastic coating dramatically displayed the HAZ as a high-strain region, Fig. 7. (The narrowing of the highly strained HAZ near the specimen edges was simply an edge effect, as confirmed by finite element analysis and by a subsequent test of a wider tensile panel.) The photograph shown as Fig. 7 was taken at a stress of 904 MPa (131.1 ksi). The strain in the HAZ reached a level of nearly 1.5 times the strain in the BM. Then strain hardening occurred in the HAZ, as shown in Fig. 6, and the strain in the BM caught up with the HAZ at a value of 2.2×10^{-2} . The overmatched weld had a strain of only 5.5×10^{-3} at this stress level, 941 MPa (136.5 ksi).

Overmatched WM and undermatched HAZ were observed for all the tests of transverse-welded tensile panels except one with a large crack in the weld, which restricted yielding in the BM and HAZ.

Table 2. HY130 specimens tests in the present study

Key: W HY130 weldment
 T HY130 tensile panel
 R HY130 welded plate for residual stress measurement
 C Through crack in specimen center
 F Full thickness crack
 B HY130 base metal
 S Surface crack

Material Type	Specimen Type	Crack Type	Specimen thickness (mm)	Specimen width (mm)	Crack length (mm)	Crack depth (mm)
W	T	--	10	89	--	--
W	R	C	25	800	to 50	F
W	T	C	10	89	8	F
W	T	C	25	912	25	F
B	T	S	10	89	25	6
B	T	S	10	89	20	1.7
B	T	S	10	89	5	1.7
W	T	S	10	89	5	1.7
W	T	S	20	254	30	2.5

4.2 Through Cracks

The second weldment test was a measurement of residual J-integral, that is, J-integral produced by residual stress. A large welded HY130 plate specimen, approximately 80 cm square and 2.5 cm thick, was instrumented with strain gages near the weld, Fig. 8. Then a crack transverse to the weld was started by drilling a hole 1.3 cm in diameter in the plate in the center of the weld, and was extended in both directions perpendicular to the weld by cutting with a saw. Cutting was interrupted periodically so that strains around the cut could be recorded. Because the initial tensile residual strains near the saw cut recovered toward a zero-strain state as the saw cut progressed, the recorded strains were negative (compressive). The longitudinal strains along the crack center-line for saw cut length 2.5 cm are plotted in Fig. 9. Analysis of the results of this test provided data on three quantities: the magnitude of the initial residual stress, the magnitude of the residual J-integral, and the width of the residually stressed area.

Extrapolation of the measured strains to the edge of the hole used to start the saw cut indicated an initial strain of 1.9×10^{-3} , which converts to a stress of 380 MPa (55 ksi), about 40 percent of the nominal yield strength. This value represents the through-thickness-average residual stress in the weldment tested.

An expression for the J-integral in the presence of residual strains, J_r , was given by Chell [17]. His expression is

$$J_r = J + \int_A dA \sigma_{ij} \partial \theta_{ij} / \partial x \quad , \quad (12)$$

where J is the usual expression for the J-integral, given above as eq (3), and the second integral on the right is the residual stress correction. This integral is taken over the area enclosed by the contour used to evaluate J; σ_{ij} is the stress tensor, θ_{ij} is the residual strain and x is distance from the crack center in the crack plane. Exact evaluation of eq (12) for an experimental situation clearly would be a formidable task. However these simplifying assumptions allow progress:

only σ_{yy} and θ_{yy} are significant;

θ_{yy} increases from zero very far from the saw cut, and reaches a constant value far from the saw cut, Fig. 10;

θ_{yy} is independent of y;

the traction-bending term in J is insignificant because the integration contour extends to infinity in the y direction;

the work density along segment CD (Fig. 10) of the contour chosen for evaluation of J can be made to vanish by choosing CD far from the crack and the residually strained region.

The area integral in eq (12) is independent of y because the thermal strain was assumed to be independent of y and located far away from the crack, which is the only possible source of y-dependence in the residual stress term of eq (12). Near the crack, where the stress does depend on distance from the crack, the residual stress gradient $\partial \theta_{yy} / \partial x$ is zero. The strains in the usual J-integral expression for the first term on the right side of eq (12) are the actual strains along the weld centerline, $\epsilon_{yy}(y)$; contributions from the other contour segments were dismissed in the assumptions listed above. Therefore we now have

$$J_r = - \int_{-\infty}^{\infty} dy \int_0^{\epsilon_{yy}(y)} \sigma_{yy}(y) d\epsilon_{yy} + \text{residual strain term} \quad (13)$$

Rewriting the area integral in the residual strain term as an integral over x and y, and assuming that the stress in the region of the residual strain gradient and near the crack depends on the strain in the usual linear elastic fashion we have

$$J_r = - \int_{-\infty}^{\infty} dy \int_0^{\epsilon_{yy}(y)} E \epsilon_{yy} d\epsilon_{yy} + \int_{-\infty}^{\infty} dy \int_0^{\epsilon_{yy,0}} E \epsilon_{yy} d\epsilon_{yy} , \quad (14)$$

where $\epsilon_{yy,0}$ is the tensile residual strain at the weld. This equation makes sense because if no crack were present $\epsilon_{yy}(y)$ would be identical to $\epsilon_{yy,0}$ and so J_r would be zero. If $\epsilon_{yy}(y)$ is relaxed below $\epsilon_{yy,0}$ near a crack, J_r will be positive. Evaluating the strain integrals we have

$$J_r = (E/2) \int_{-\infty}^{\infty} dy [\epsilon_{yy}(y)^2 - \epsilon_{yy,0}^2] . \quad (15)$$

As shown by the data plotted in Fig. 9, the measured strain relaxation values near the crack $\epsilon_{yy}(y)$ can be represented as

$$\bar{\epsilon}_{yy}(Y) = -\epsilon_{yy,p} \exp(-y/y_0) \quad (16)$$

Where $\epsilon_{yy,p}$ and y_0 are fitting parameters. The magnitude of the residual strain, $\epsilon_{yy,0}$, was calculated from eq (16) using the y value at the radius of the starter hole, y_n :

$$\epsilon_{yy,0} = \epsilon_{yy,p} \exp(-y_n/y_0) \quad (17)$$

The tensile residual stresses remaining in the plate along the y axis after partial saw cutting can be deduced from the strain gage data and the fitting function, eq (16).

Far from the saw-cut, the strains are constant at the residual strain value, $\epsilon_{yy,0}$. Near the cut, the strains are relaxed as shown in Fig. 9. The residual strain can be expressed as a function of saw cut length as

$$\begin{aligned}\epsilon_{yy}(y) &= \epsilon_{yy,0} - \epsilon_{yy,p} \exp(-y/y_0) \\ &= \epsilon_{yy,0} [1 - (\epsilon_{yy,p}/\epsilon_{yy,0}) \exp(-y/y_0)].\end{aligned}\tag{18}$$

When evaluating eq (18) only y values greater than y_n , the radius of the starter hole, correspond to actual strains. Substituting the strain function of eq (18) into eq (15) and evaluating the integral, one finds

$$J_r = \frac{3}{2} E \epsilon_{yy,0}^2 y_0.\tag{19}$$

A plot of residual J-integrals calculated from eq (19) plotted against saw-cut length is shown in Fig. 11. These values are well below the critical J value, J_{IC} , for HY130. But, if the residual strain were near yield instead of less than half of yield, the residual J values would quadruple, and would then be approximately J_{IC} for cracks several centimeters long. This implies that for residual strains at their maximum value, yield strain, and cracks about 5 cm long, tearing could initiate in HY130 at sharp cracks under residual strain alone.

The residual J values plotted against crack length in Fig. 11 can be compared to J values $J(K)$, calculated using the usual expression for the stress intensity factor for a center-cracked panel, with the saw cut length and the measured residual stress. At a saw cut length of 4.4 cm, for example, the value for $J(K)$ was 50kJ/m² (288 lb/in) which was 25 percent above the value calculated by integrating strains. This difference probably indicates that the saw cut was approaching the region of the residual stress gradient. A stressed tensile panel has tensile stresses across its whole width. Residual stresses only part-way across a panel would be expected to produce lower applied J-integral values. The breakdown of the near-linear dependence of J on saw-cut lengths (Fig. 11) for cut lengths less than about 2 cm is attributed to: inadequacy of eq (16), for strain as a function of position, near the hole, 1.3 cm in diameter, used to start the saw cut; variability of the actual residual strain along the saw cut; and breakdown of the assumptions, listed above, used in evaluating the residual J-integral.

It is concluded from the results discussed above that residual strains produce strain distributions of the same general character as those produced by mechanical strains, and that similar relationships among stress level, crack size, and applied J-integral should hold for residual and mechanical stresses.

The next through-cracked specimen tested was a transverse-welded, center-cracked tensile panel. The through crack intercepted about 10 per cent of the cross-sectional area. Its instrumentation layout is shown in Fig. 12. As shown by the the strain gage results and photoelastic coating, Figs. 13 and 14, net section yielding occurred. Figures 15a-k verify the expected rapid increase of applied J-integral and crack mouth opening displacement with strain for net section yielding behavior. This test showed that in weldments, as in base plate, net section yielding occurs when the crack intercepts 10 per cent or more of the specimen cross-section. The exact crack area separating net section yielding from gross section yielding was pursued further for surface flaws in weldments, as discussed below.

Figures 16-19 depict the instrumentation layout and behavior of the third through-cracked specimen, a much larger welded tensile panel with the weld along the tensile axis. The results of this test showed that residual stresses and size scaling have no first order effects on tensile panel behavior for the crack sizes and strain levels considered here, namely, a crack intercepting 2.8 per cent of the specimen area. Net section yielding occurred as expected, Figs. 17-18. The residual applied J-integral was about 20 kJ/m² (120 lb/in), as calculated from the crack size and the residual

stress measurement described above. This level of applied J-integral might be significant in a very brittle material, but it is insignificant for a crack growing toward HY130 base metal.

4.3 Surface Cracks

The goals of the tests of surface-cracked tensile panels were three: to verify the effects of gross and net section yielding on applied J-integral values, to locate more precisely the boundary between NSY and GSY, and to determine effective crack sizes for several sets of crack lengths and depths.

The behavior of a large surface crack (17 percent of cross-section area) was reported previously [3]. The data are repeated here for completeness. The instrumentation layout is shown in Fig. 20, strain gage results are plotted in Fig. 21, strain patterns revealed by the brittle lacquer coating are shown in Fig. 22, and the strain and stress dependence of J-integral and crack mouth opening displacement are displayed in Figs. 23 a-k. This test showed that for surface cracks, as for through cracks, net section yielding occurs and produces a rapid increase in applied J-integral with applied strain. It also showed the necessity of accounting for ligament yielding in surface cracks.

Surface cracks, being geometrically more complex than through flaws, have an additional yielding pattern, ligament yielding. As can be seen in Fig. 24, ligament yielding means that the plastic zone emanating from the crack root has reached the back face of the specimen, but has not reached the sides of the specimen. Ligament yielding is a sort of local net section yielding, restrained by the elastic strain field between the specimen sides and the end of the crack's plastic zone. As might be expected, ligament yielding produces a rapid increase in crack driving force, but not as rapid as net section yielding at a through flaw.

Two additional experiments on surface-cracked base metal specimens were conducted to locate the transition from NSY and GSY and to measure effective crack sizes for GSY for surface cracks. Instrumentation layouts for these two specimens are shown in Figs. 25 and 26. The behavior of these two surface-cracked base-metal panels was complicated by nonuniformity of tensile properties along the panel tensile axis. For both specimens, one end had a lower flow strength than the remaining material; strains in the soft end were much larger than elsewhere in the specimen, as indicated in Fig. 27. The qualitative strain asymmetry was revealed by the photoelastic coating on the specimens. Because strain gages were present, by chance, only on the harder specimen end, the form of the strain on the softer end could only be estimated from the fringes in the photoelastic coating and from the total strain over the whole specimen, obtained from measured displacements. Because of this strain asymmetry, some of the data pertain only to the specimen end instrumented with strain gages, while others pertain to the overall specimen length. Figures 28 and 29 show the strain gage strains and photoelastic strain patterns for the specimen with the longer crack, and Figs. 30 and 31 show these data for the specimen with the shorter crack. Because the behaviors of the two ends of these specimens were different, overall-length data cannot be combined with half-length data to give a complete description of specimen behavior. Instead, the two data sets must be separately considered and compared. Quantities pertaining to the instrumented half-length are the contour J-integral, the remote strain as given by a strain gage away from the crack, the gage length strain as calculated by integrating strains from individual gages, and the stress. Plots showing the interdependence of these quantities for the two base-metal, surface-cracked specimens are referred to as half-length plots, and are presented in Figs. 32 and 34. Quantities relevant to the full length include crack mouth opening displacement (CMOD), gage length strain from LVDTs, and stress. Plots relating these quantities are called full-length plots, Figs. 33 and 35.

On the 89 x 10 mm specimen with a surface crack 10 mm by 1.7 mm (crack intercepted 2 percent of cross section area), deformation patterns indicative of net section yielding were visible. This confirmed the previous result that for cracks larger than 1 percent of the cross section area net section yielding can be expected.

The smallest surface crack tested in a base metal tensile panel, 1.7 mm deep by 5 mm long in a panel with a 10 x 89 mm cross section (crack intercepts 1 percent of cross section) showed no signs of net section yielding. Gross section yielding occurred, followed by yielding to failure in the soft end.

For the through-cracked specimens covered by the previous report, the GSY part of the applied J-integral was clearly distinguishable from the NSY part. However for surface cracks, deformation bands extend from the crack root to the back surface for both ligament yielding and NSY. Therefore, no clear distinction between the NSY and GSY parts of the applied J-integral is available. Therefore, these base-metal surface-cracked specimens provided an upper bound to the effective crack size, but not a definitive value.

The effective crack size is that value of the parameter a in the J-integral estimation curve (eqs (1) and (2), above) that forces the estimated J values to be equal to the measured values for a specific case. Effective crack sizes for the base metal specimen with the longer surface crack were calculated from the plot of J-integral against remote strain (half-length data) and from the plot of CMOD against gage length strain (full-length data). The effective crack sizes were 0.92 and 0.77 of the actual crack depth. Because some NSY occurred in this test, these effective crack sizes are overestimates of the GSY part of the applied J-integral.

For the specimen with the shorter crack, the strain-gaged end of the specimen did not reach strains above yield. Therefore an effective crack length for this specimen was obtained from the full-length plot of CMOD against gage length strain, Fig. 34b. The J-integral was taken to be the product of CMOD and yield strength, a relationship provided by the previous series of tests [3]. Net section yielding at the crack did not occur in this specimen as shown by the photoelastic coating, Fig. 30. Therefore the gage length strain provided a good measure of the average remote strain. The effective crack size was 0.5 of the actual crack depth.

Two transverse-welded surface-cracked tensile panels were tested, one 10 mm thick by 89 mm wide (0.4 x 3.5 in) and one 20 mm thick by 250 mm wide (0.77 x 10 in). Instrumentation layouts for these specimens are shown in Figs. 36 and 37. The CMOD for the smaller specimen was measured using a traveling microscope, because the crack was too small for a clip-on gage. Strain gage strains and photoelastic coating strain patterns are shown as Figs. 38, 39, 40 and 41. Stress and strain dependences of the J-integral and crack mouth opening displacement are shown as Figs. 42 and 43. The measured CMOD values for the smaller specimen contained a scatter of about ± 0.03 mm because of the optical measurement method used. These tests clearly demonstrated the behavior of small surface cracks in HY130 weldments. The key results are the importance of overmatching weld metal strength, crack sizes small enough to ensure gross section yielding, and small crack depths in limiting crack driving force. Overmatching was expected because of the results of the test uncracked welded tensile panel and confirmed by the strain vs position results and strain patterns from the surface-cracked weldments. The cracks machined in these two tensile panels were 1 and 1.6 percent, respectively, of their cross-sectioned areas. The absence of NSY is evident from the strain vs position results and the strain patterns. The effect of crack depth can be seen from analysis of the J-integral results. For the smaller tensile panel, the J-integral was obtained in the usual way. For the larger specimen the measured strains were complicated by the presence of a natural flaw in the weld, in addition to the crack introduced intentionally. The complicated strains prevented contour J-integral measurement for this specimen. The J-integral was estimated as the product of yield strength and CMOD. Effective crack sizes were obtained by requiring that the J-integral values given by the estimation curve matched the measured values. The ratio of effective crack size to actual crack depth decreased from 0.72 to 0.028, for the smaller specimen, and from 0.76 to 0.084 for the larger one as the strain increased from 0.004, near yield, to 0.007, where the high weld metal flow strength prevented further plastic strains in the weld metal. The ratios of effective crack size to actual crack depth in the elastic-plastic strain range in the two specimens were 0.72 and 0.76, even though the crack aspect ratios (depth to total length) were 0.34 and 0.083, the crack depth to plate thickness ratios were

0.17 and 0.13, and the ratios of crack length to plate width were 0.06 and 0.12. The fact that the ratio of effective crack size to actual crack depth was not noticeably influenced by aspect ratio, crack depth to plate thickness ratio, or crack length to panel width ratio indicates the predominant effect of crack depth on effective crack size. Both of these tests demonstrated the conservatism of using the actual crack depth as the effective crack size. In fact these two tests, together with the results from the surface-cracked base-metal tests, indicate that for gross section yielding and for surface cracks with aspect ratios greater than 0.08 the effective size for surface cracks can be taken as 0.75 of the actual crack depth. The aspect ratio restriction excludes very long cracks, for which the effective size is the full depth.

A natural weld flaw in addition to the machined flaw in the larger surface-cracked specimen provided the opportunity to draw another conclusion about the effects of weld defects: a weld defect can cause unstable tearing in a tensile panel. The natural defect was a buried part-through crack in a plane approximately perpendicular to the panel tensile axis. The crack extended in the transverse direction from one edge of the specimen almost to its center line and was approximately 2 mm in depth (plate thickness direction). This crack caused local yielding, evidenced by local strains revealed by the photoelastic coating, Fig. 41, and eventually caused unstable tearing of half the panel width at an applied remote strain of 0.013. The tearing arrested near the end of the natural flaw, at about the center of the specimen.

From the two experiments on surface cracks in transverse-welded tensile panels discussed here, it was concluded that surface cracks in weldments can be treated using the J-integral estimation curve previously reported for base metals. For surface cracks the effective crack size a for GSY should be taken as 0.75 of the crack depth for relatively short cracks (length to depth ratio 12 or less). For longer cracks the effective size is to be taken as the full depth.

For the HY130 weldments tested here, the post-yield strain in the weld increased much less than the post-yield strain in the base metal, because of overmatching. While for the welds in this study the effective crack size for GSY was definitely less than 10 percent and more than 1.6 of the actual crack depth for strains above 0.007, the specific fraction might depend on the exact weld process and weld chemistry used.

5. Conclusions

From tests of 3 surface-cracked HY130 base metal tensile panels and 6 uncracked, through-cracked, and surface-cracked HY130 weldments, the following conclusions of the previous report [3] on base metal tests have been sustained:

1. Applied J-integral is controlled qualitatively by deformation pattern. Net section yielding produces large applied J-integral values, while gross section yielding produces small applied J-integral values.
2. Fitness-for-service assessment for contained plasticity and gross section yielding can be performed using a J-integral estimation curve to obtain applied J-integral as a function of applied strain and crack size.
3. Net section yielding is intolerable. This yielding pattern can be avoided in tensile panels by restricting crack size to 1 percent or less of load-bearing-cross-sectional area.
4. Estimation of applied J-integral values for surface flaws requires consideration of ligament yielding as well as contained and gross section yielding. Contributions of each of these yielding patterns to applied J-integral can be evaluated using estimation curves specific to each yielding pattern.

The following additional conclusions have been obtained for surface cracks generally and surface cracks in weldments:

5. Surface-crack depth has a dominant effect on the crack driving force.
6. Overmatching weld metal flow strength is a powerful means of lowering crack driving forces for cracks in welds transverse to the tensile axis. A five percent strength overmatch can reduce effective crack size by a factor of 10 in HY130, assuming that adequate weld toughness can be maintained.
7. Residual stresses in HY130 weldments produce applied J-integrals at cracks within the stress fields. The residual stress field measured in this study had a magnitude of slightly less than half yield, and could have initiated tearing in HY130 at a through-crack 12 cm long, if such a large residual stress field were possible.
8. Net section yielding from cracks in HY130 welds transverse to the tensile axis is prevented by restricting crack size to 1.5 percent of the load-bearing-cross-sectional area. This restriction applies for welds ground flush. The presence of a weld crown might allow further relaxation of this restriction.
9. For surface flaws in HY130 base- and weld-metal tensile panels, the effective crack size for gross section yielding can safely be taken as 0.75 of the actual crack depth for cracks with length to depth ratio 12 or less; the effective size can be taken as the full crack depth for longer cracks.
10. The applied J-integral at the crack root is the appropriate measure of crack driving force in surface cracks in base plates and in weldments. The usual line J-integral in the plane perpendicular to the crack root at the crack center is sufficiently path independent for practical purposes.

6. Acknowledgments

Financial support from the Fracture Control Technology Program of the Naval Sea Systems Command is gratefully acknowledged.

The contributions of J. D. McColskey as technician on this project are gratefully acknowledged. Helpful discussions with J. P. Gudas, H. I. McHenry, R. B. King, and Y. W. Cheng, assistance in data plotting by B. Gunther, and manuscript preparation by J. Wilken are appreciated.

7. References

- [1] R. W. Judy, Jr., T. W. Crooker, J. A. Corrods, J. E. Beach, J. A. Hauser, Review of Fracture control technology in the U.S. Navy. Presented at the Second Program Review, Fracture Control Technology for Ships and Submarines; 1979 November 30; Annapolis, MD.
- [2] D. T. Read and H. I. McHenry, Interim Progress Report: J-Integral Method for Fitness-for-Service Assessment, National Bureau of Standards Interagency Report NBSIR 81-1648, May 1981.
- [3] D. T. Read, Applied J-Integral in HY130 Tensile Panels and Implications for Fitness-for-Service Assessment, National Bureau of Standards Interagency Report NBSIR 82-1670, July 1982.
- [4] J. R. Rice, A Path Independent Integral and Approximate Analysis of Strain Concentration by Notches and Cracks, Journal of Applied Mechanics 35, 1968, pp. 379-386.

- [5] W. A. Logsdon, Elastic Plastic (J_{IC}) Fracture Toughness Values: Their Experimental Determination and Comparison with Conventional Linear Elastic (K_{IC}) Fracture Toughness Values for five Materials, Mechanics of Crack Growth STP 560, American Society for Testing and Materials, Philadelphia, 1976, pp. 43-60.
- [6] J. A. Begley and J. D. Landes, The J Integral as a Fracture Criterion, Fracture Toughness, STP 514, American Society for Testing and Materials, Philadelphia, 1972, pp. 1-20.
- [7] J. D. Landes and J. A. Begley, The Effect of Specimen Geometry on J_{IC} , Fracture Toughness, STP 514, American Society for Testing and Materials, Philadelphia, 1972, pp. 24-39.
- [8] M. G. Dawes, The COD Design Curve, in Advances in Elasto-Plastic Fracture Mechanics, edited by L. H. Larsson, Applied Science Publishers, London, 1980, pp. 279-300.
- [9] J. A. Begley, J. D. Landes, and W. K. Wilson, An Estimation Model for the Application of the J-Integral, Fracture Analysis, STP 560, American Society for Testing and Materials, Philadelphia, 1974, pp. 155-169.
- [10] C. E. Turner, Elastic-Plastic Aspects of Fracture Stress Analysis: Methods for other than Standardized Test Conditions, in Fracture Mechanics in Design and Service, Phil. Trans. R. Soc. Lond. A299, 1981, pp. 73-92.
- [11] H. I. McHenry, D. T. Read, and J. A. Begley, Fracture Mechanics Analysis of Pipeline Girthwelds, Elastic-Plastic Fracture, STP 668, American Society for Testing and Materials, Philadelphia, 1979, pp. 155-169.
- [12] R. deWit and J. H. Smith, Development of Some Analytical Fracture Mechanics Models for Pipeline Girth Welds, Fracture Mechanics, STP 700, American Society for Testing and Materials, Philadelphia, 1980, pp. 513-528.
- [13] Y. W. Cheng, H. I. McHenry, and D. T. Read, Crack-opening Displacement of Surface Cracks in Pipeline Steel Plates, Proceedings of the Fourteenth National Symposium on Fracture Mechanics, June 30-July 2, 1981, Los Angeles, CA.
- [14] Y. W. Cheng, R. B. King, D. T. Read, and H. I. McHenry, Post-yield Crack-opening Displacement of Surface Cracks in Steel Weldments. Proceedings of the Fifteenth National Symposium on Fracture Mechanics. July 7-9, 1982, College Park, MD.
- [15] K. Kishimoto, S. Aoki, and M. Sakata, On the Path Independent Integral \hat{J} , Engineering Fracture Mechanics 13, 1980, pp. 841-850.
- [16] R. B. King, Y. W. Cheng, D. T. Read, and H. I. McHenry, J-Integral Analysis of Surface Cracks in Pipeline Steel Plates. Proceedings of second International Symposium on Elastic-Plastic Fracture Mechanics, October 6-9, 1981, Philadelphia, PA.
- [17] G. G. Chell, Elastic-Plastic Fracture Mechanics, in Developments in Fracture Mechanics-1, edited by G. G. Chell, Applied Science Publishers, London, 1979, p. 97.

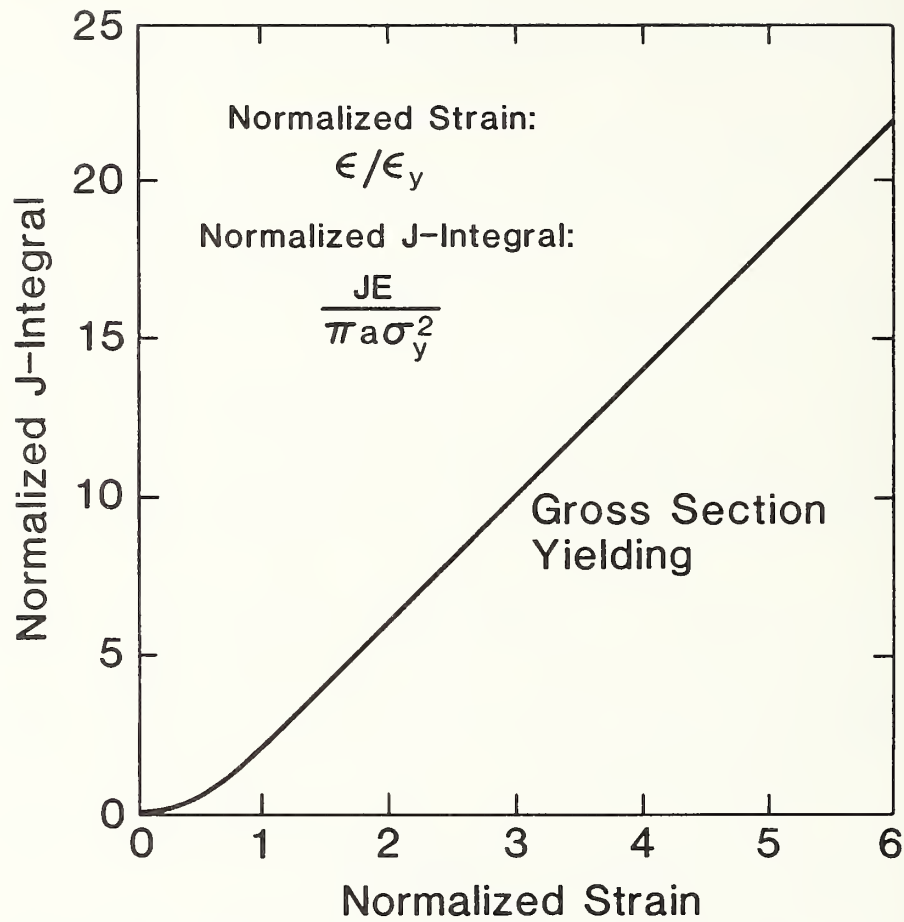


Figure 1. Experimentally derived J-integral estimation curve for contained yielding and gross section yielding in HY130 in tension.

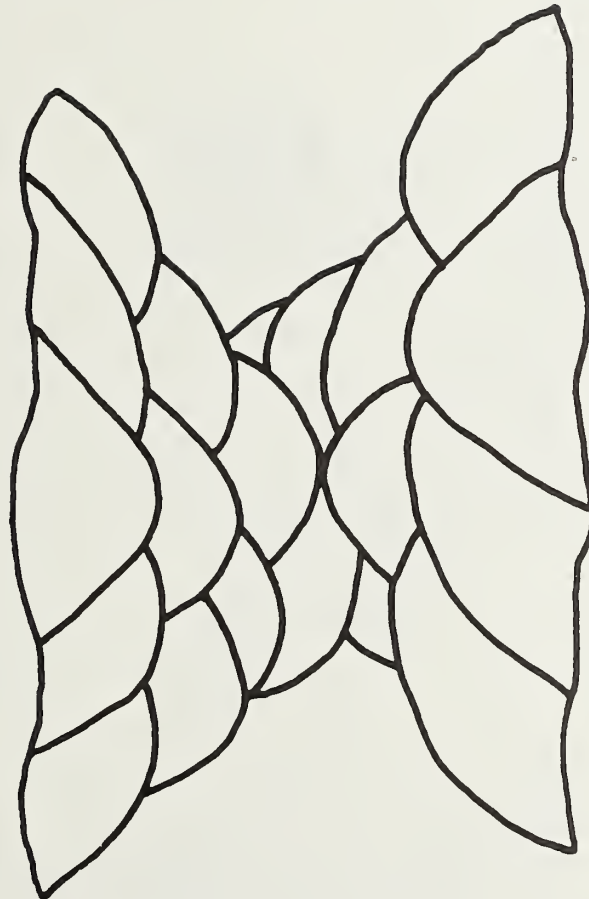


Figure 2a. Weld bead placement in HY130 GMAW-process butt weld used in the present study.

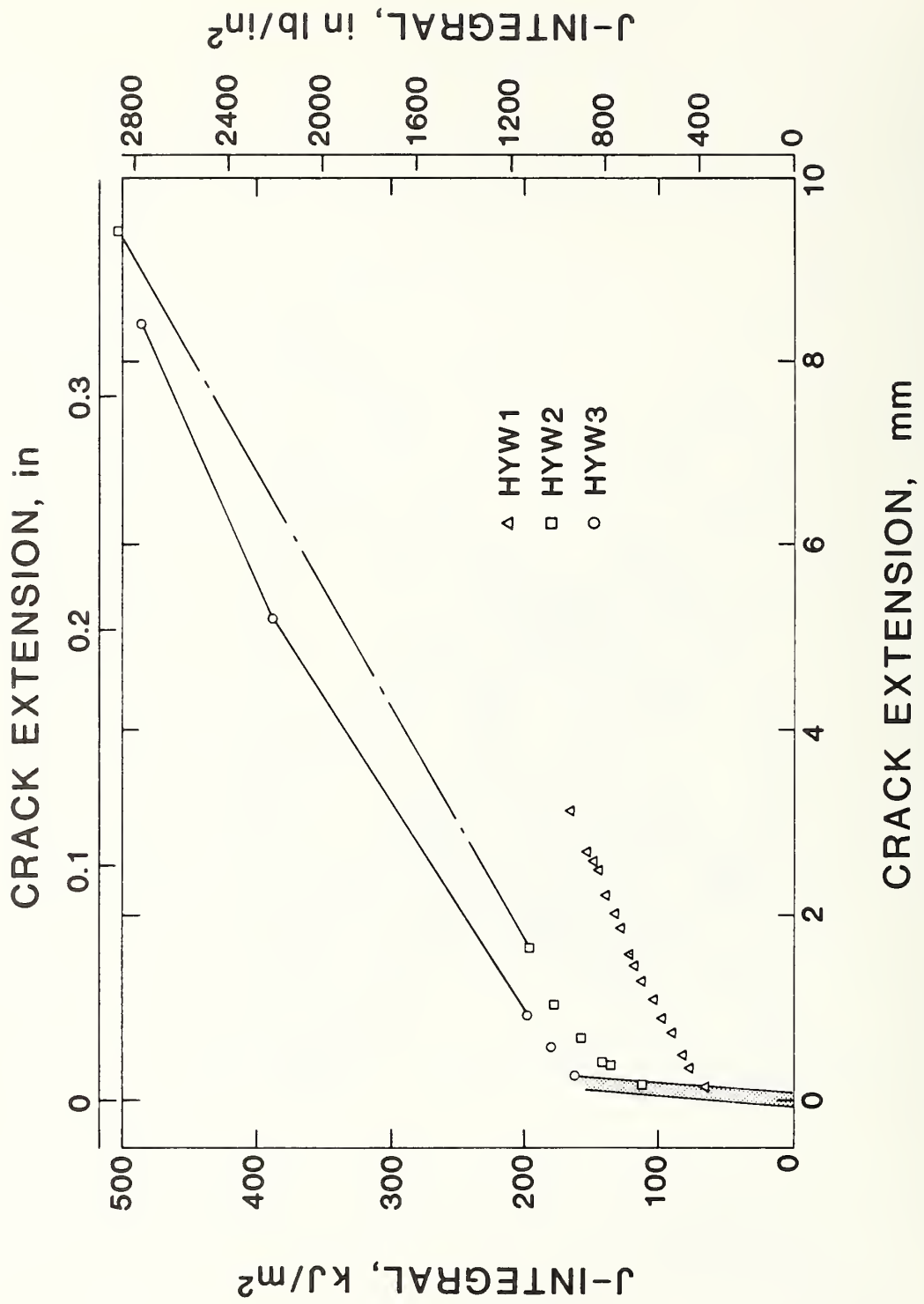


Figure 2b. J-R curves for the weld metal of the present study.

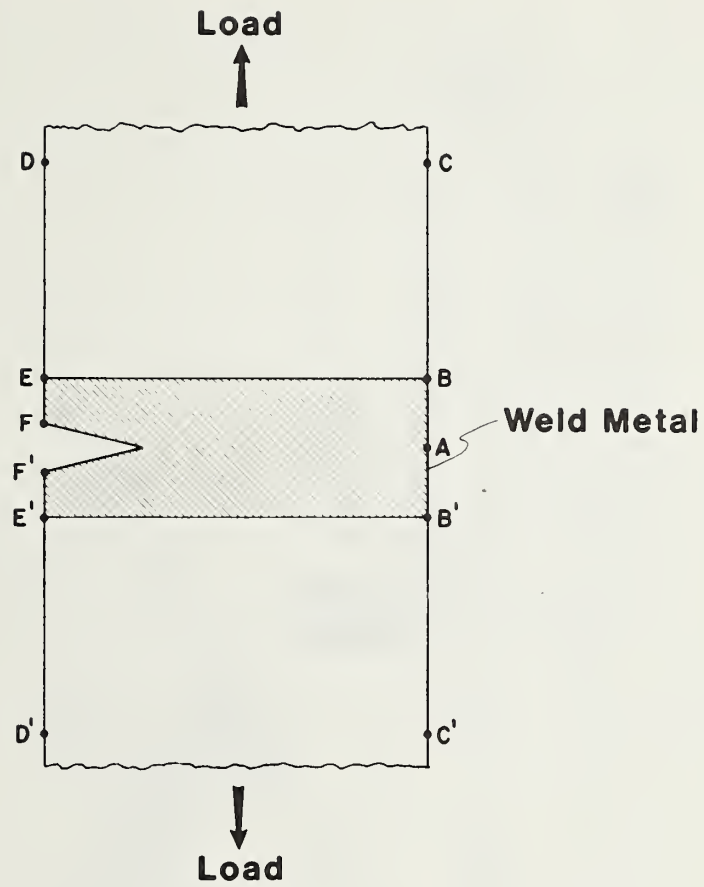


Figure 3. Integration paths for the J-integral for a crack in a weldment.

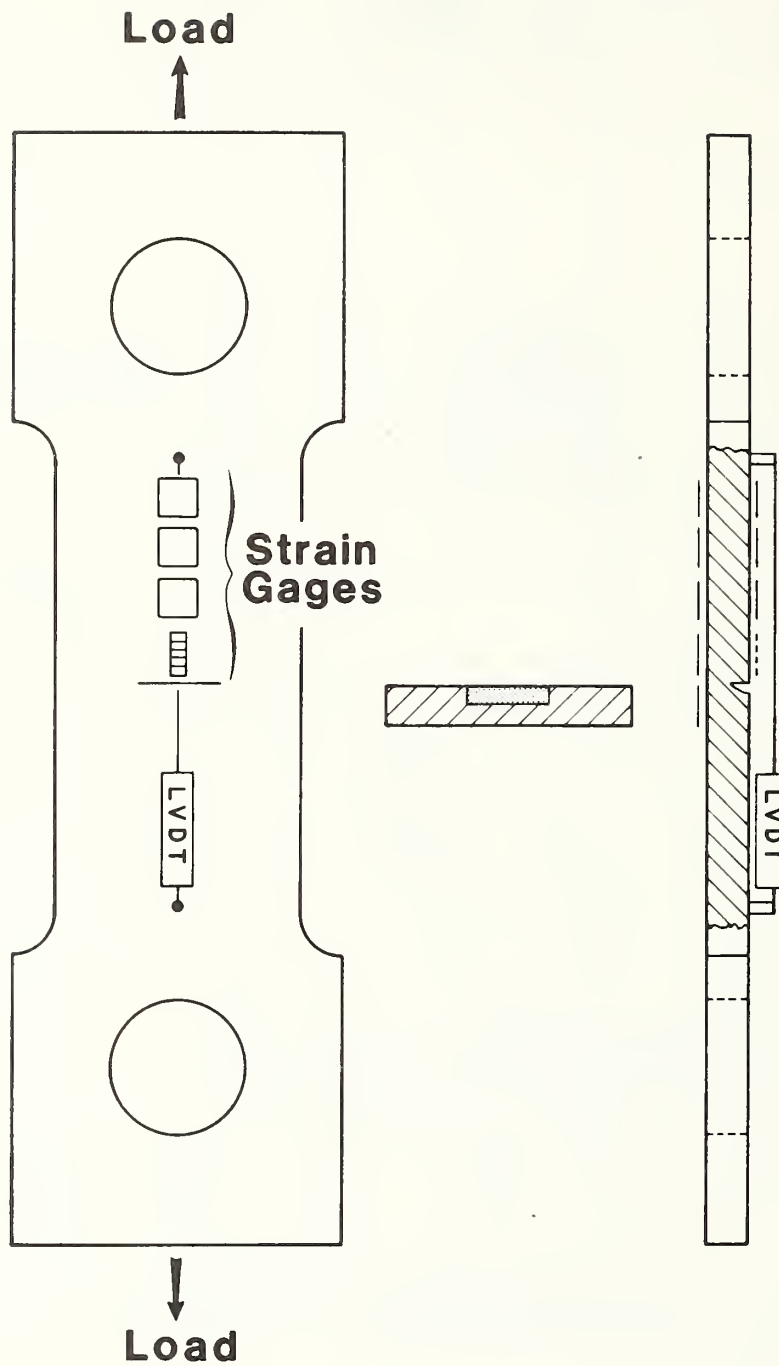


Figure 4. Schematic diagram of surface-cracked tensile panel instrumented with strain gages and LVDTs for direct measurement of the contour J-integral.

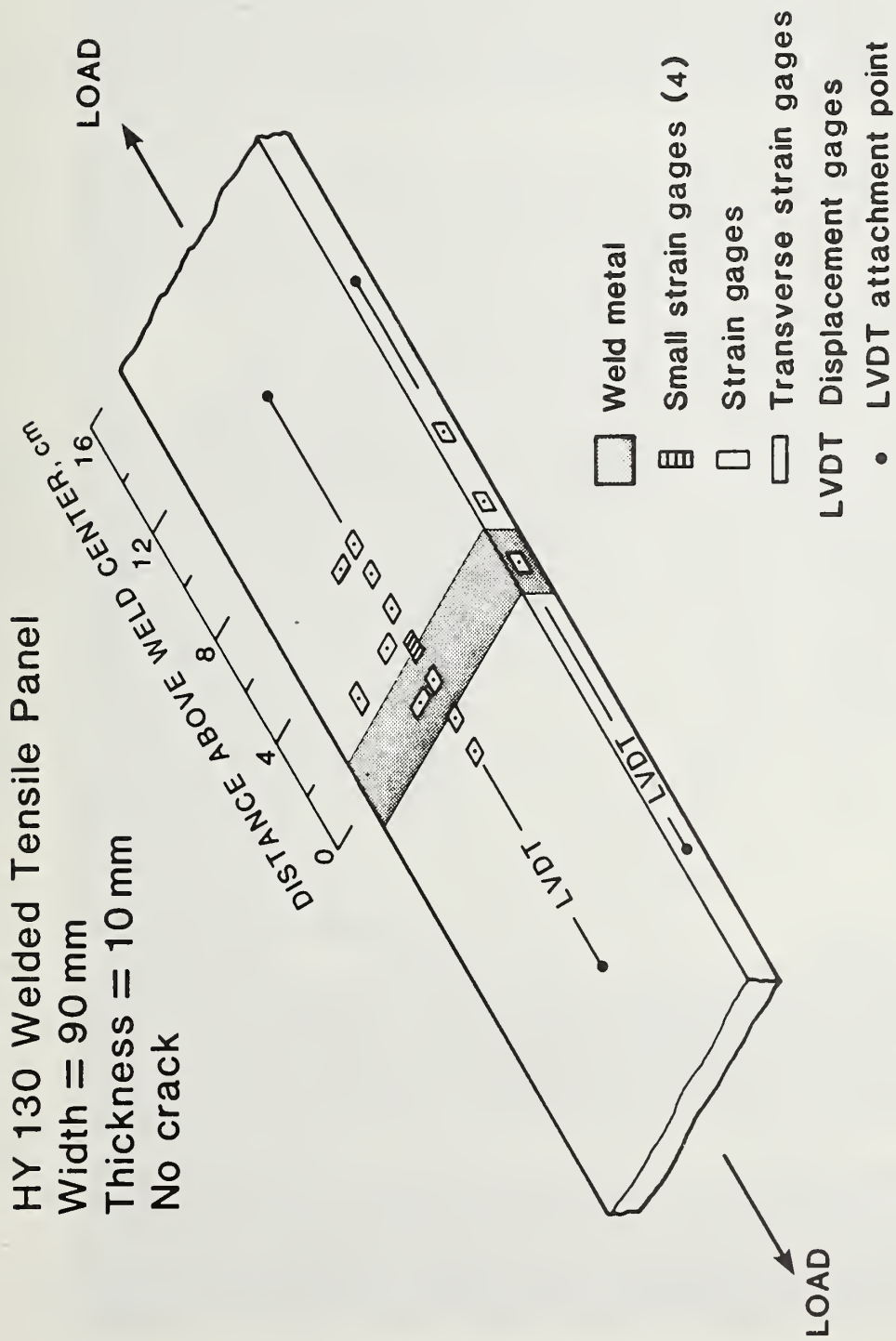


Figure 5. Instrumentation layout for transverse-welded uncracked HY130 tensile panel.

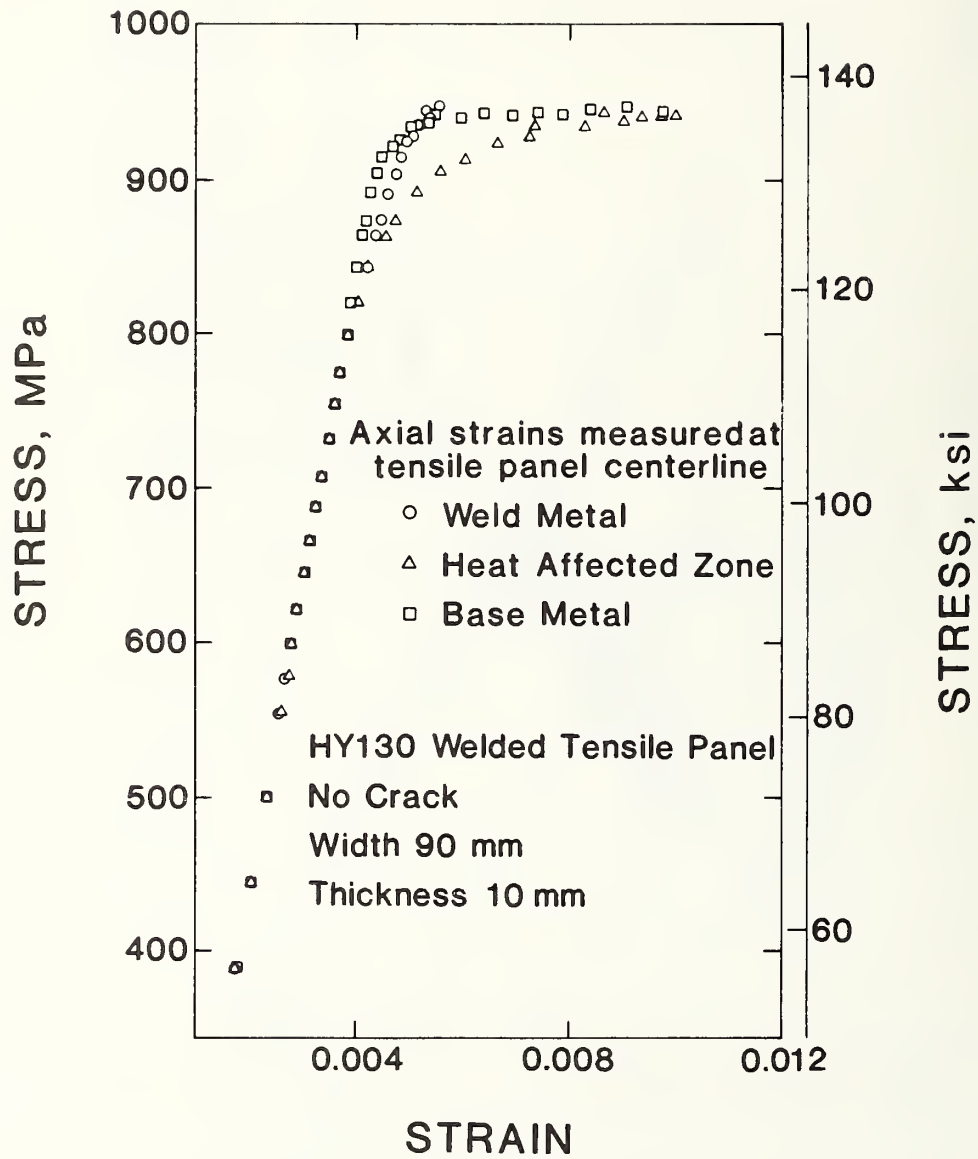


Figure 6. Longitudinal strain in weld metal (WM), heat-affected-zone (HAZ), and base metal (BM) plotted against stress for transverse-welded uncracked HY130 tensile panel.

HY130 Welded Tensile Panel No Crack
Width 90 mm Thickness 10 mm Stress 904 MPa



Figure 7. Photograph showing highly strained HAZ of transverse-welded uncracked HY130 tensile panel, at a stress of 904 MPa (131.1 ksi).

HY-130 Welded Plate

**Residual J measurement by
cutting instrumented plate**

Plate size 100 x 100 cm

Plate thickness 25 mm

Saw-cut starter hole at center of plate

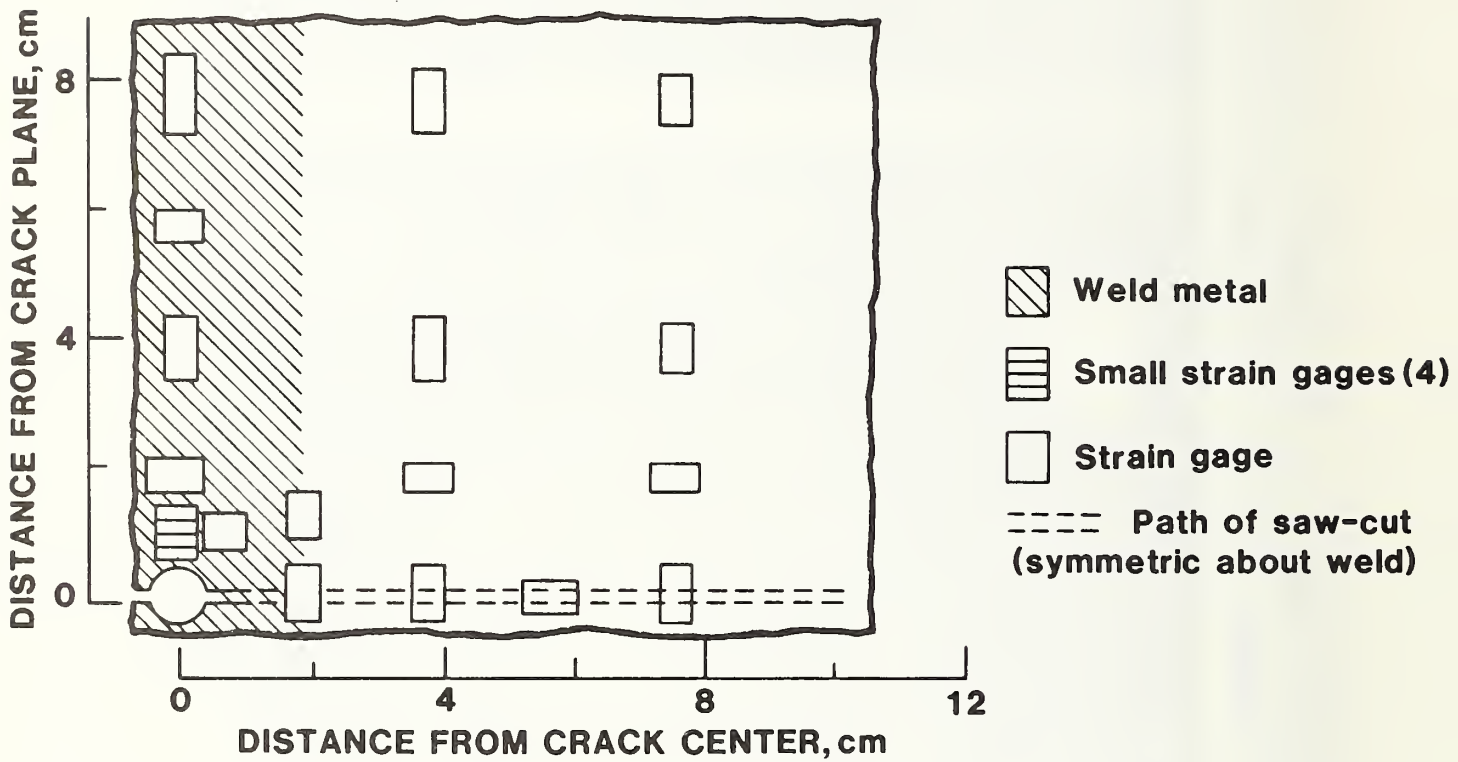


Figure 8. Instrumentation layout for large welded HY130 plate specimen for residual J-integral measurement.

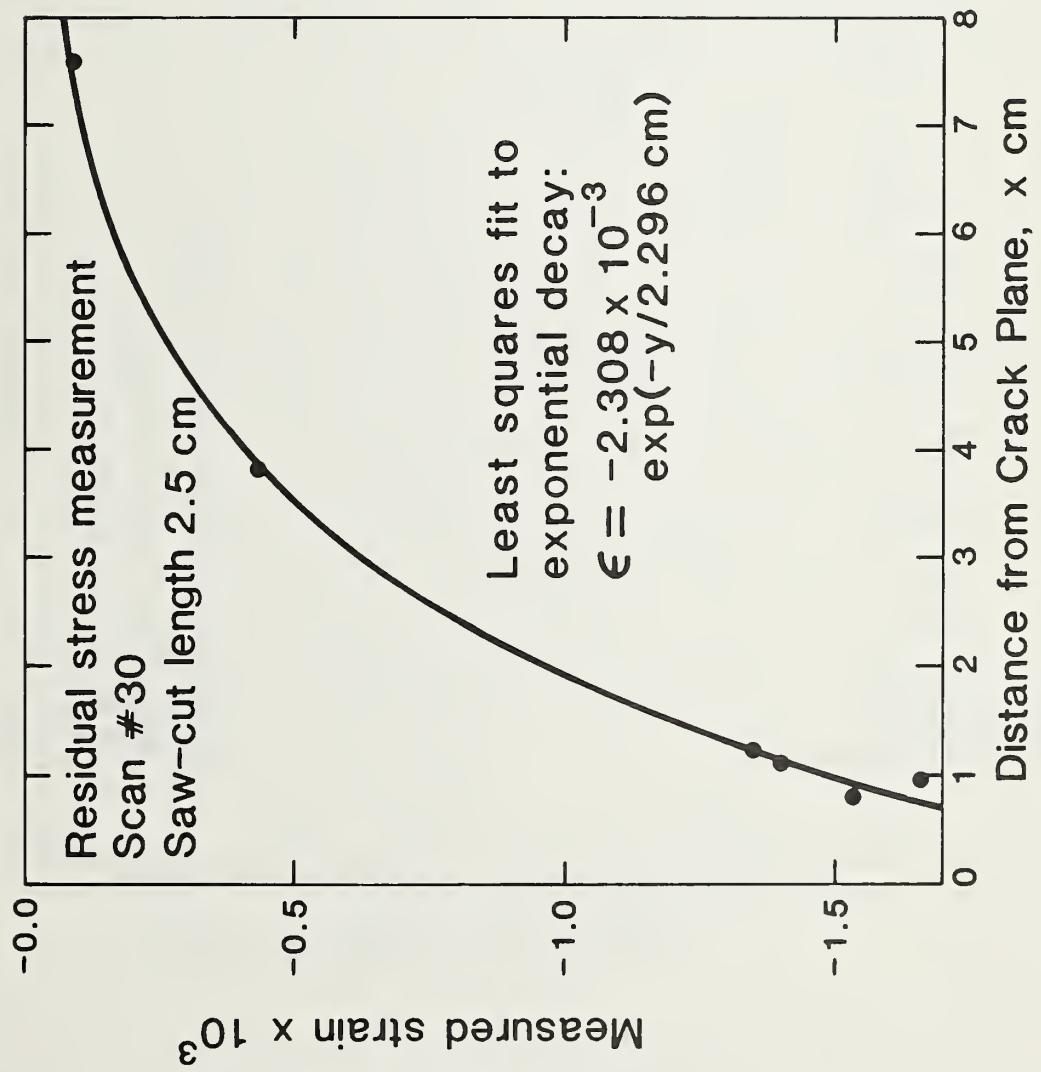


Figure 9. Measured strains near saw-cut in HY130 weldment with residual strain. Also shown is the fitting function used for evaluation of contour J-integral.

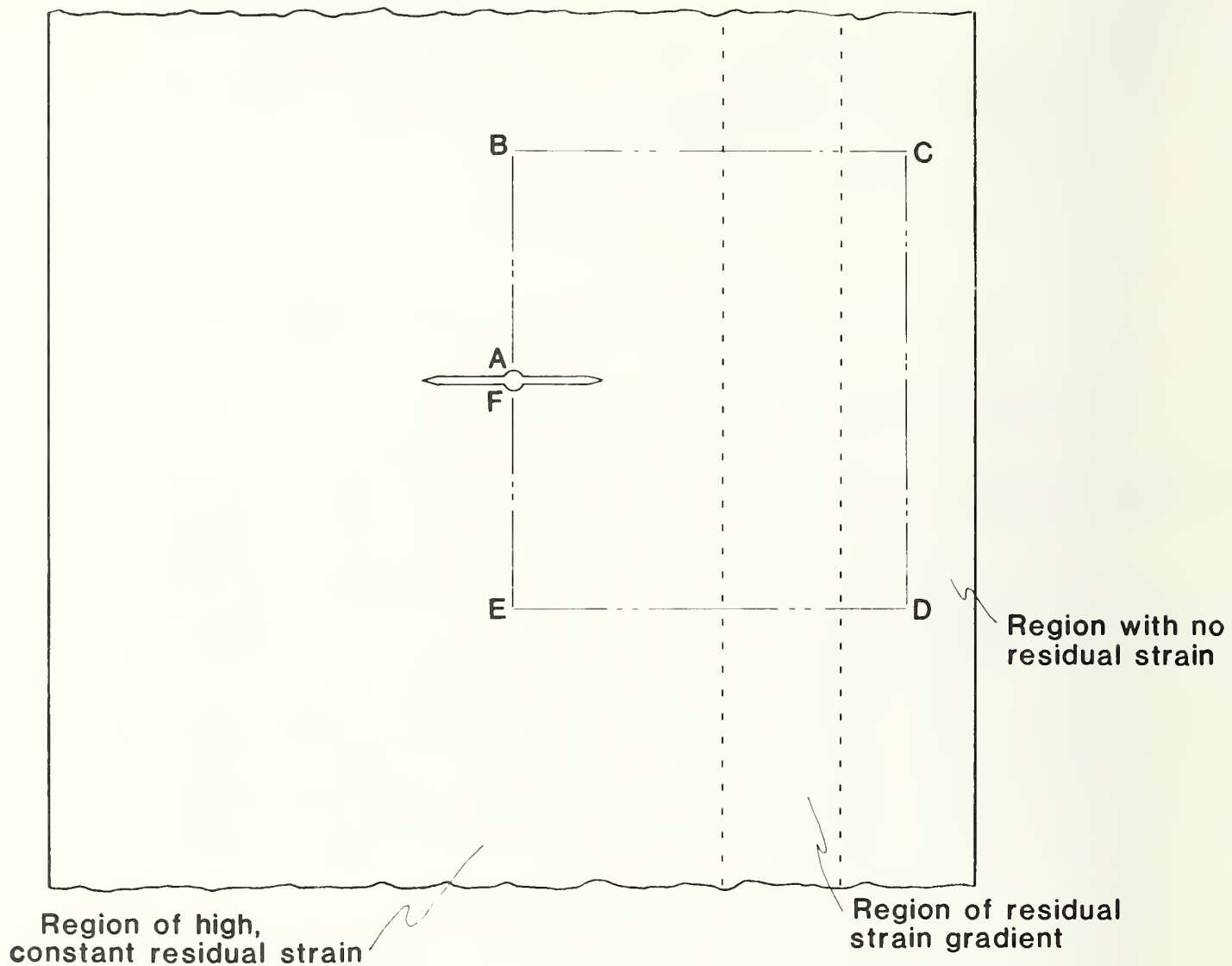


Figure 10. Diagram showing location of contour for J-integral evaluation in a plate with residual strains.

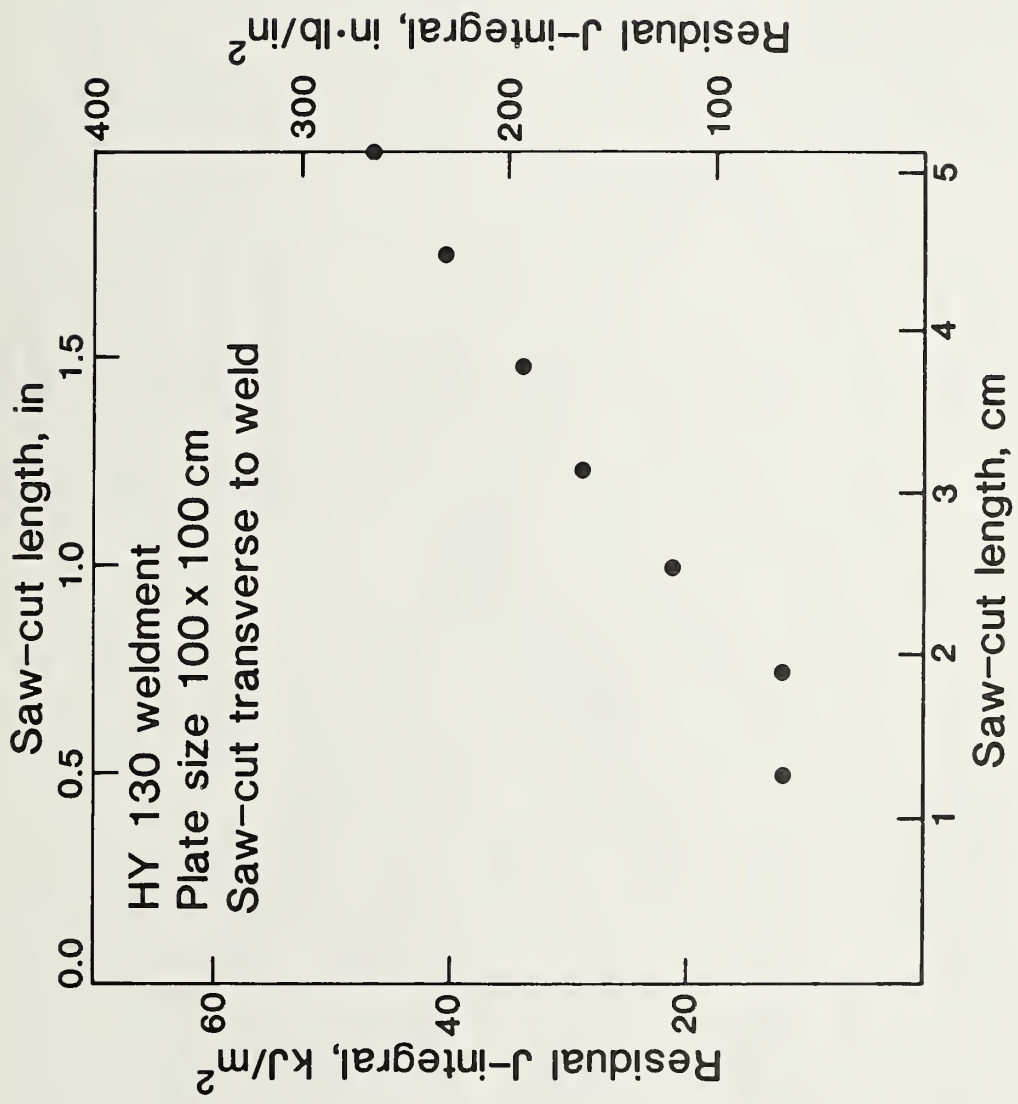


Figure 11. Experimentally obtained residual J-integral values plotted against total saw-cut length for HY130 weldment with residual strains.

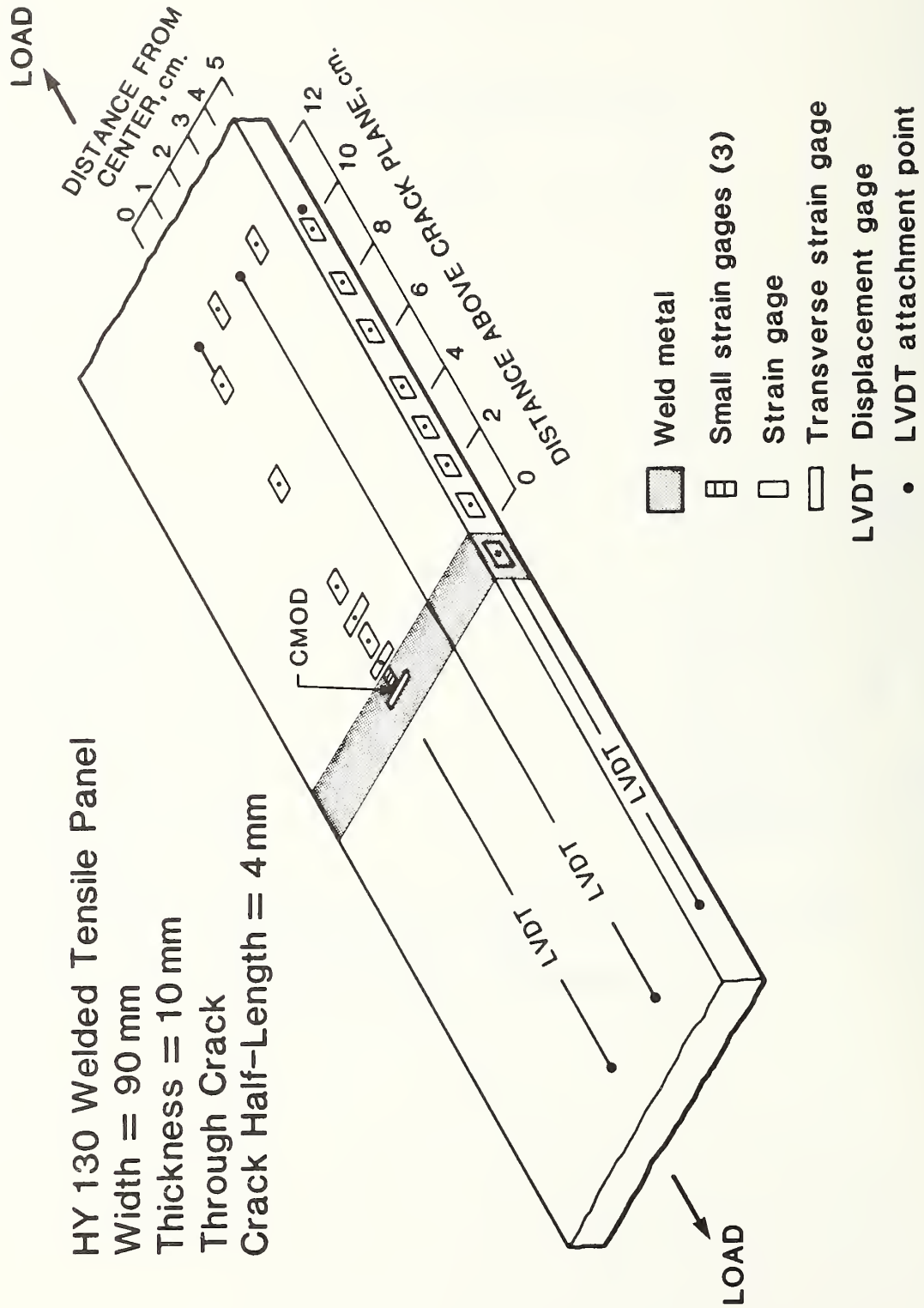


Figure 12. Instrumentation layout for transverse-welded center cracked HY130 tensile panel.

HY130 Welded Tensile Panel Center-Cracked

Crack Half- Length 4mm

Scan Number	26	33	80
Gage Length Strain	0.0039	0.0052	0.0130
Remote Strain	0.0035	0.0042	0.0043
J-Integral (kN/m) ^{1/2}	62	172	1415

$\sigma = 1 \text{ kN/m} = 5.71 \text{ lb/in}$

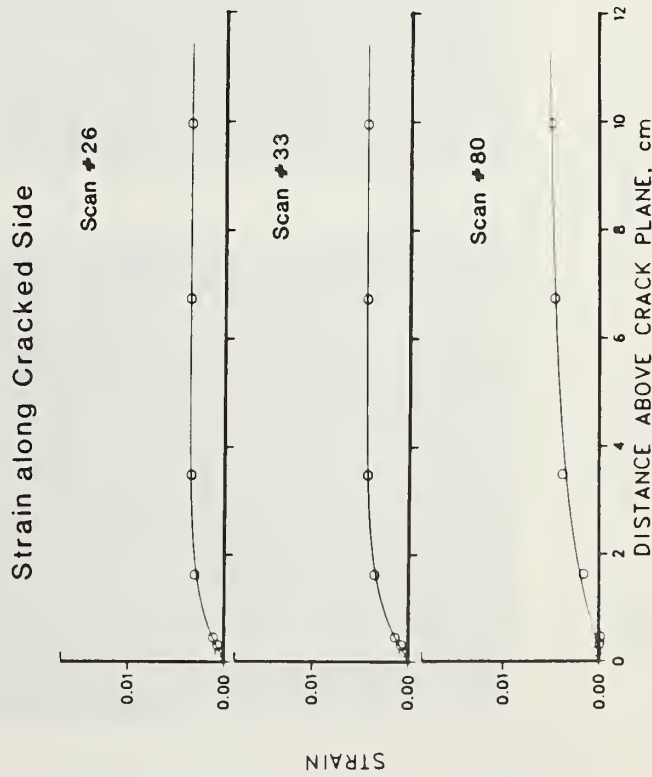
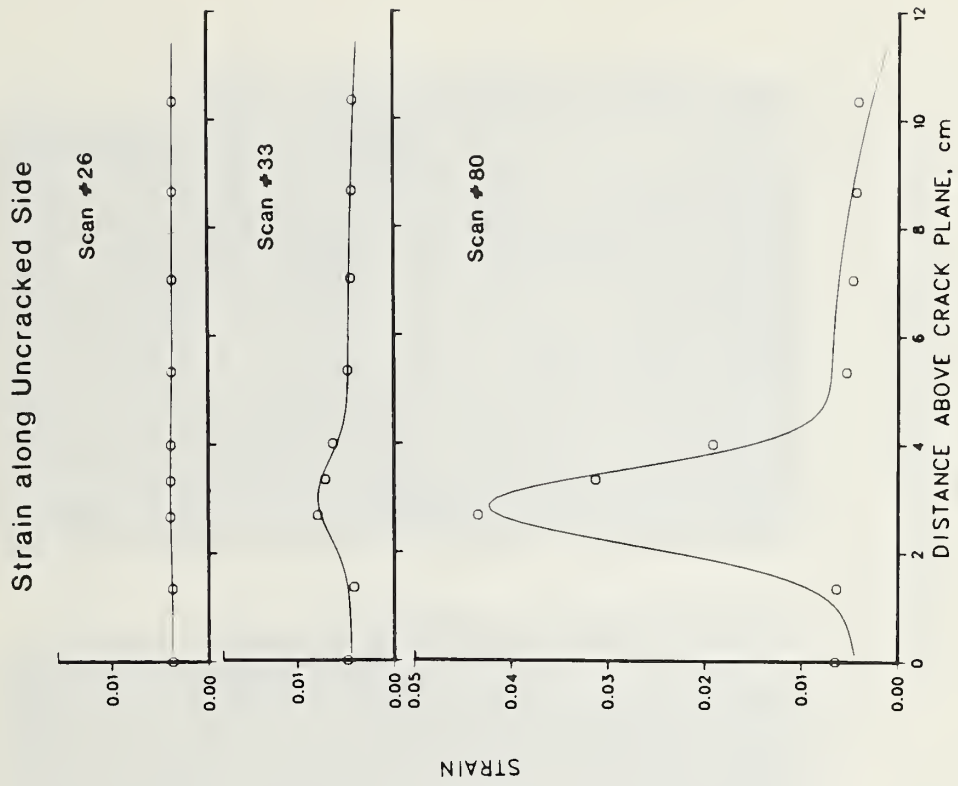
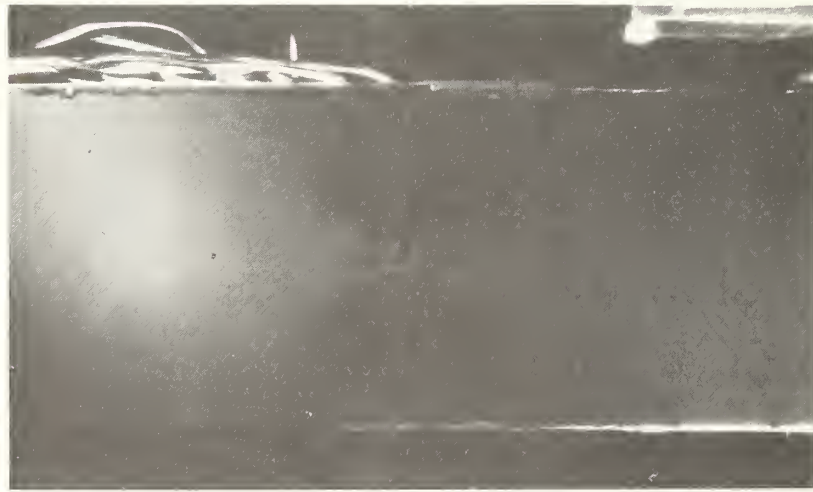


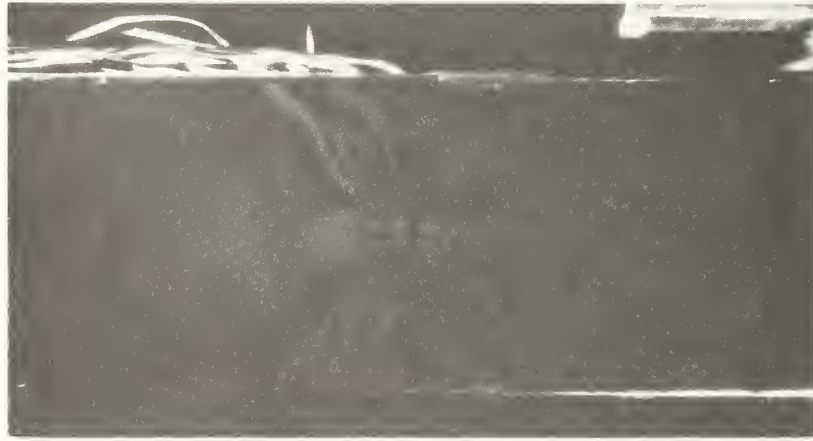
Figure 13. Strain distribution in transverse-welded center-cracked HY130 tensile panel at three applied strain levels.

HY 130 Welded Tensile Panel Center-Cracked

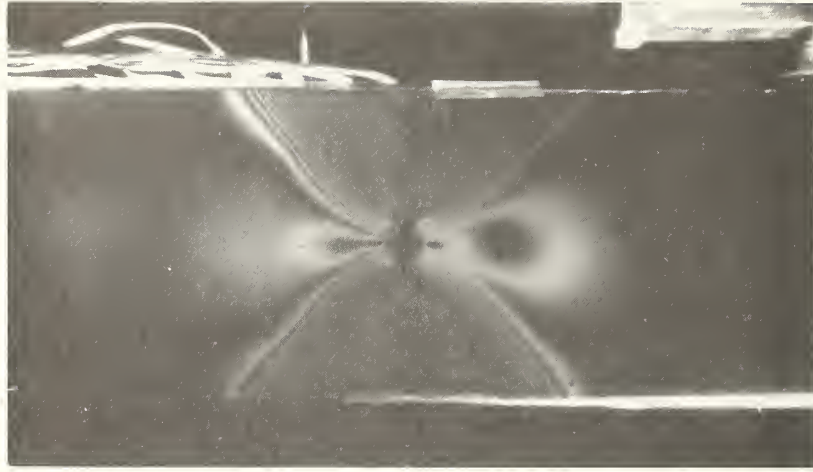
Width 90 mm Thickness 10 mm Crack Half-Length 4 mm



Scan #26



Scan #33



Scan #80

Figure 14. Transverse-welded center-cracked HY130 tensile panel, crack half-length 4 mm, with photoelastic coating to show strain pattern, at the three strain values used for figure 13.

Figure 15a-k. Dependence of J-integral, stress, and crack mouth opening displacement on strain for transverse-welded center-cracked HY130 tensile panel.

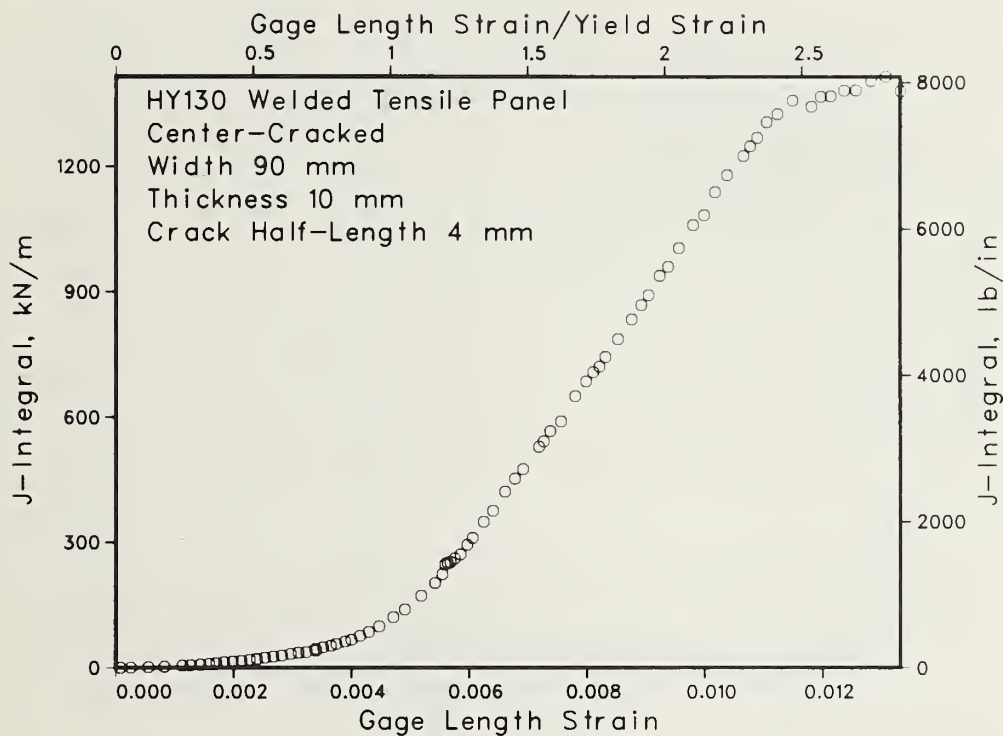


Figure 15a.

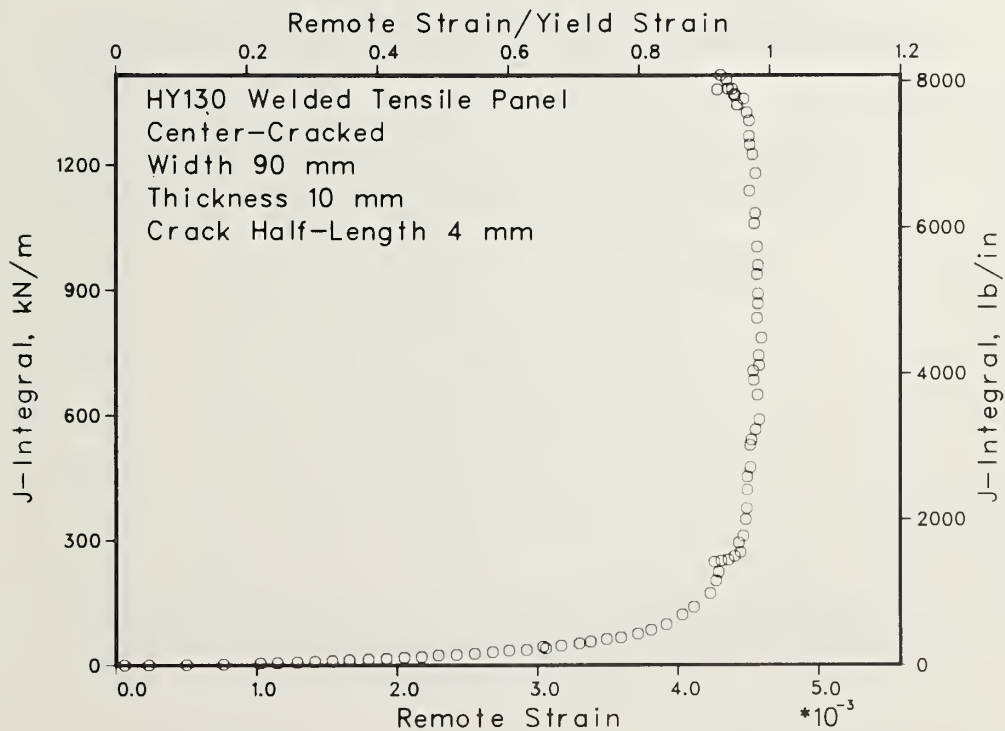


Figure 15b.

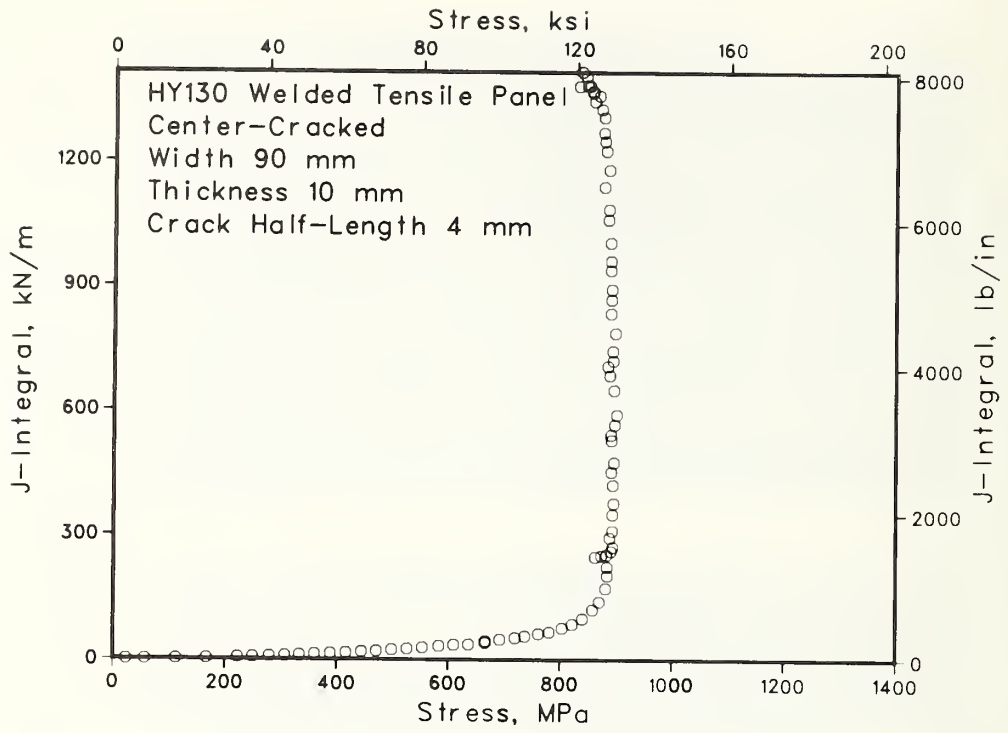


Figure 15c.

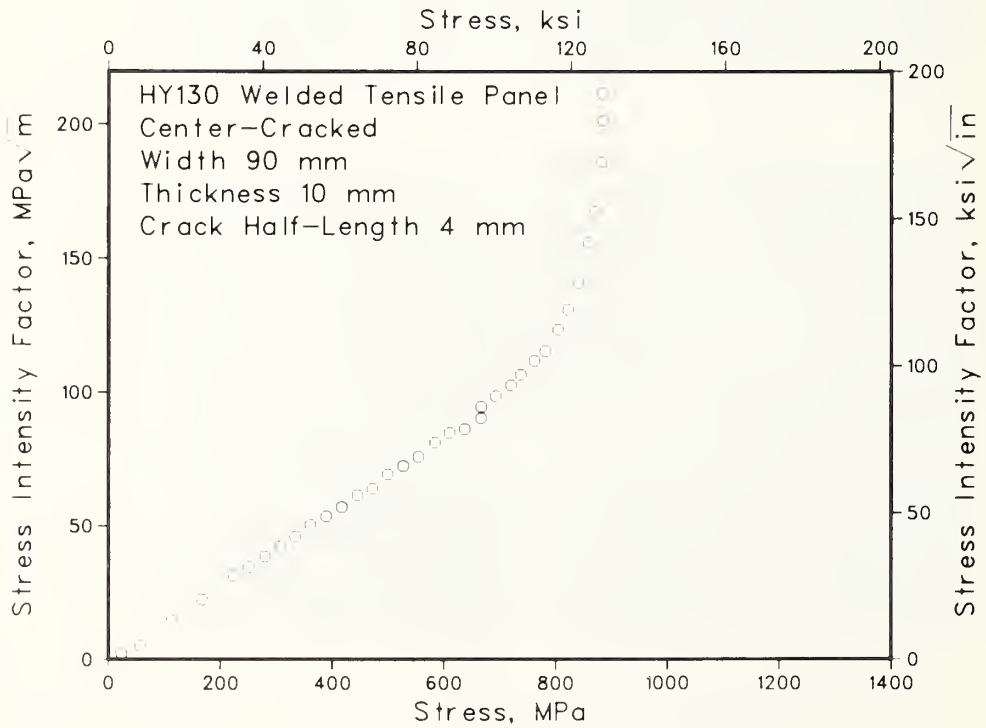


Figure 15d.

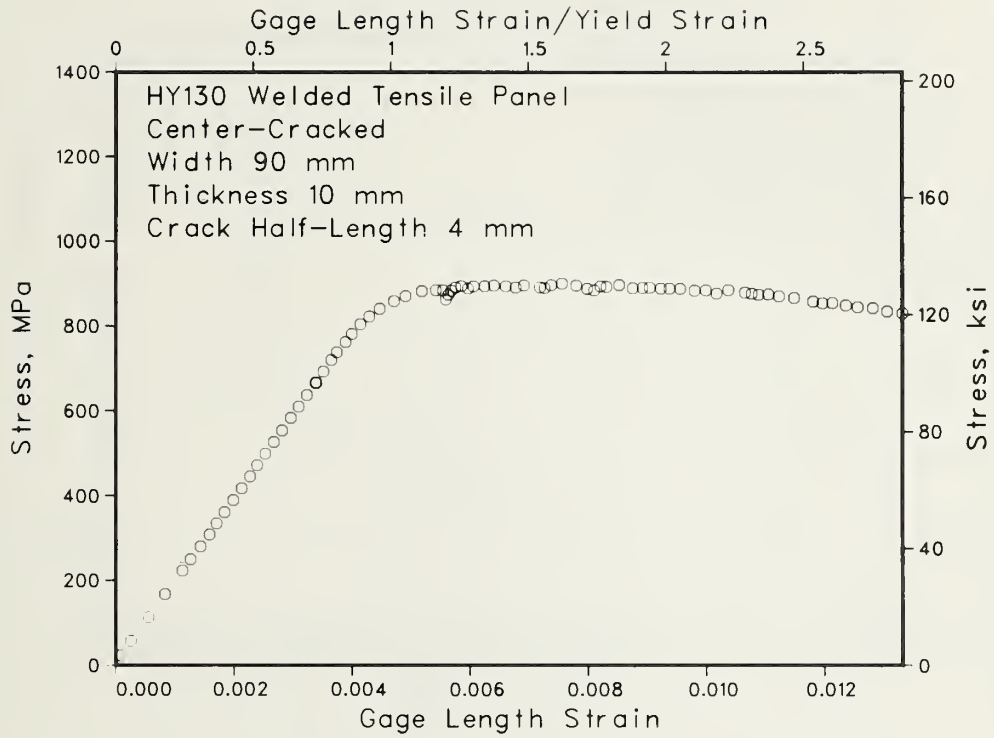


Figure 15e.

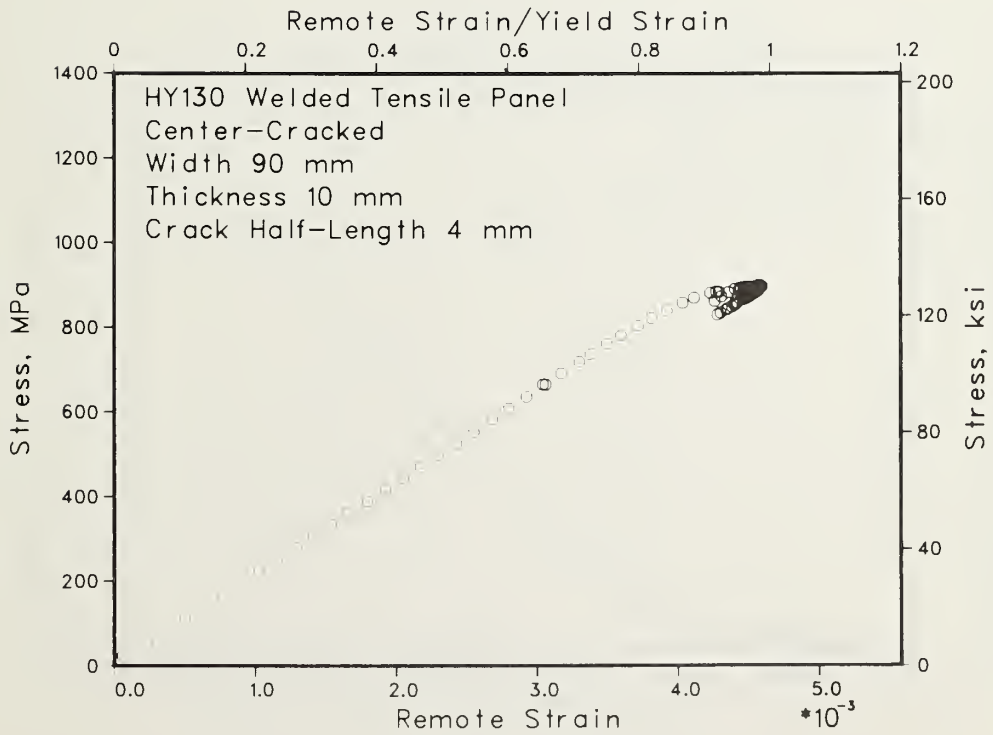


Figure 15f.

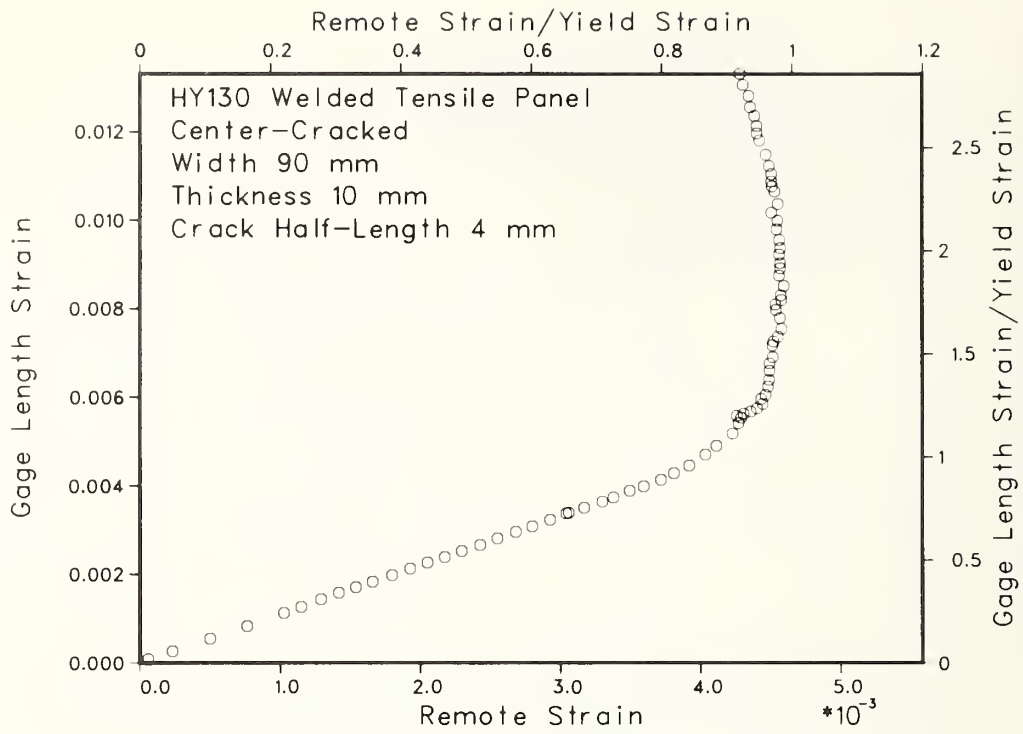


Figure 15g.

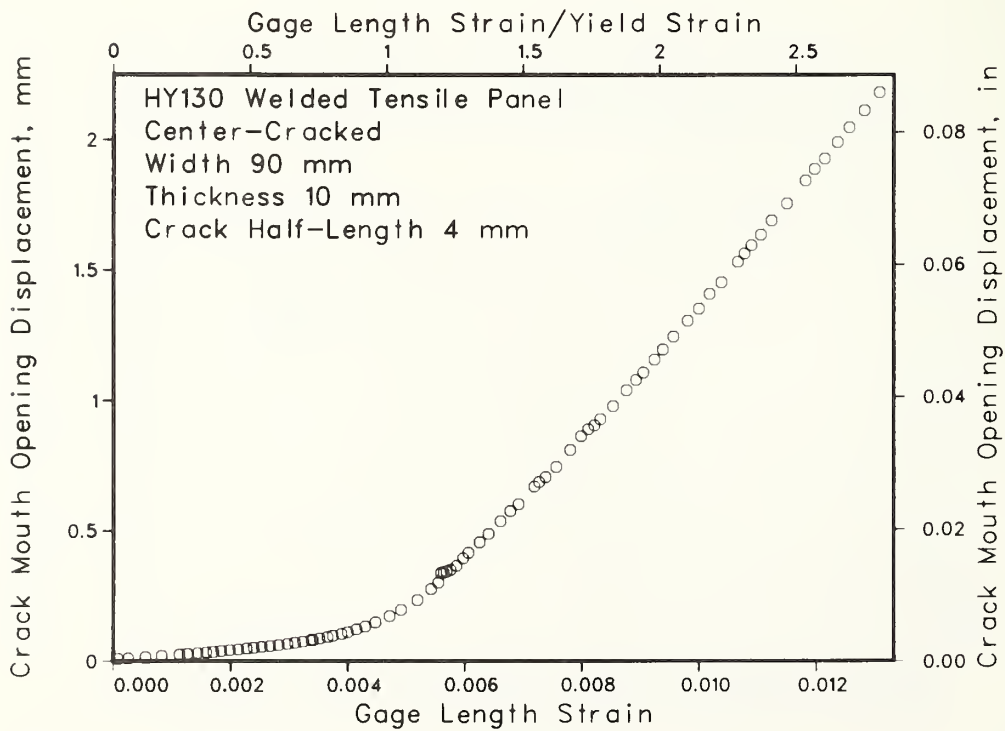


Figure 15h.

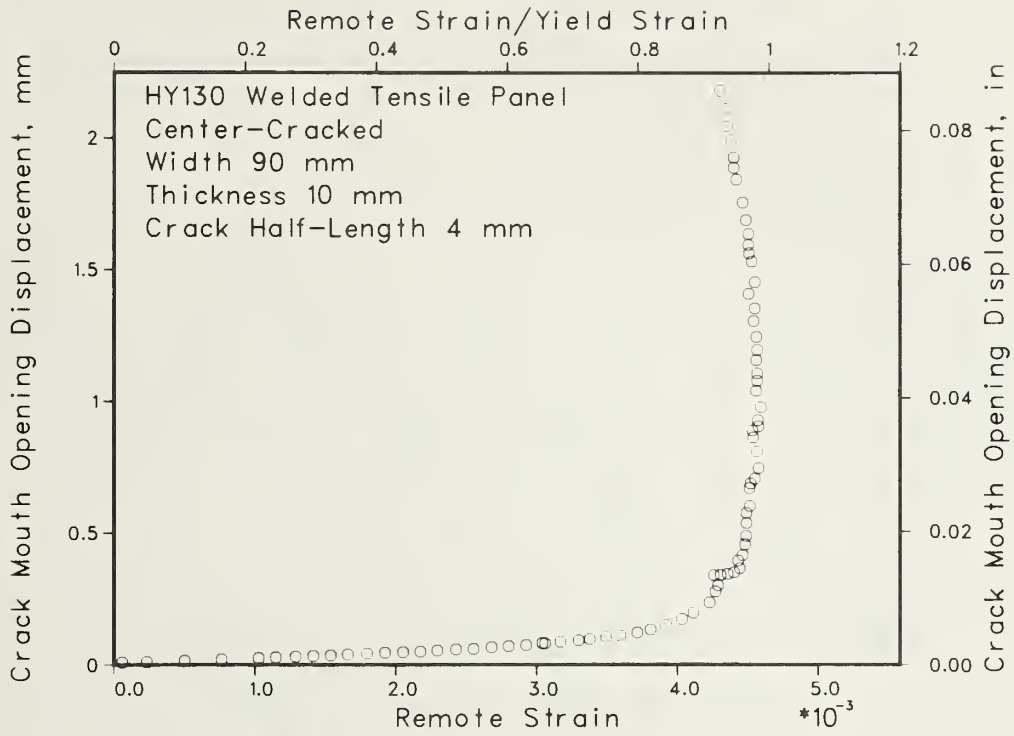


Figure 15i.

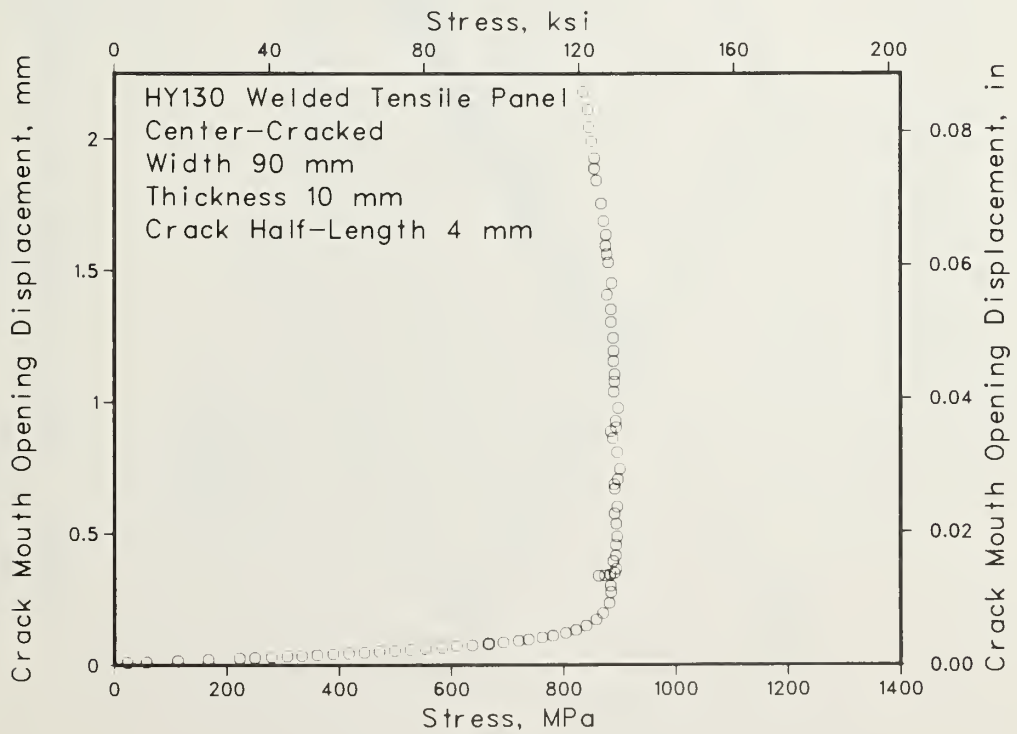


Figure 15j.

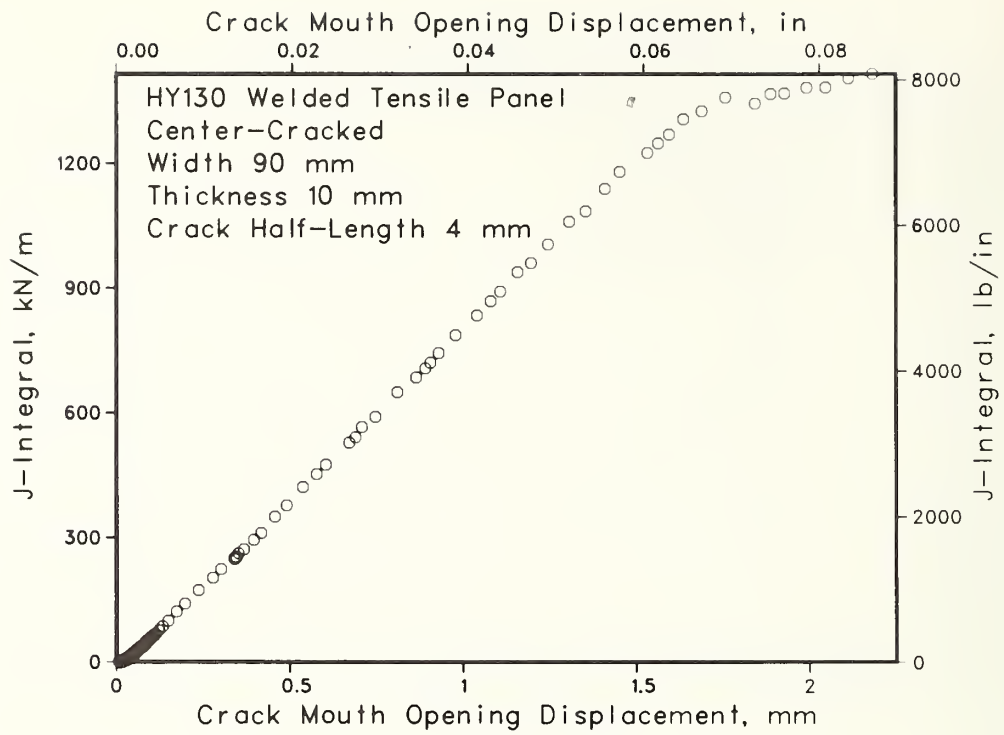


Figure 15k.

HY 130 Welded Tensile Panel
 Width = 912 mm
 Thickness = 25 mm
 Crack Half-Length = 12.5 mm

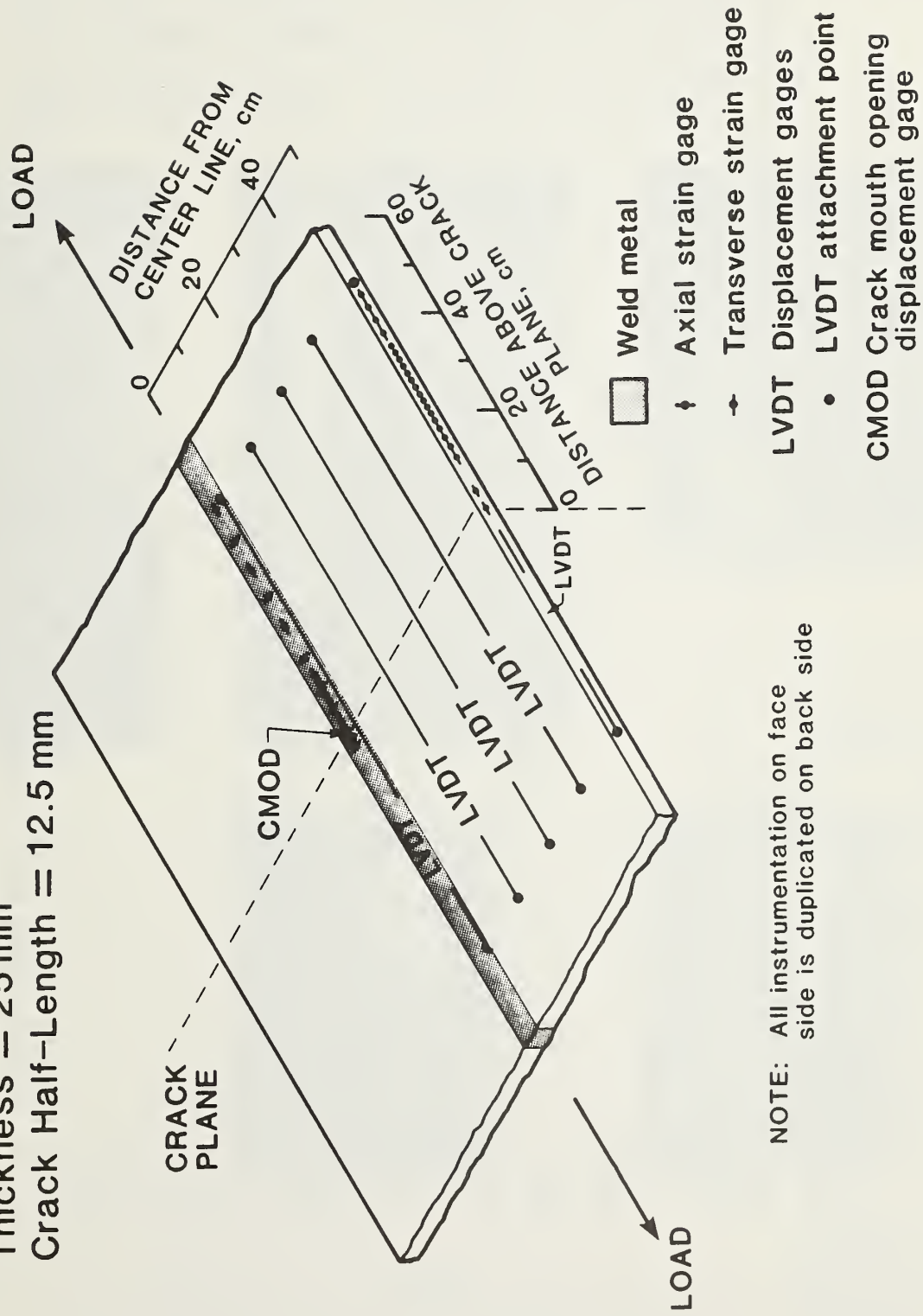


Figure 16. Instrumentation layout for large axial-welded center-cracked HY130 tensile panel.

HY 130 Welded Tensile Panel (Weld along tensile axis)
 Specimen Width 910 mm Crack Half-Length 12.5 mm

Scan Number	35	45	49
Gage Length Strain	0.0043	0.0056	0.0079
Remote Strain	0.0041	0.0050	0.0059
J-Integral (kN/m) [#]	407	1028	2634

[#] 1 kN/m = 5.71 lb/in

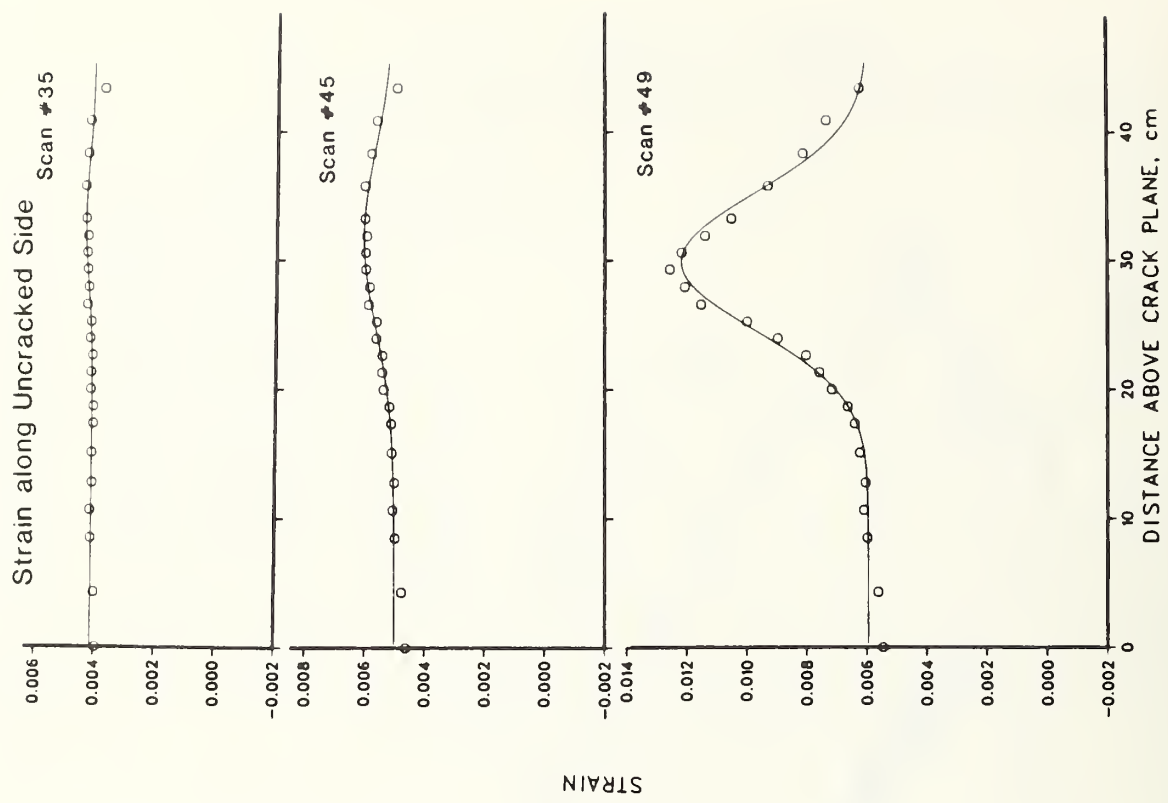
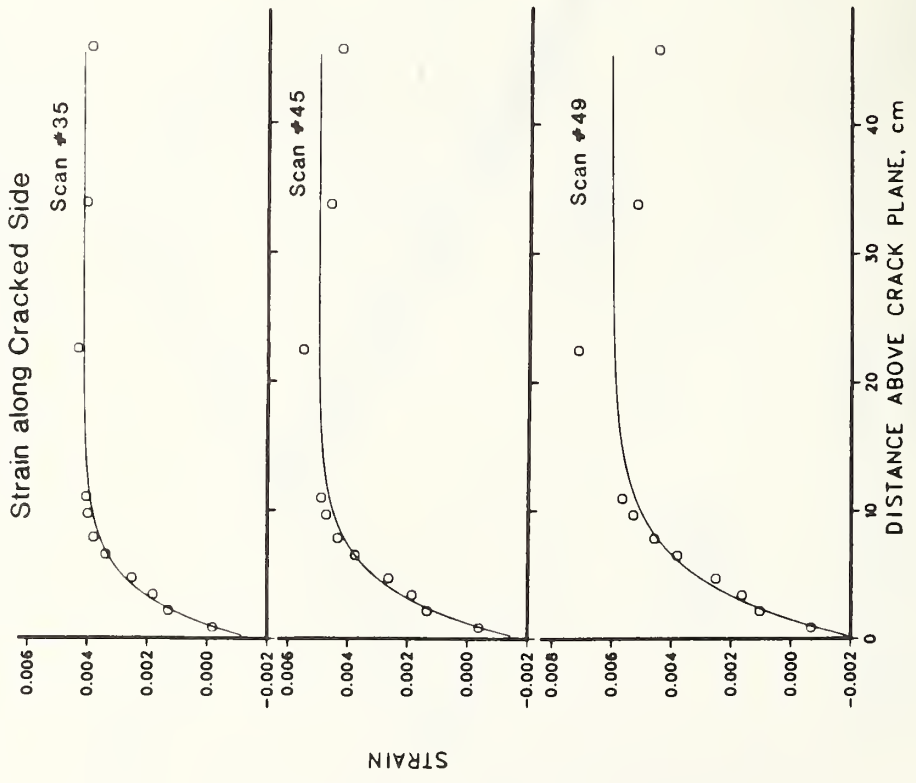


Figure 17. Strain distribution in large axial-welded center-cracked HY130 tensile panel.

HY130 Welded Tensile Panel Weld along Tensile Axis
Center-Cracked Width 910 mm
Thickness 25 mm Crack Half-Length 12.5 mm



Scan #35



Scan #45



Scan #49



Scan #45



Scan #49

Figure 18. Strain pattern as revealed by photoelastic coating on large axial-welded center-cracked HY130 tensile panel.

Figure 19a-k. Dependence of J-integral, stress, and crack mouth opening displacement on strain for transverse-welded center-cracked HY130 tensile panel.

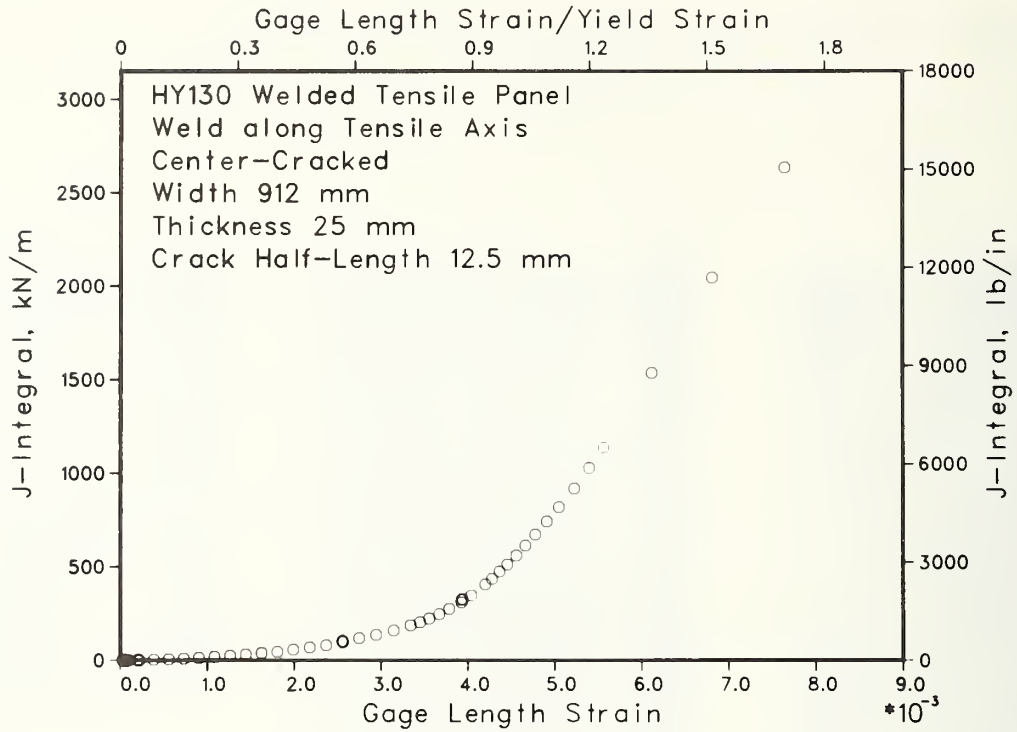


Figure 19a.

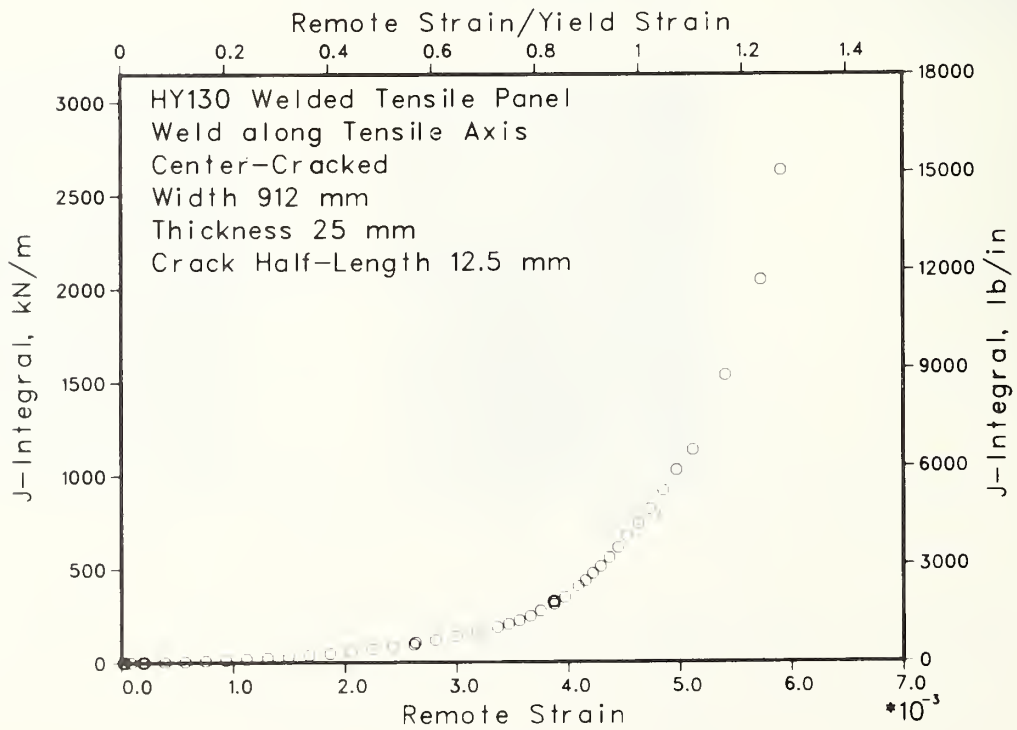


Figure 19b.

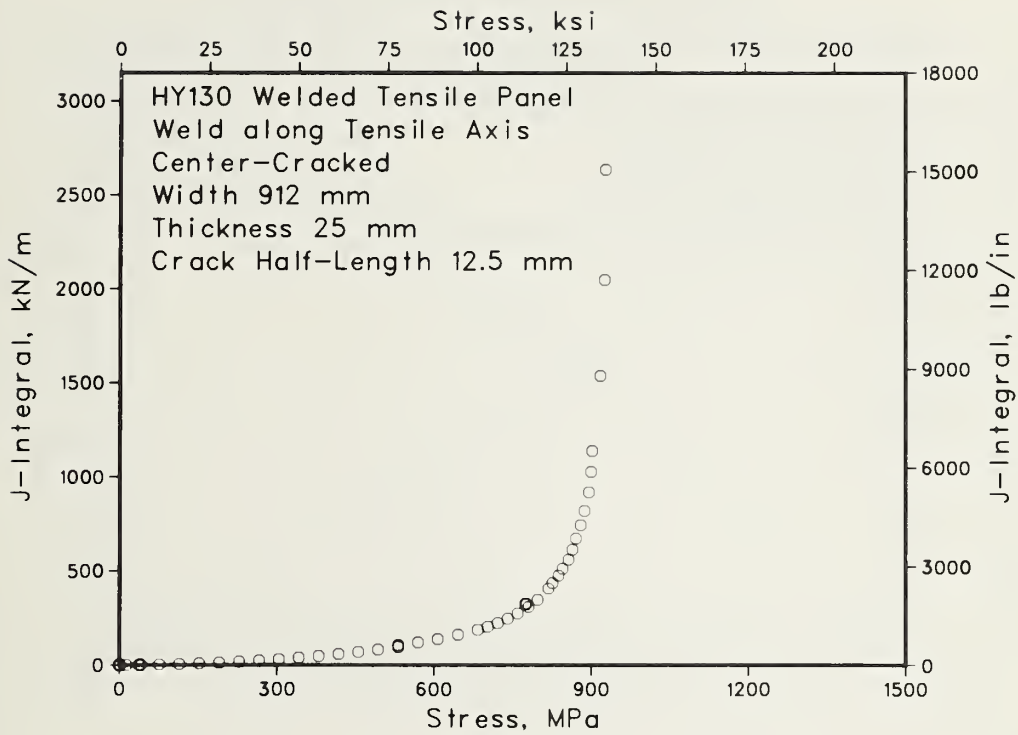


Figure 19c.

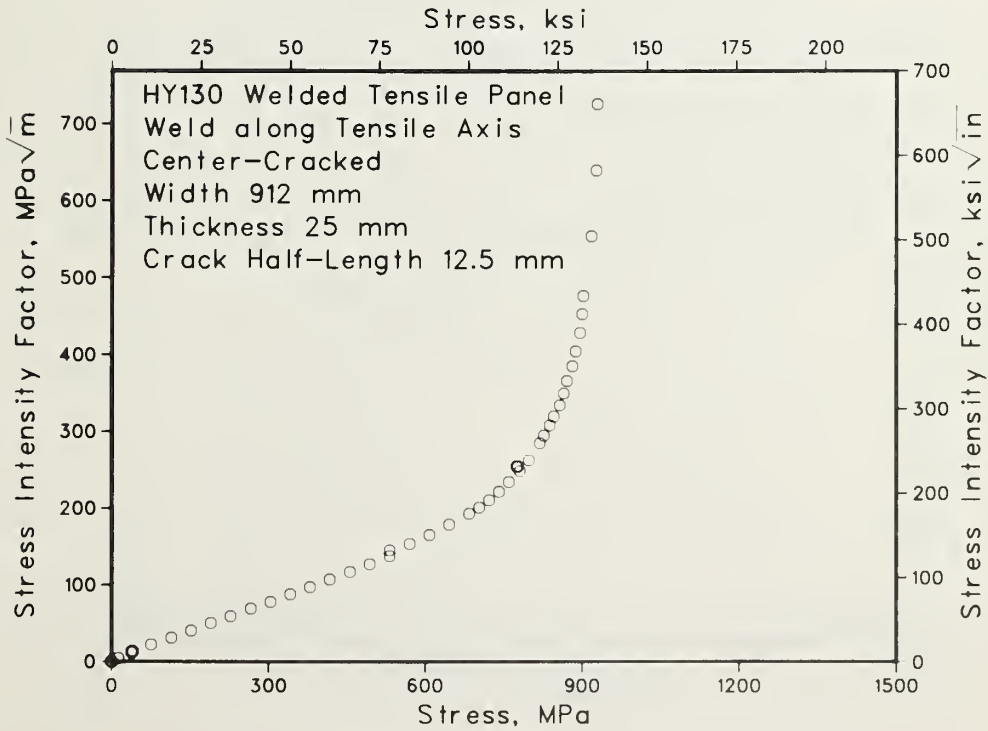


Figure 19d.

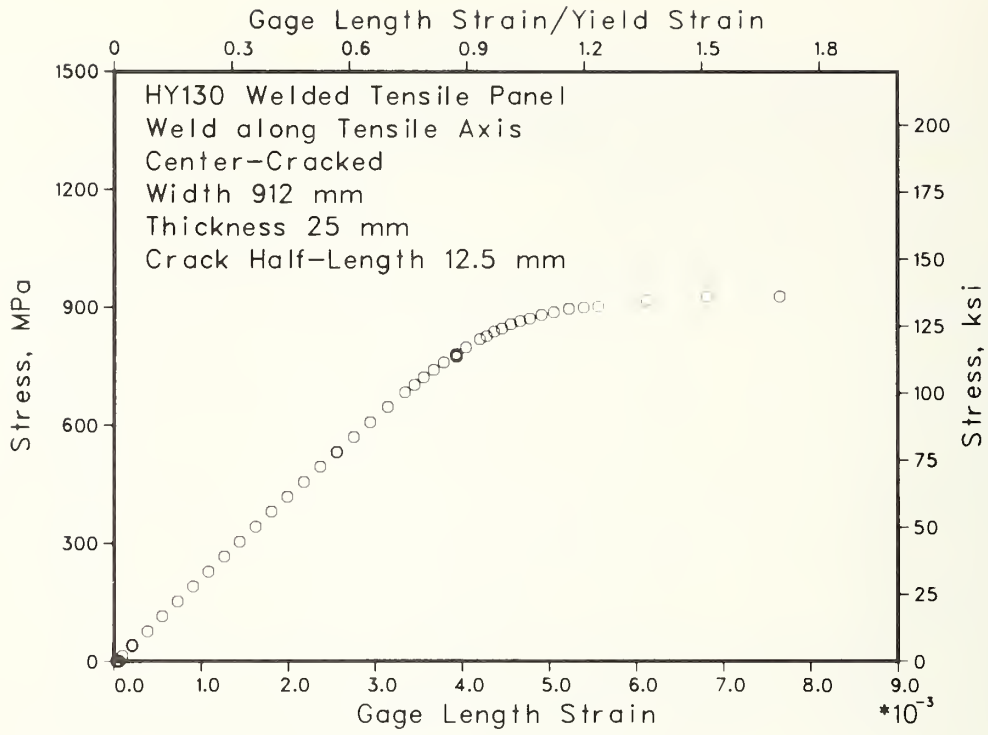


Figure 19e.

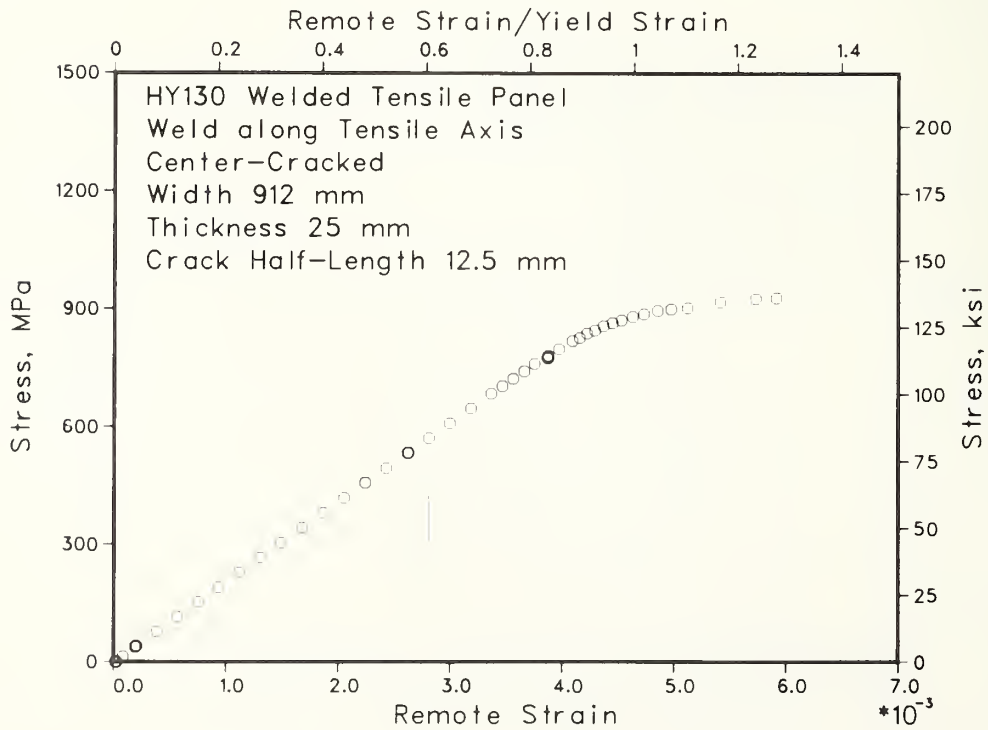


Figure 19f.

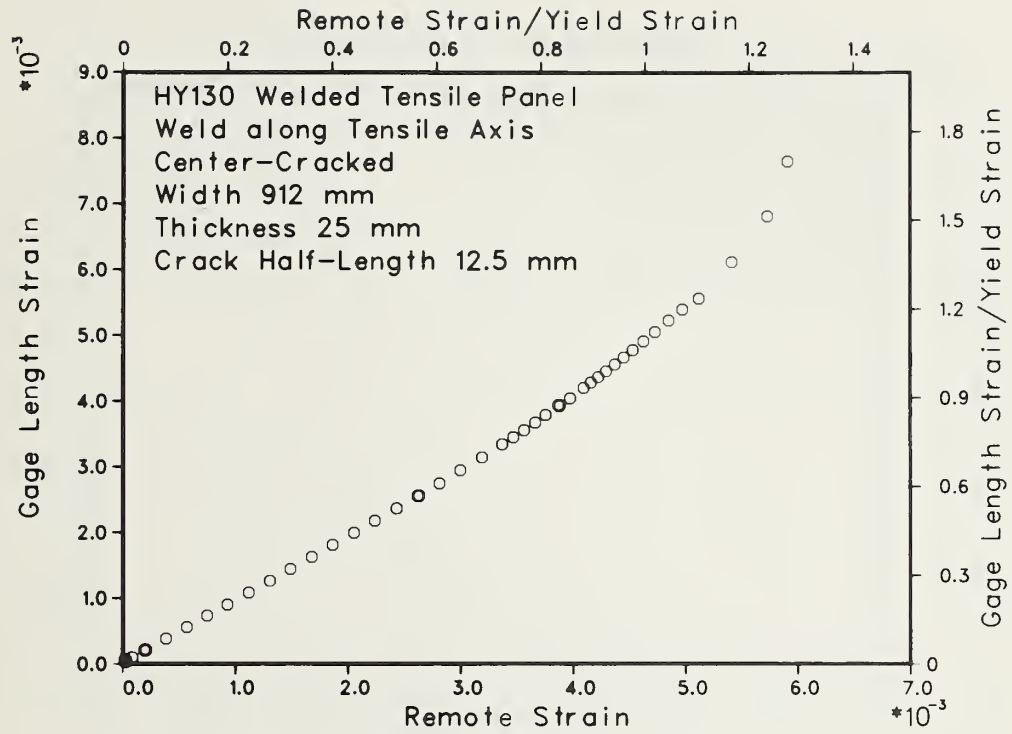


Figure 19g.

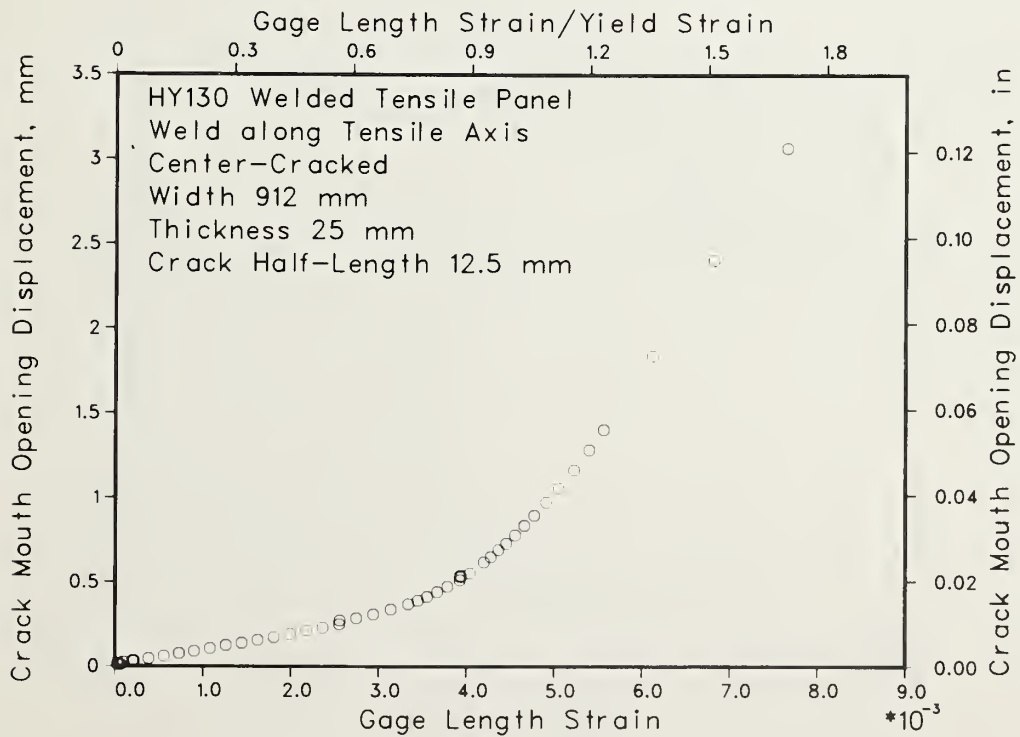


Figure 19h.

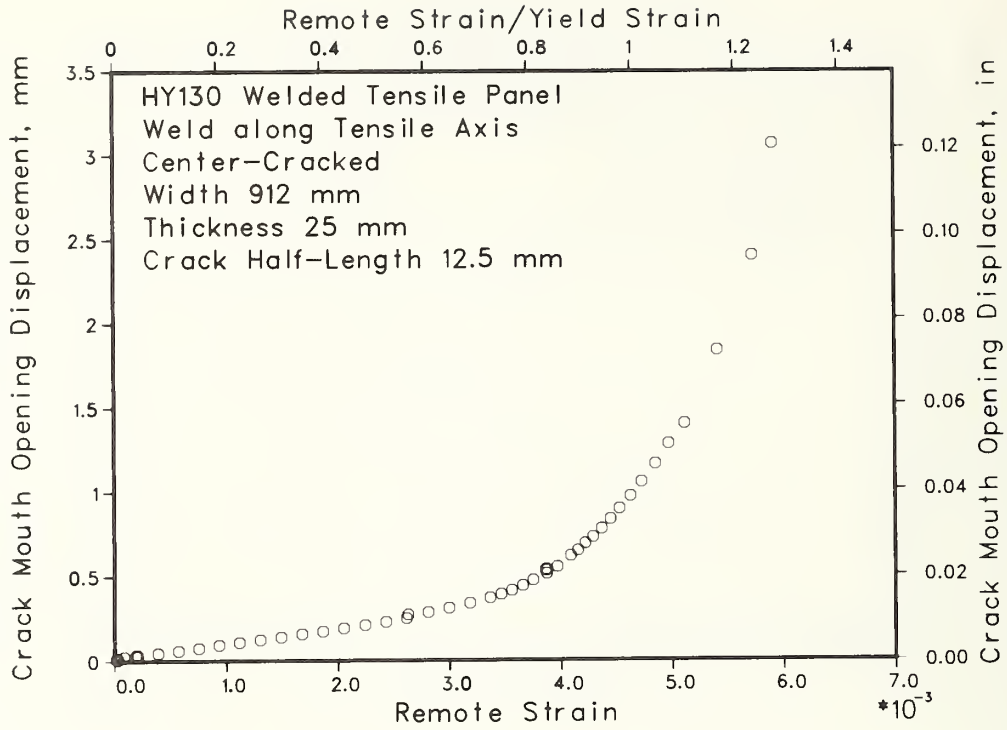


Figure 19i.

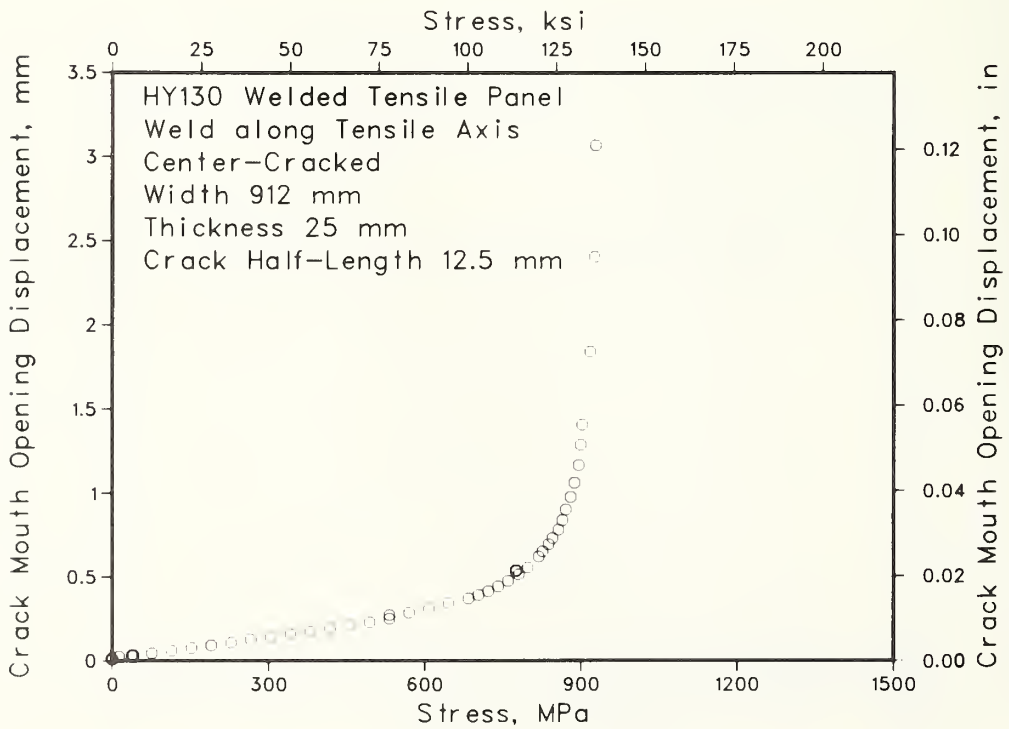


Figure 19j.

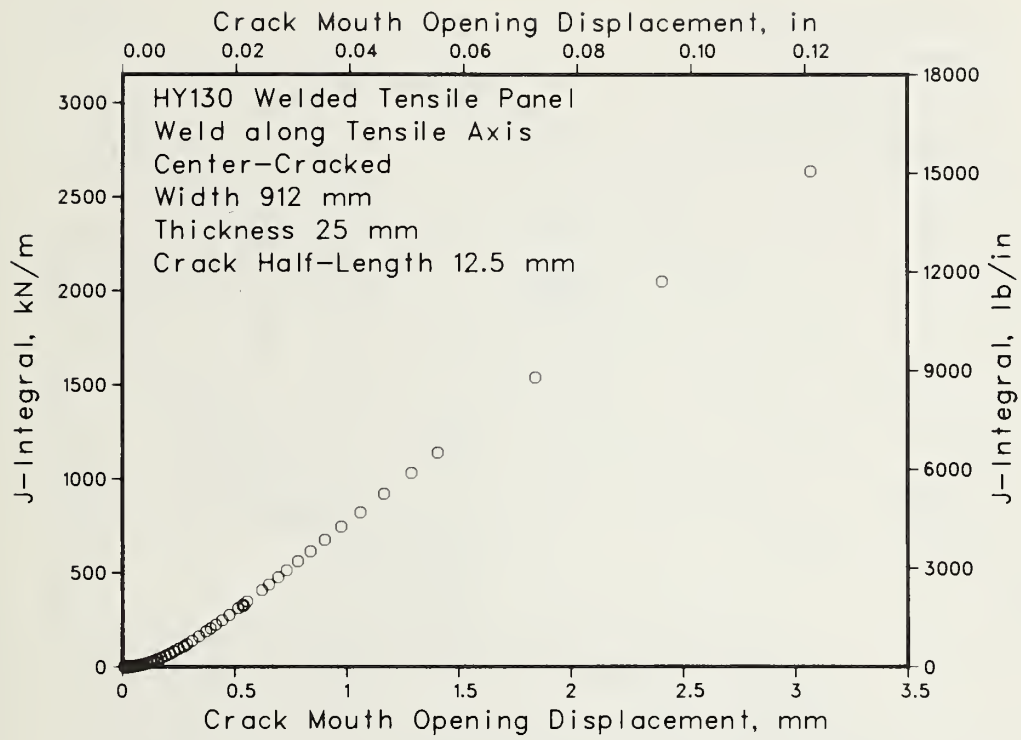


Figure 19k.

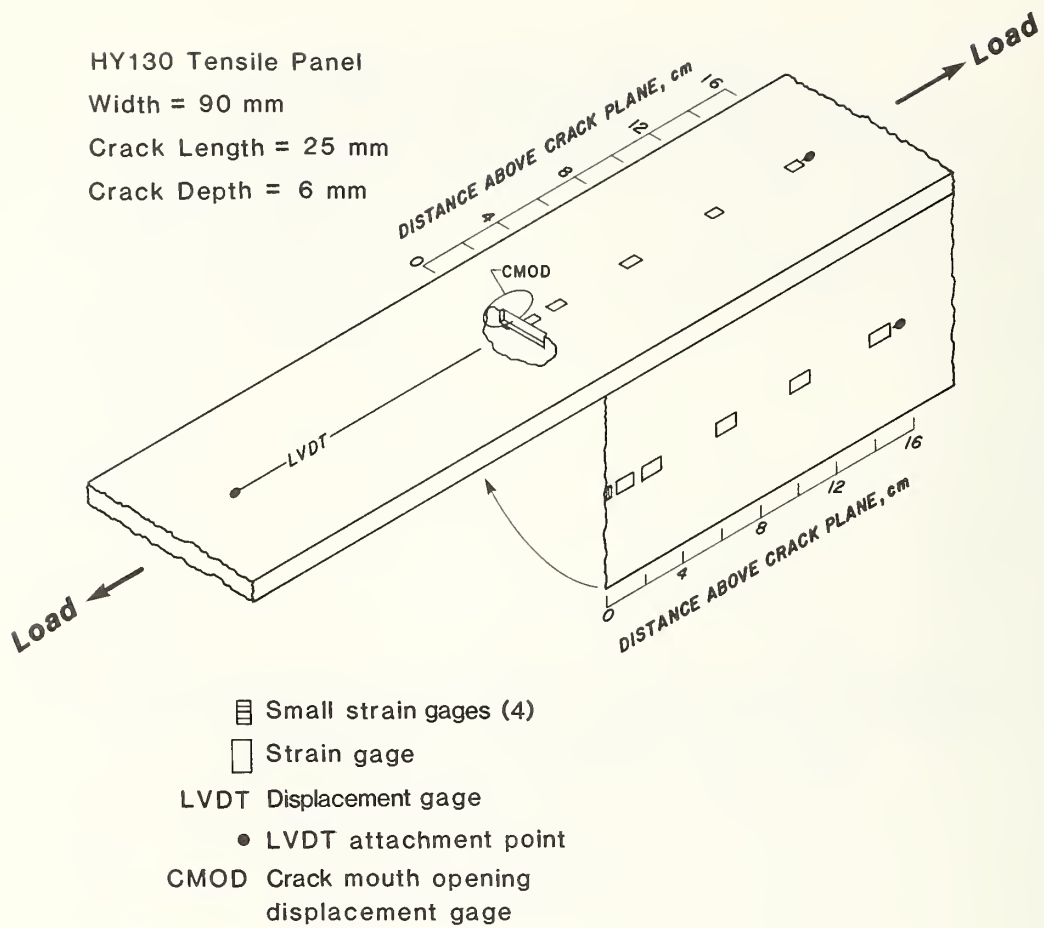


Figure 20. Instrumentation layout for surface-cracked tensile panel, crack depth 6 mm, crack length 25 mm.

HY130 Tensile Panel Surface-Cracked

Crack Length = 25 mm. Crack Depth = 6 mm. Specimen Width = 90 mm.
 Panel Thickness = 10 mm.

Scan Number	33	60	90
Gage Length Strain	0.0012	0.0025	0.0058
Remote Strain	0.0012	0.0024	0.0030
J-Integral (kN/m)*	6.89	42.04	628.39

*1 kN/m = 6.369 lb/in

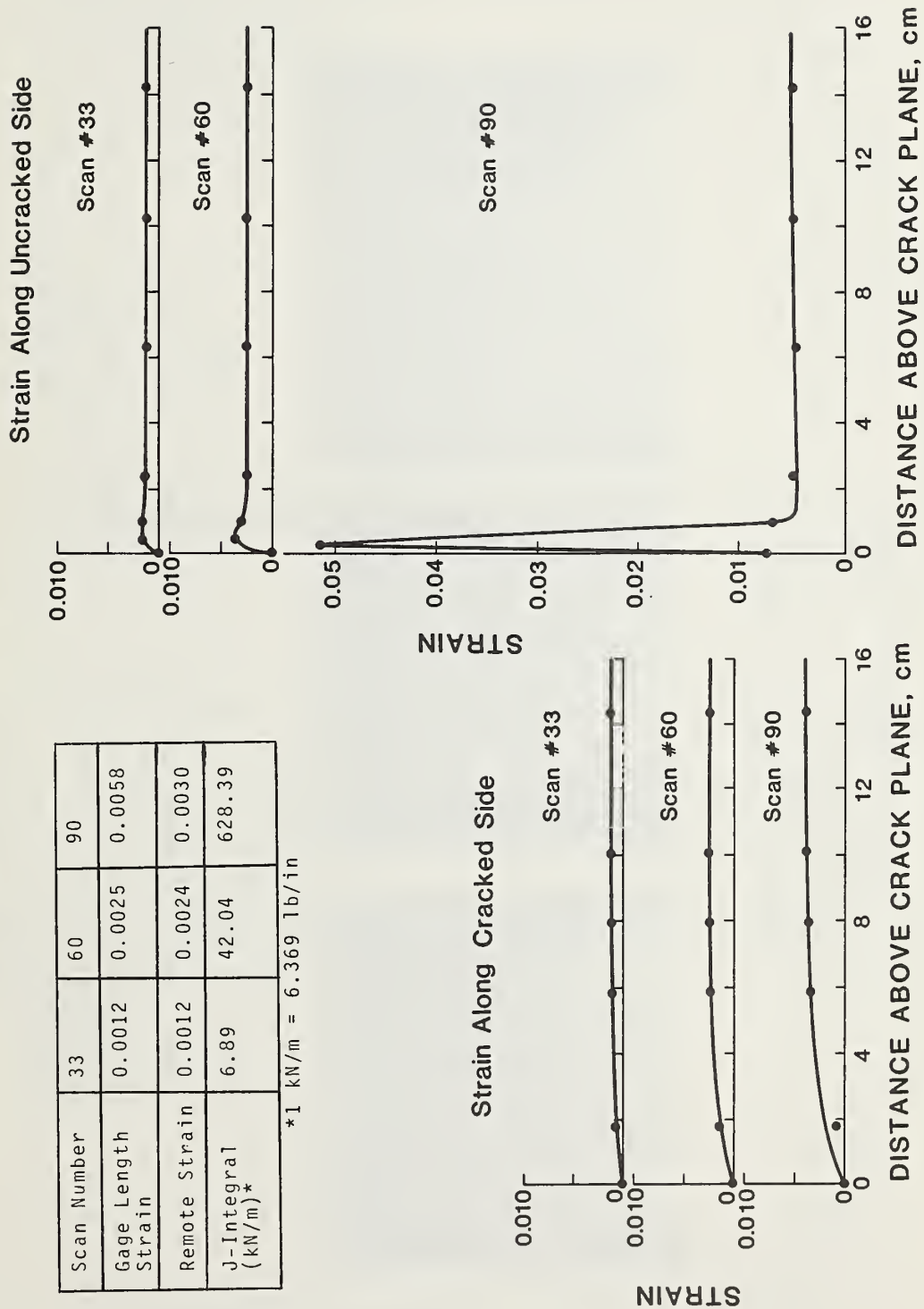


Figure 21. Strain distribution in surface-cracked tensile panel with crack depth 6 mm and crack length 25 mm at three strain levels.

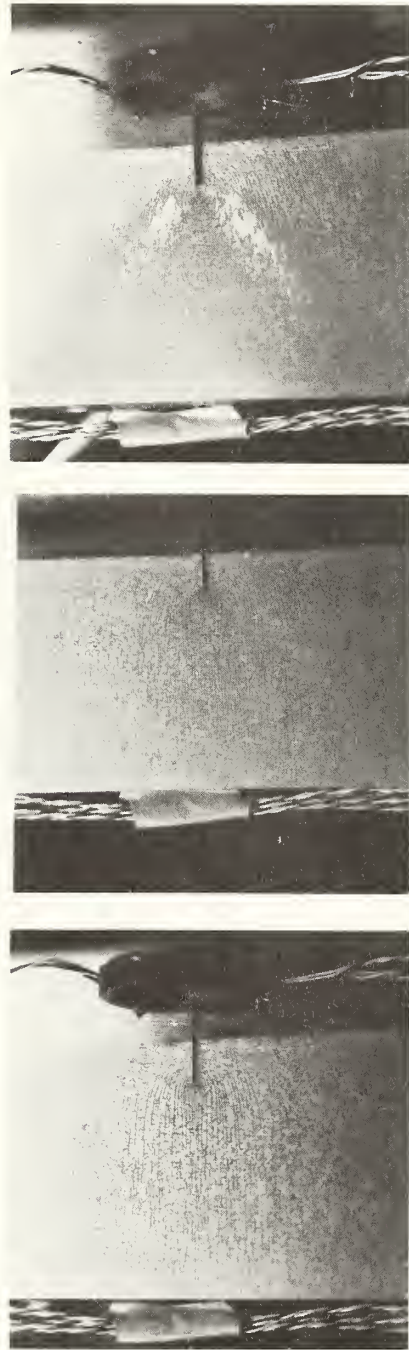
HY130 Tensile Panel Surface-Cracked

Crack Length = 25 mm.

Crack Depth = 6 mm.

Panel Thickness = 10 mm.

Specimen Width = 90 mm.



Scan Number	33	60	90
Gage Length Strain	0.0012	0.0025	0.0058
Remote Strain	0.0012	0.0024	0.0030
J-Integral (kN/m)*	7	42	628

* 1 kN/m = 5.71 lb/in

Figure 22. Surface-cracked tensile panel, crack depth 6 mm, crack length 25 mm, with brittle lacquer coating to show strain distribution at three strain levels.

Figure 23a-k. Strain and stress dependence of J-integral and crack mouth opening displacement for surface-cracked HY130 base metal tensile panel with crack length 25.4 mm and crack depth 6.4 mm.

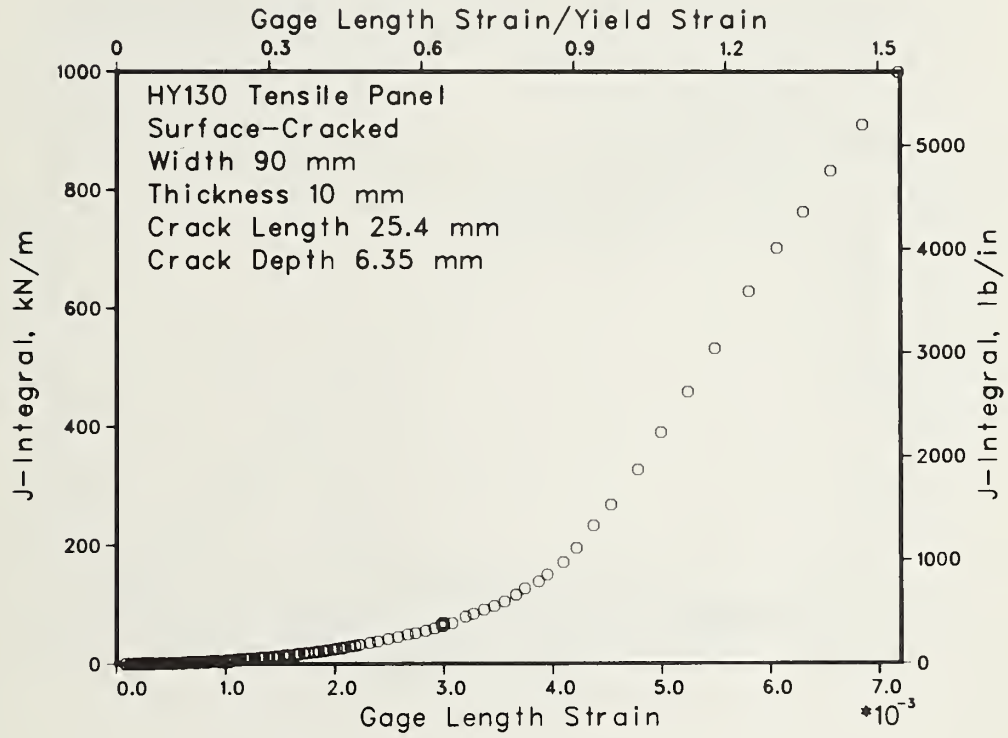


Figure 23a.

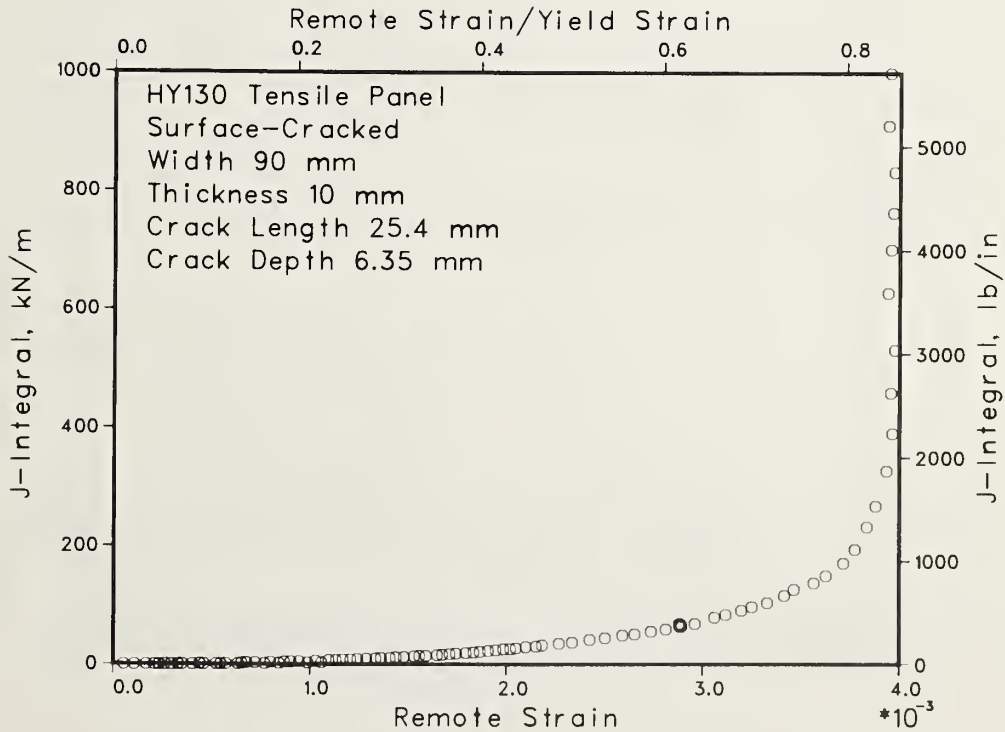


Figure 23b.

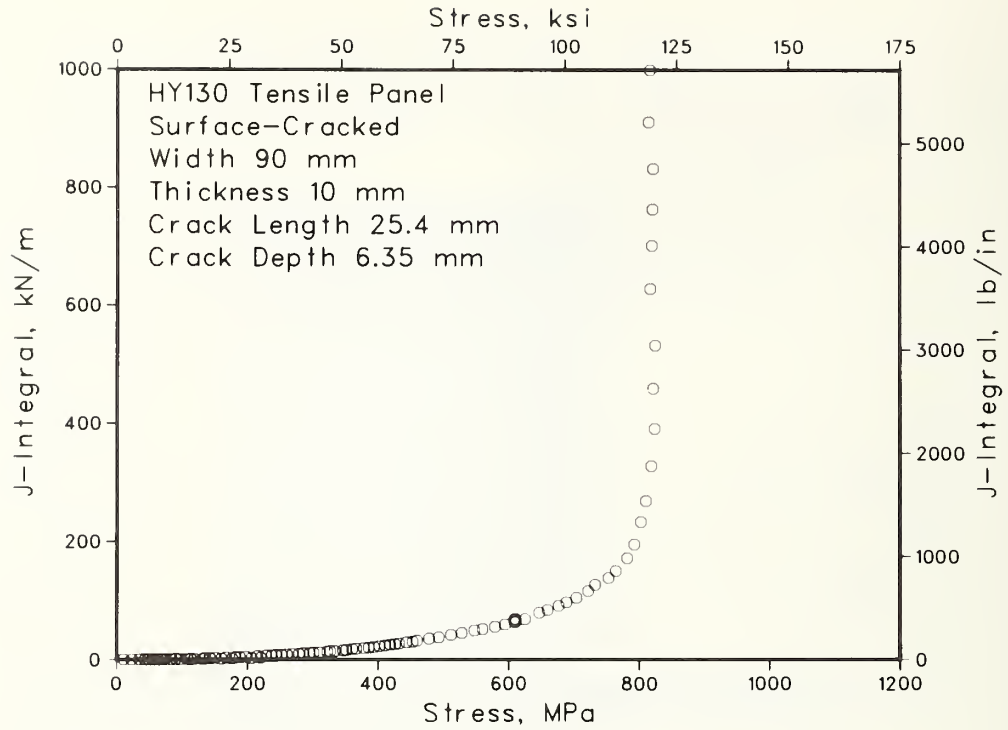


Figure 23c.

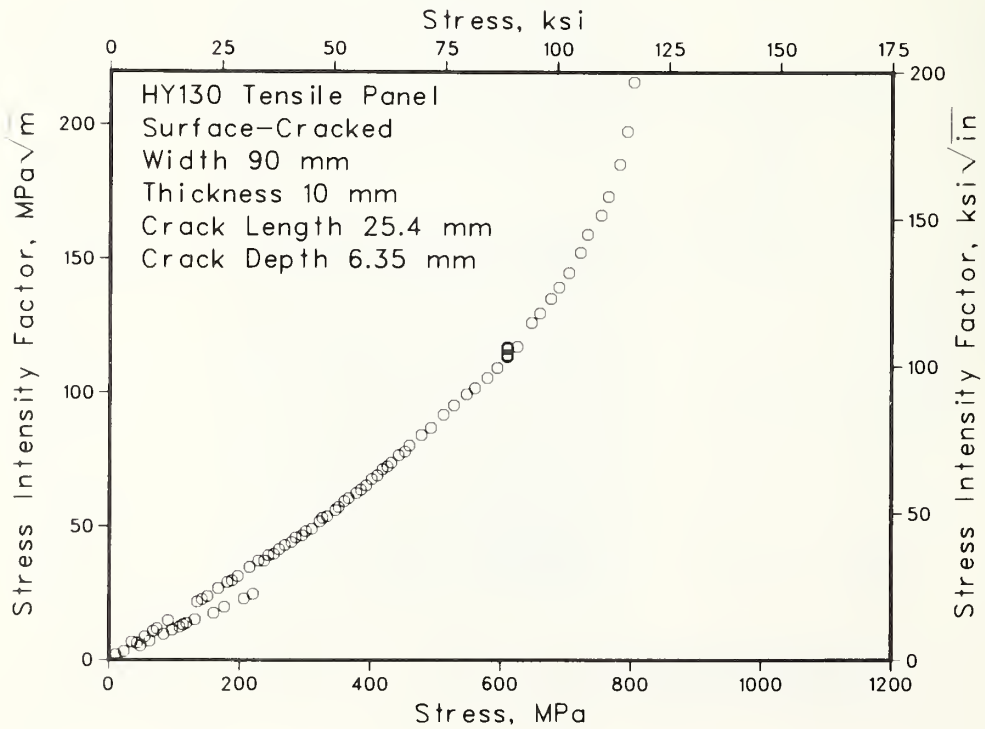


Figure 23d.

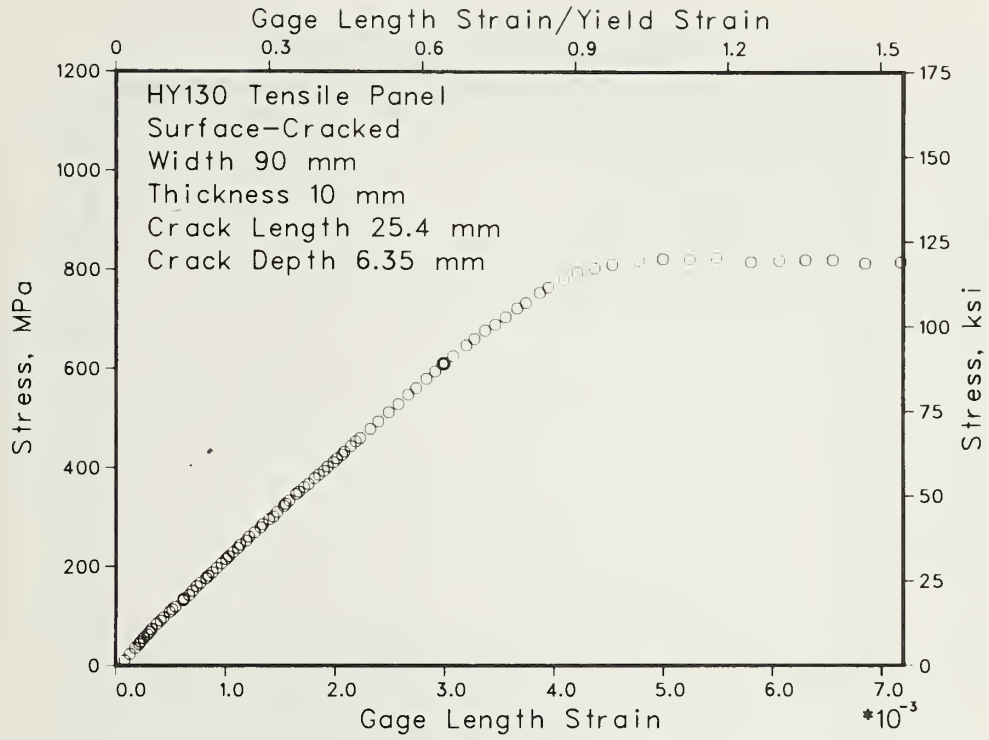


Figure 23e.

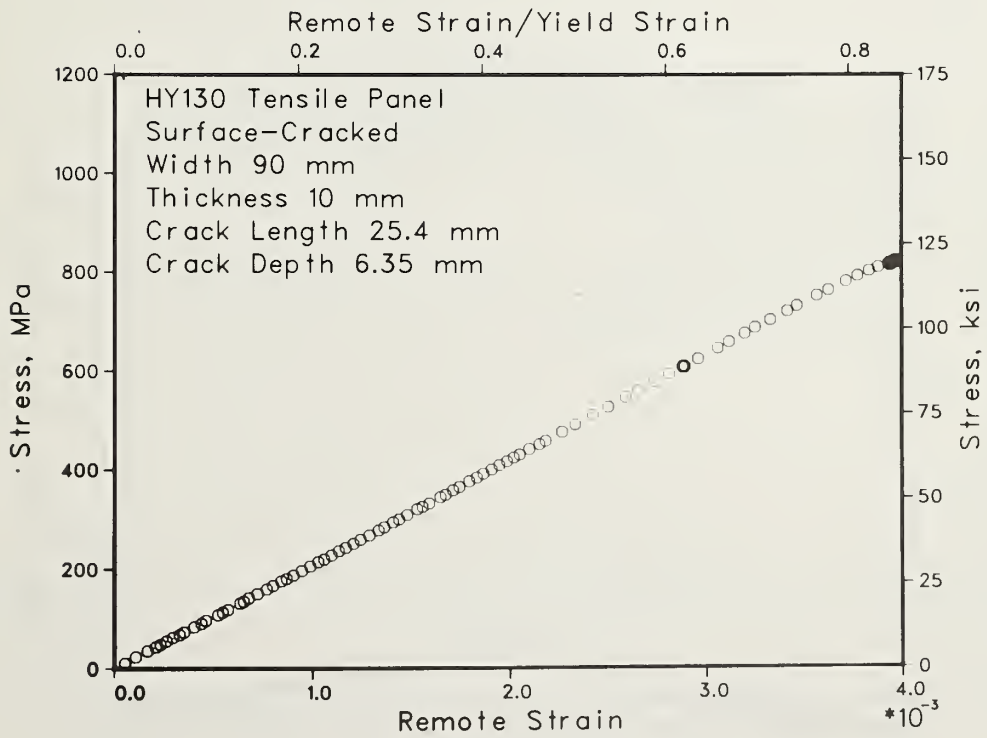


Figure 23f.

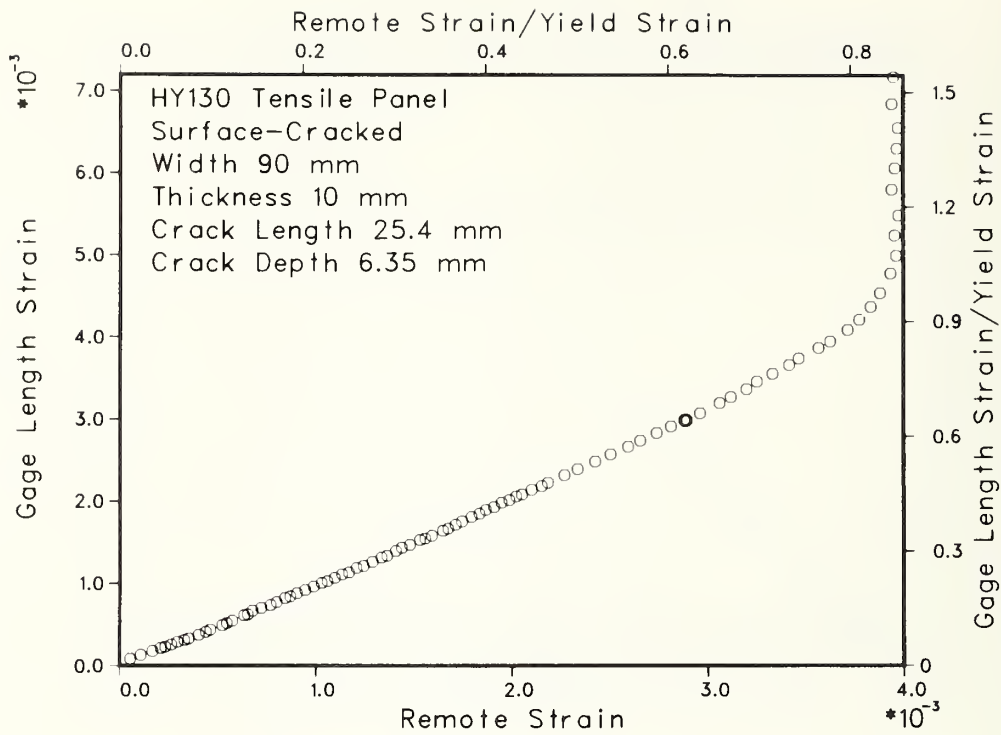


Figure 23g.

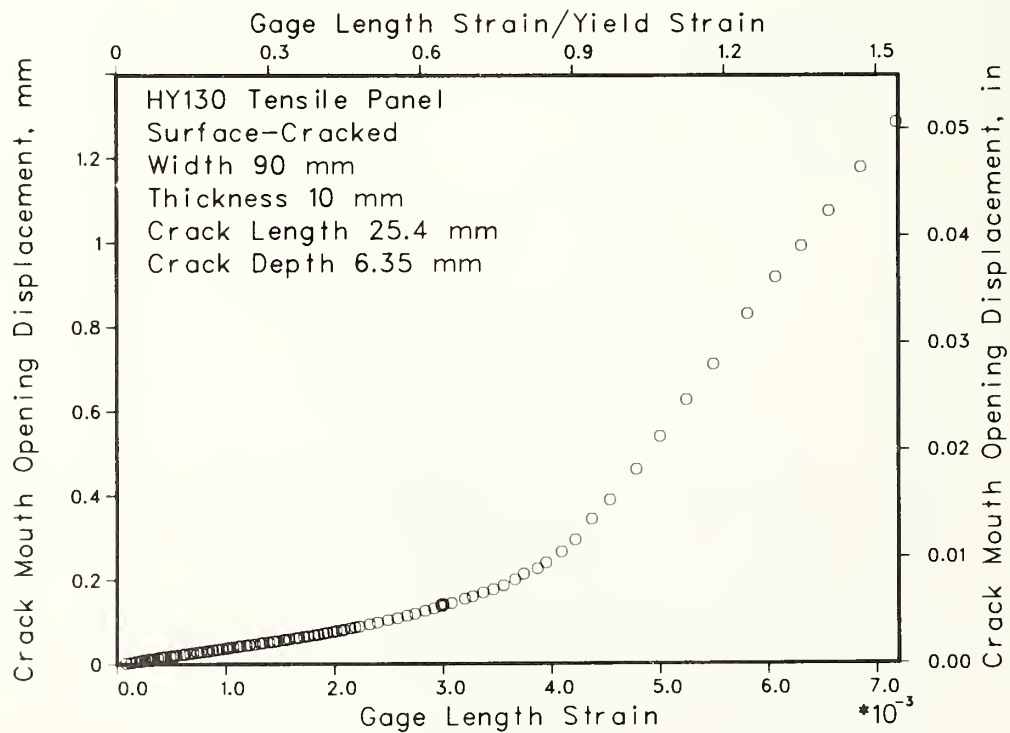


Figure 23h.

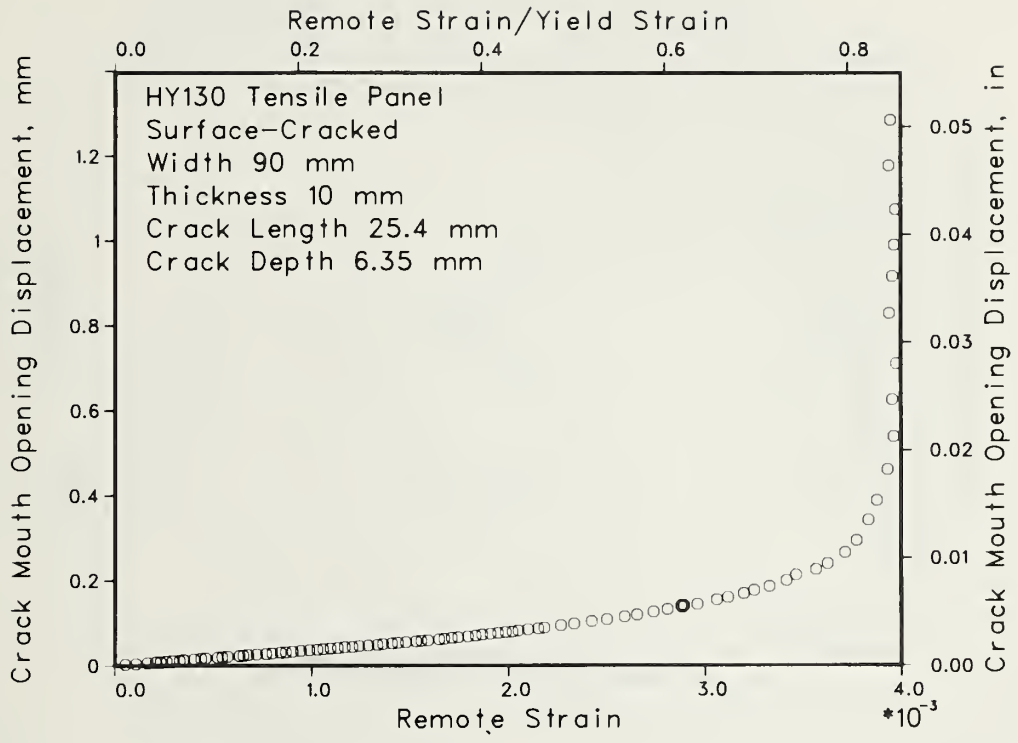


Figure 23i.

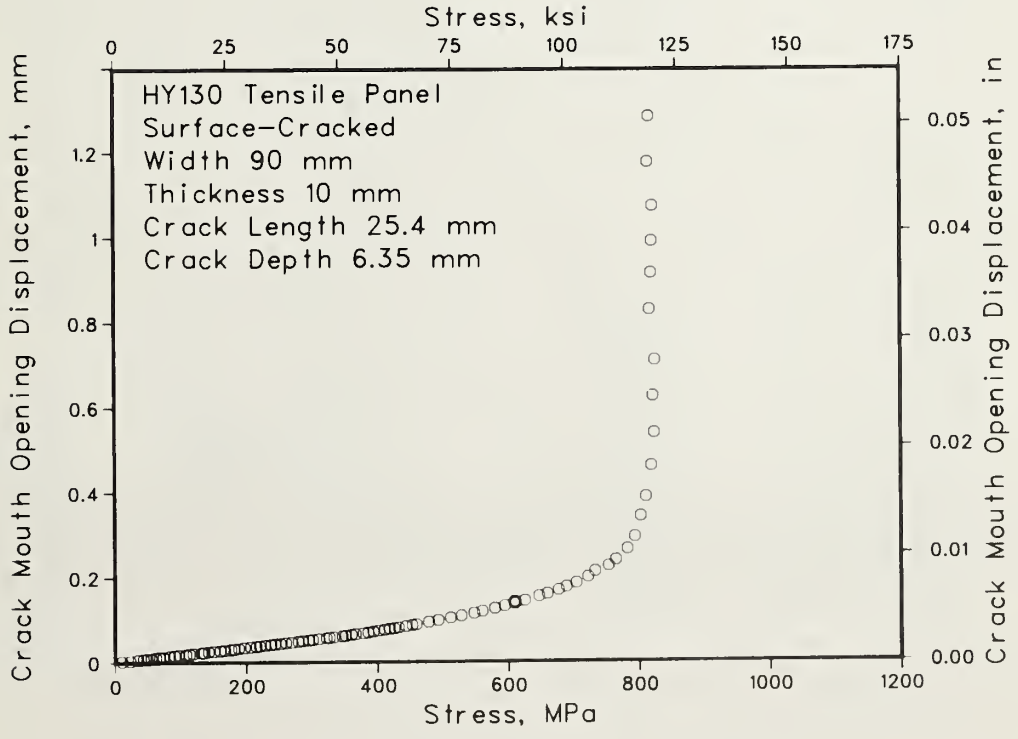


Figure 23j.

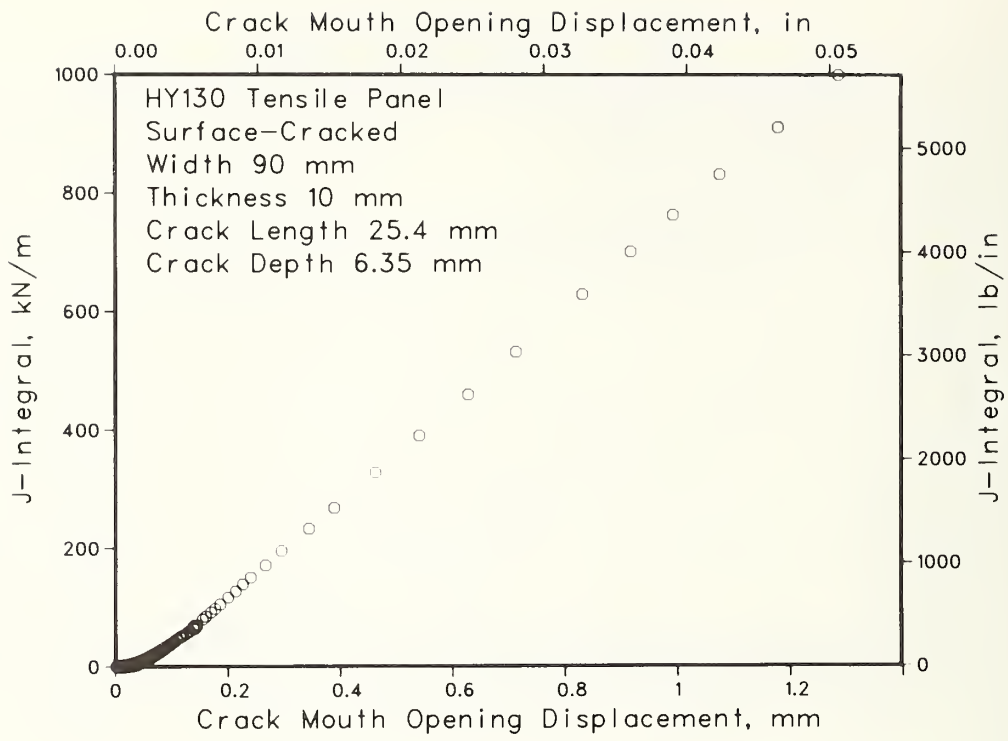
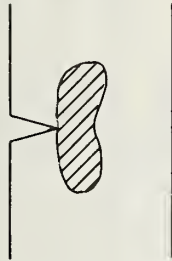


Figure 23k.

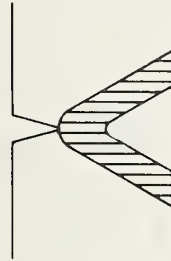
Yielding Patterns (no bending)

(shading indicates yielding)

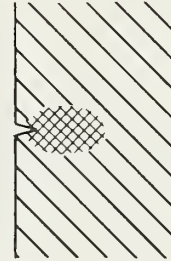
Through Cracks



Yielding Confined to Crack Tip Region



Net Section Yielding



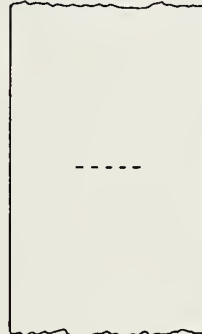
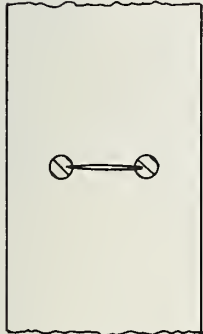
Gross Section Yielding

Surface Cracks

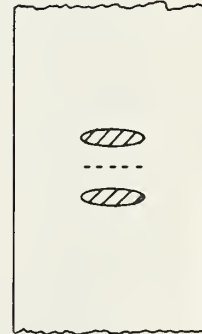
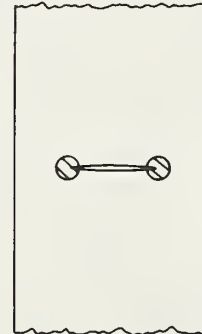
Side

Front

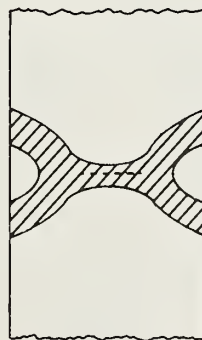
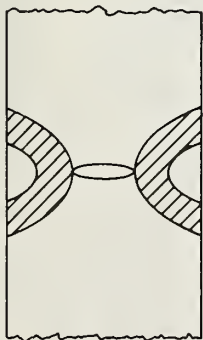
Back



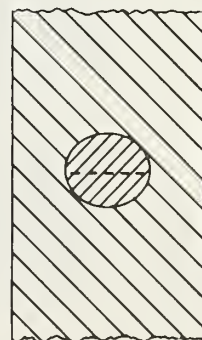
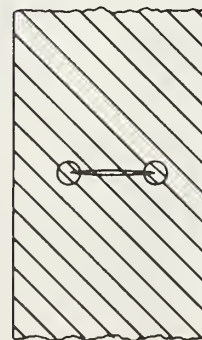
Confined Yielding



Ligament Yielding



Net Section Yielding



Gross Section Yielding

Figure 24. Yielding patterns for surface cracks compared to those for through cracks.

HY 130 Tensile Panel
 Width = 90 mm
 Thickness = 10 mm
 Crack Length = 10 mm
 Crack Depth = 1.7 mm

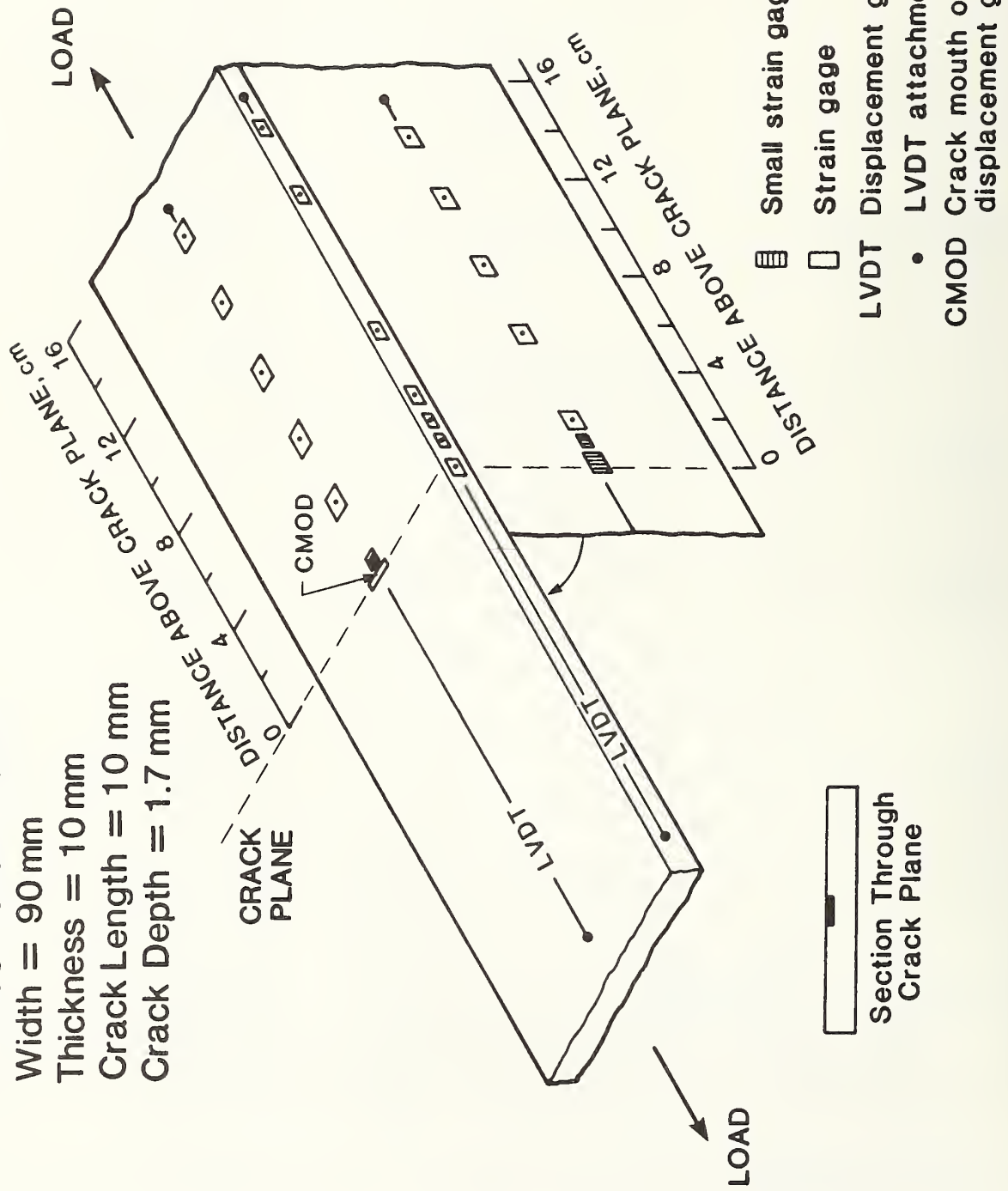
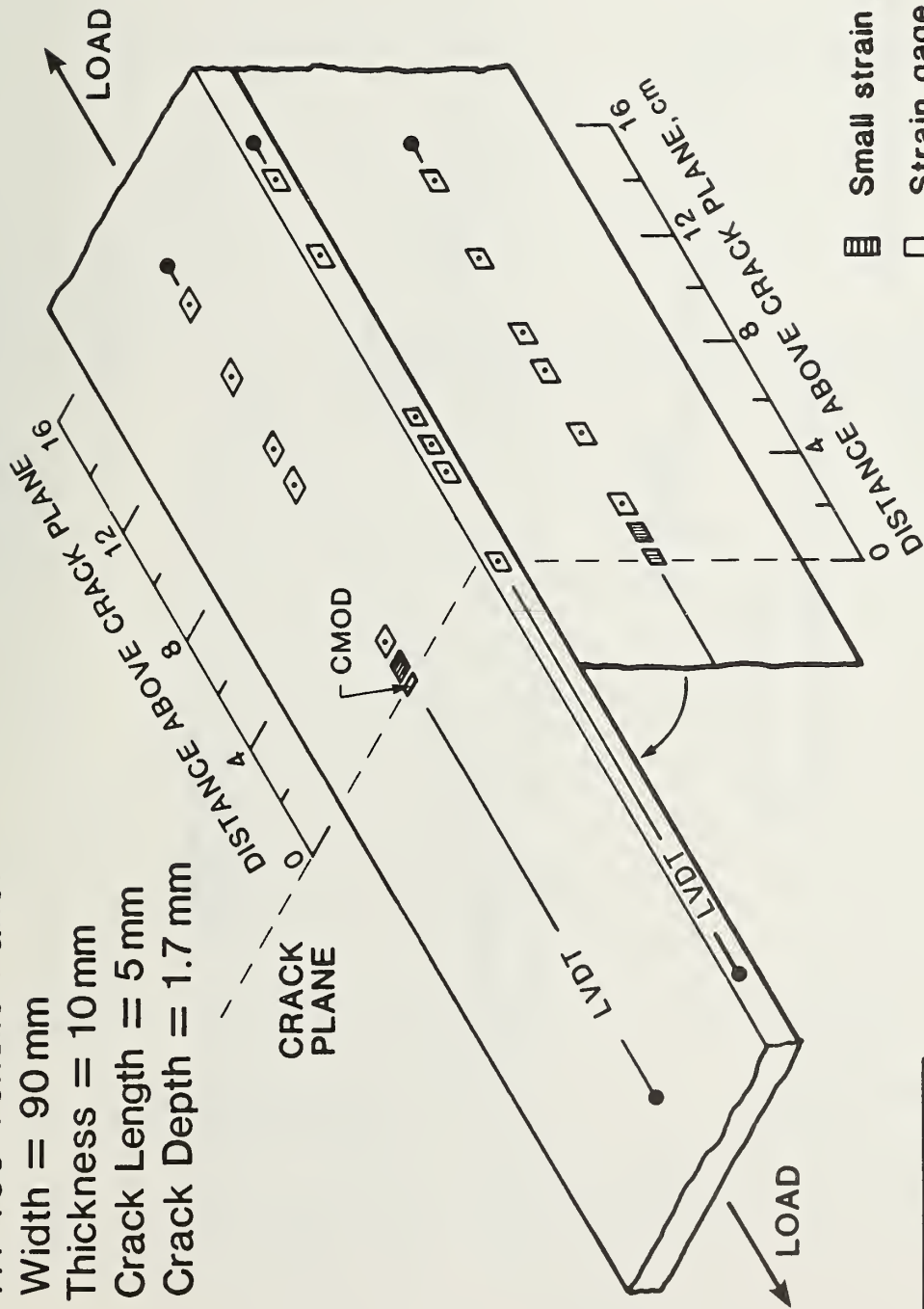


Figure 25. Instrumentation layout for surface-cracked HY130 base metal tensile panel, crack length 10 mm, crack depth 1.7 mm.

HY 130 Tensile Panel
 Width = 90 mm
 Thickness = 10 mm
 Crack Length = 5 mm
 Crack Depth = 1.7 mm



Section Through
 Crack Plane

-  Small strain gages (5)
-  Strain gage
-  LVDT Displacement gage
-  LVDT attachment point
-  CMOD Crack mouth opening displacement gage

Figure 26. Instrumentation layout for surface-cracked HY130 base metal tensile panel, crack length 5 mm, crack depth 1.7 mm.

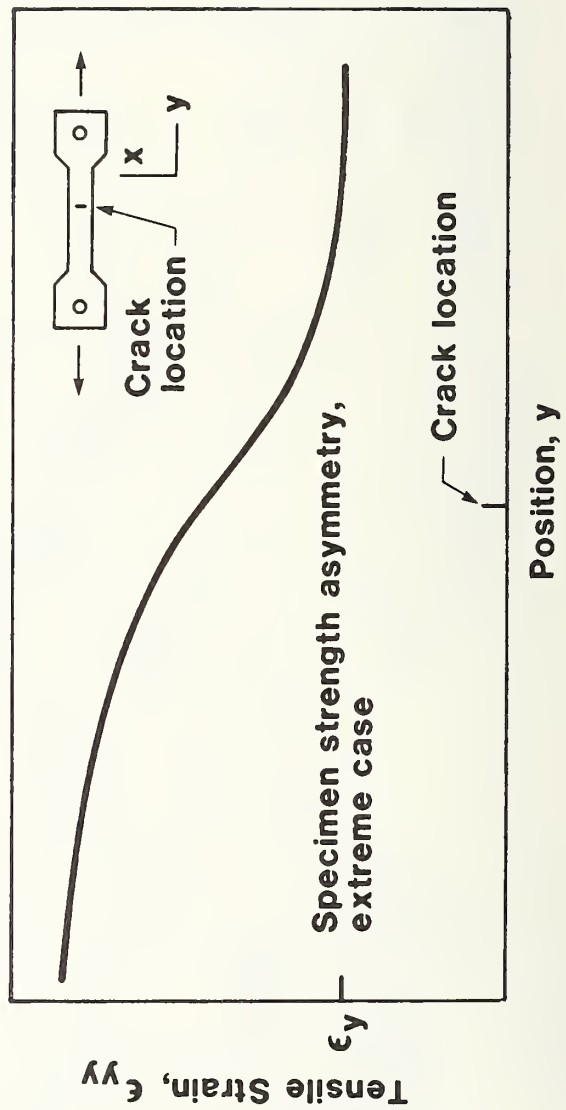
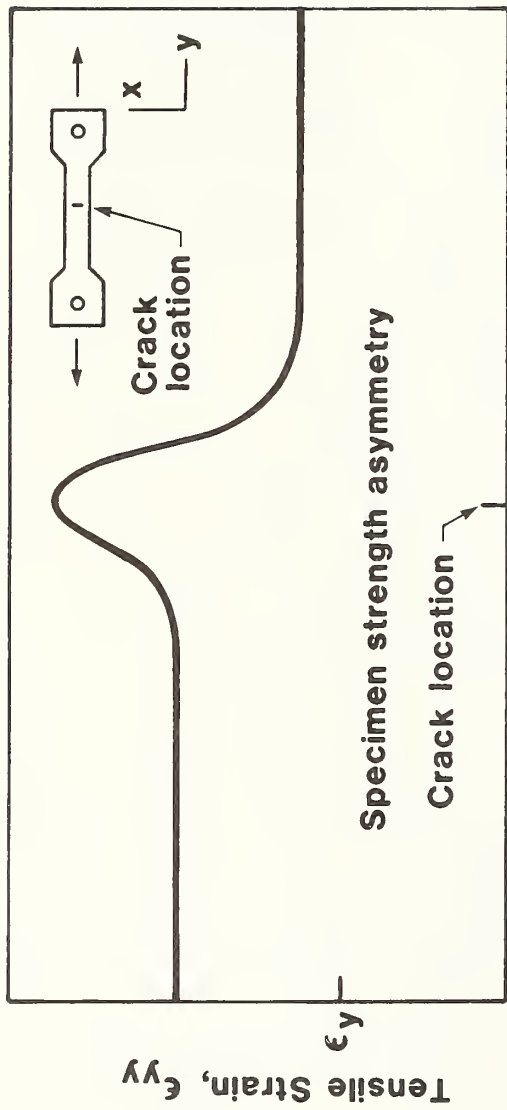
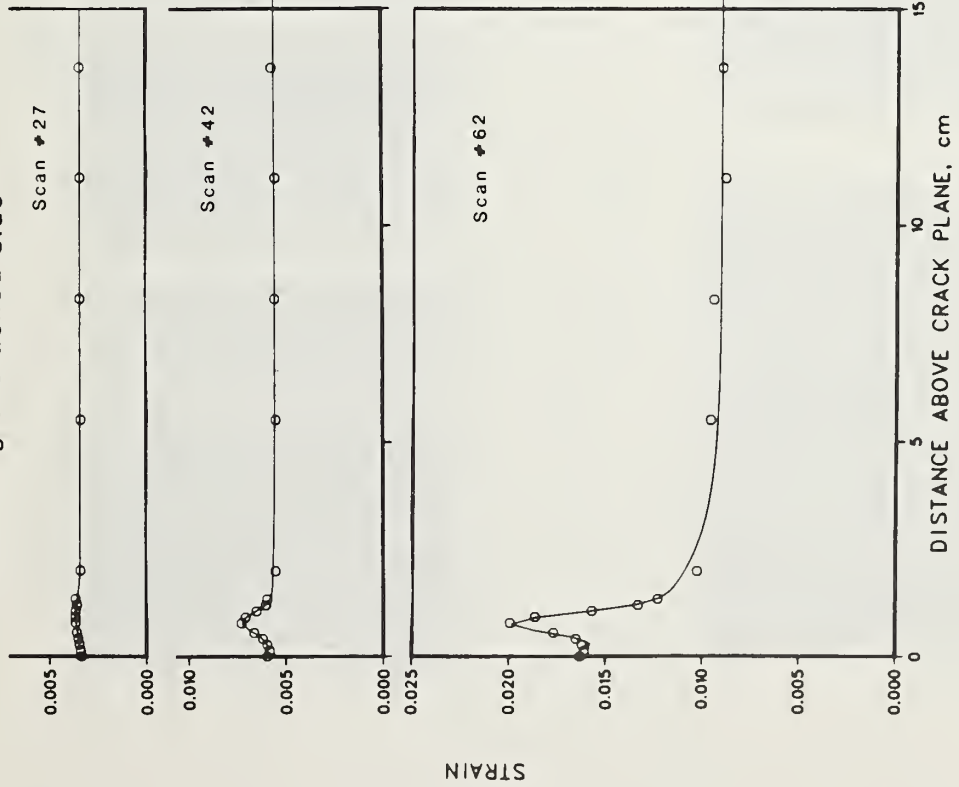


Figure 27. Strain asymmetry produced by strength asymmetry of surface-cracked base-metal tensile panels.

HY 130 Tensile Panel Surface-Cracked
 Crack Depth 1.7mm Crack Length 10mm

Strain along Uncracked Side



Scan Number	27	42	62
Gage Length Strain	0.0034	0.0056	0.0099
Remote Strain	0.0034	0.0055	0.0091
J-Integral (kN/m) [*]	10	32	104

^{*} 1 kN/m = 5.71 lb/in

Strain along Cracked Side

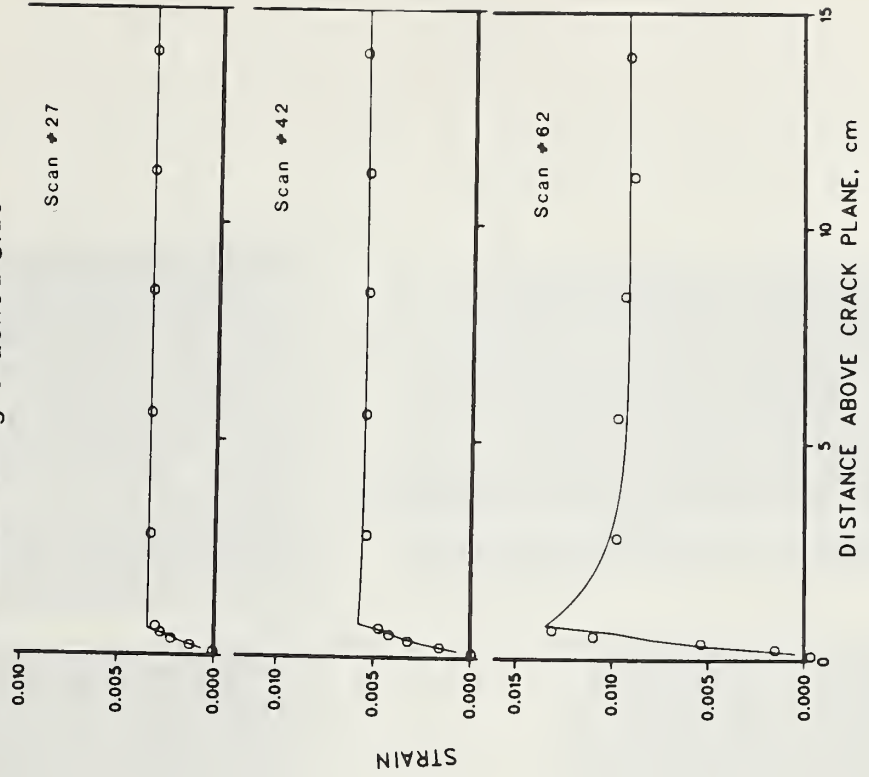


Figure 28. Strain gage strains plotted against position for surface cracked HY130 base metal tensile panel with crack length 10 mm and crack depth 1.7 mm.

HY130 Tensile Panel Surface-Cracked Width 90 mm
 Thickness 10 mm Crack Length 10 mm Crack Depth 1.7 mm



Scan #27



Scan #42



Scan #62



Scan #27



Scan #42



Scan #62

Figure 29. Strain pattern as revealed by photoelastic coating on surface-cracked HY130 base metal tensile panel with crack length 10 mm and crack depth 1.7 mm.

HY 130 Tensile Panel Surface-Cracked Specimen Width 90mm Crack Depth 1.7mm Crack Length 5mm

Scan Number	35	52	59
Remote Strain	0.0041	0.0047	0.0049
J-Integral(kN/m) [#]	21	47	57

[#] 1 kN/m = 5.71 lb/in

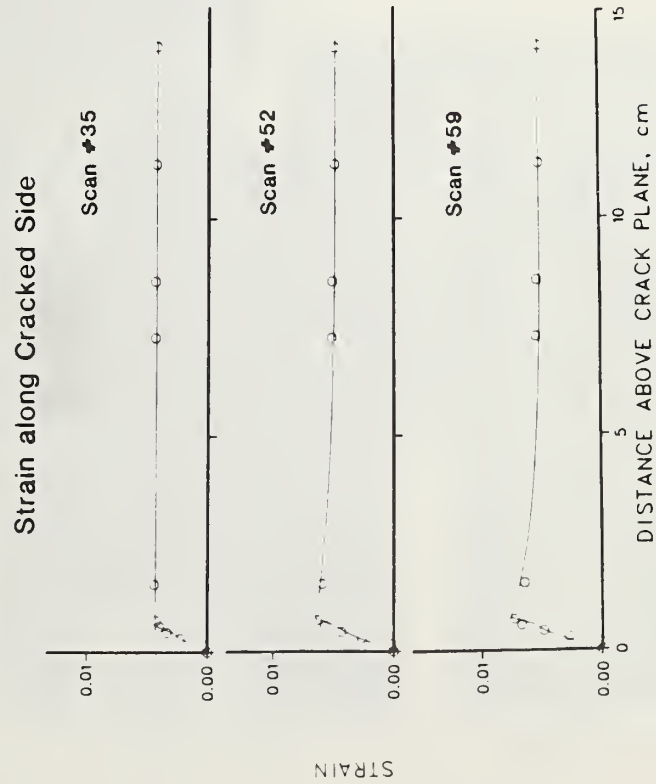
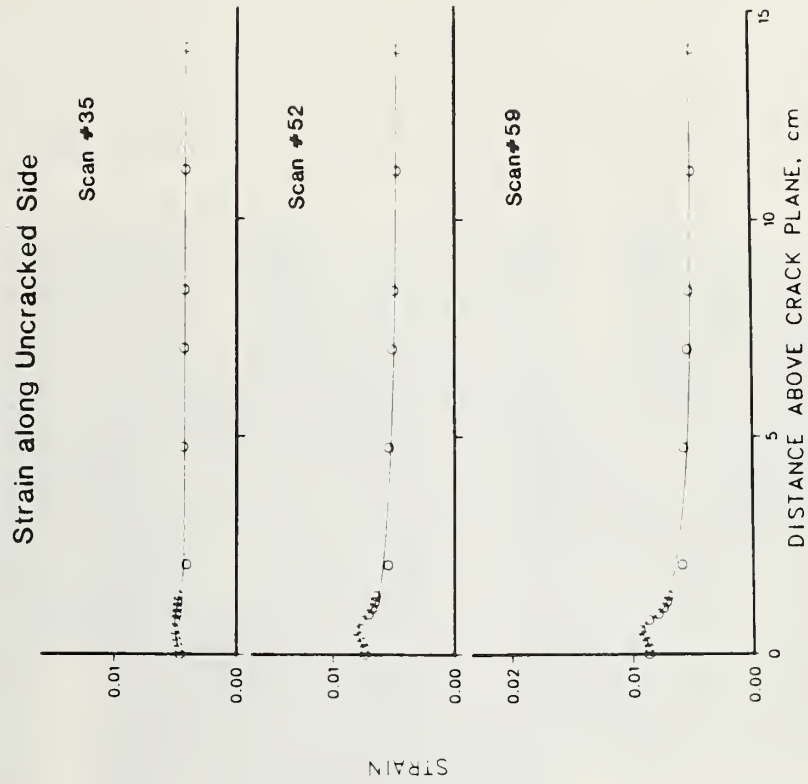


Figure 30. Strain gage strains plotted against position for surface cracked HY130 base metal tensile panel with crack length 5 mm and crack depth 1.7 mm.

HY130 Welded Tensile Panel Surface-Cracked
Width 90 mm Thickness 10 mm
Crack Length 5mm Crack Depth 1.7 mm



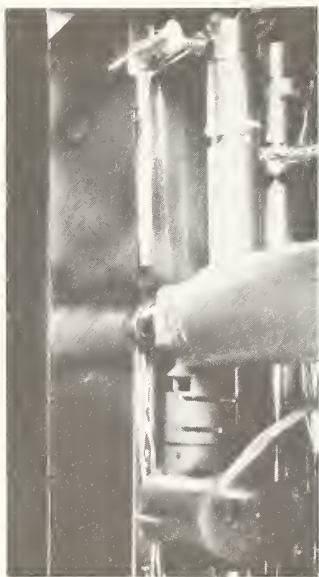
Scan #29



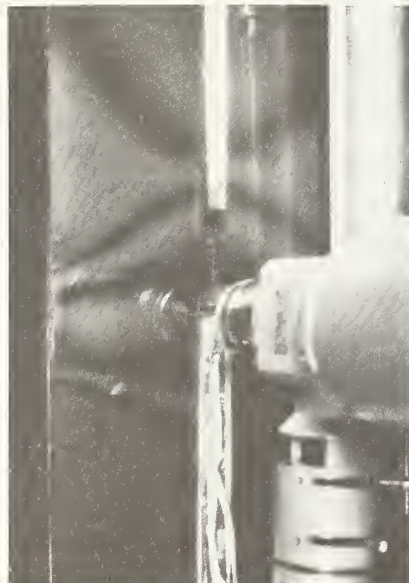
Scan #33



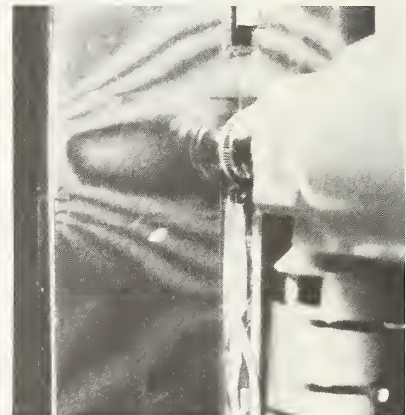
Scan #40



Scan #48

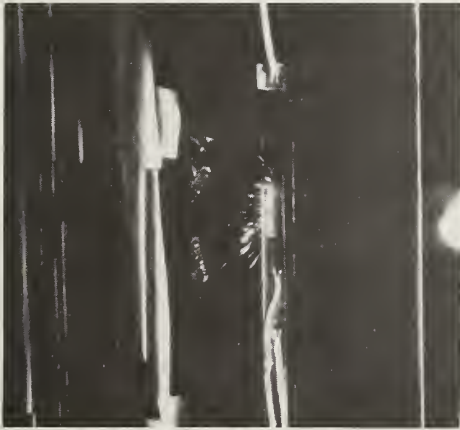


Scan #61



Scan #77

Figure 31. Strain pattern as revealed by photoelastic coating on surface-cracked HY130 base metal tensile panel with crack length 5 mm and crack depth 1.7 mm.



Scan #29



Scan #33



Scan #40



Scan #48



Scan #61



Scan #77

Figure 31, continued.

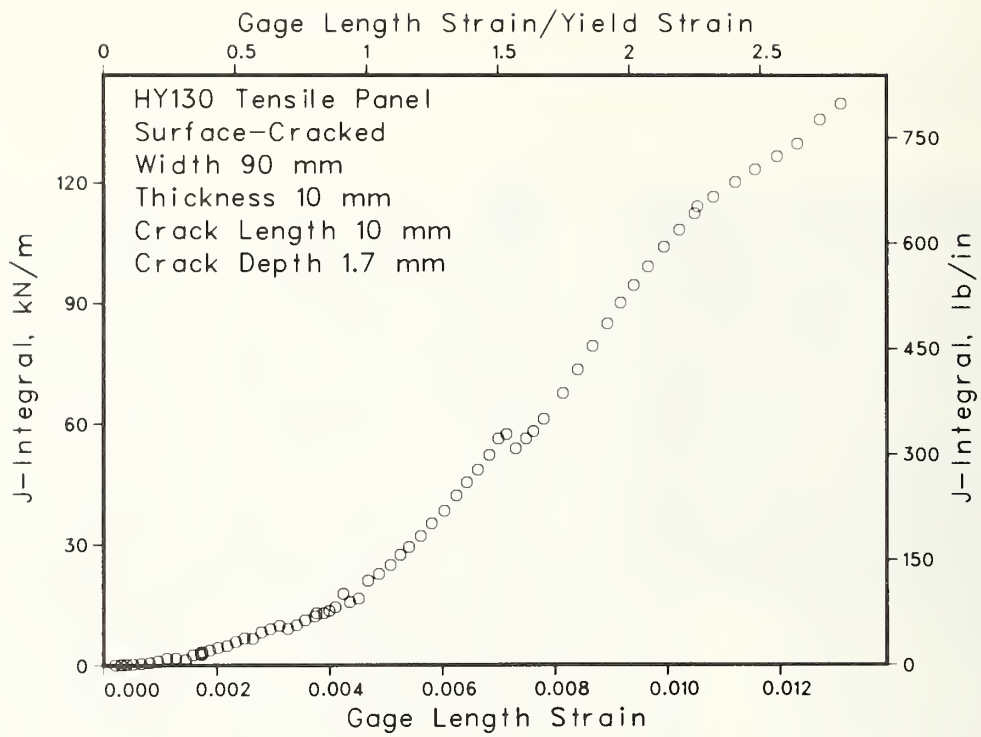


Figure 32a.

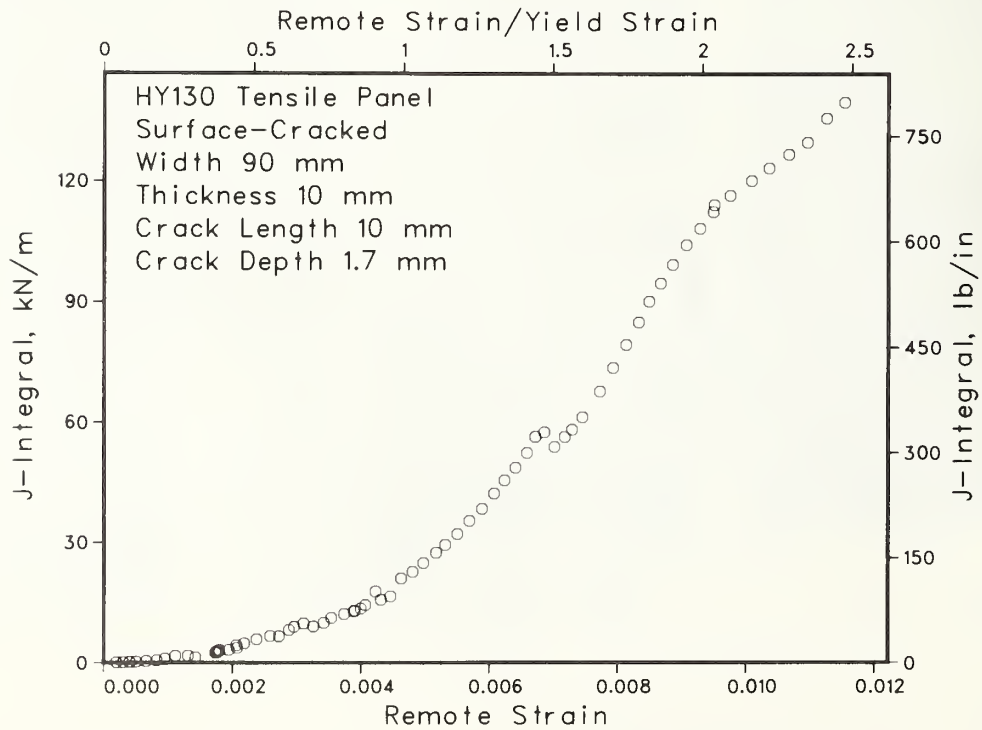


Figure 32b.

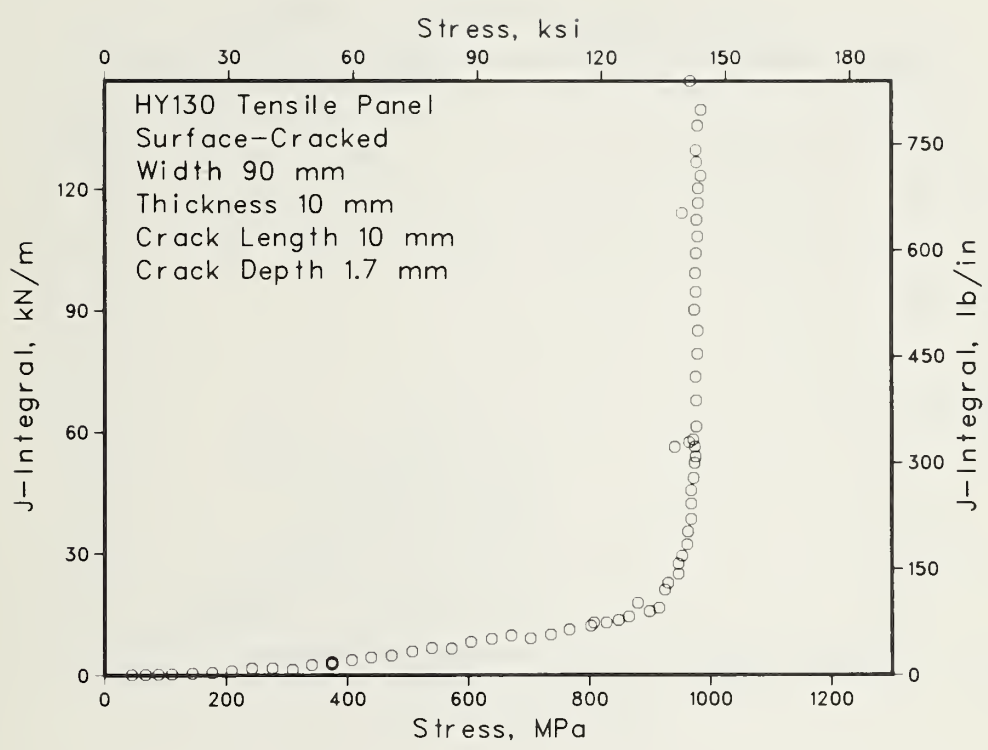


Figure 32c.

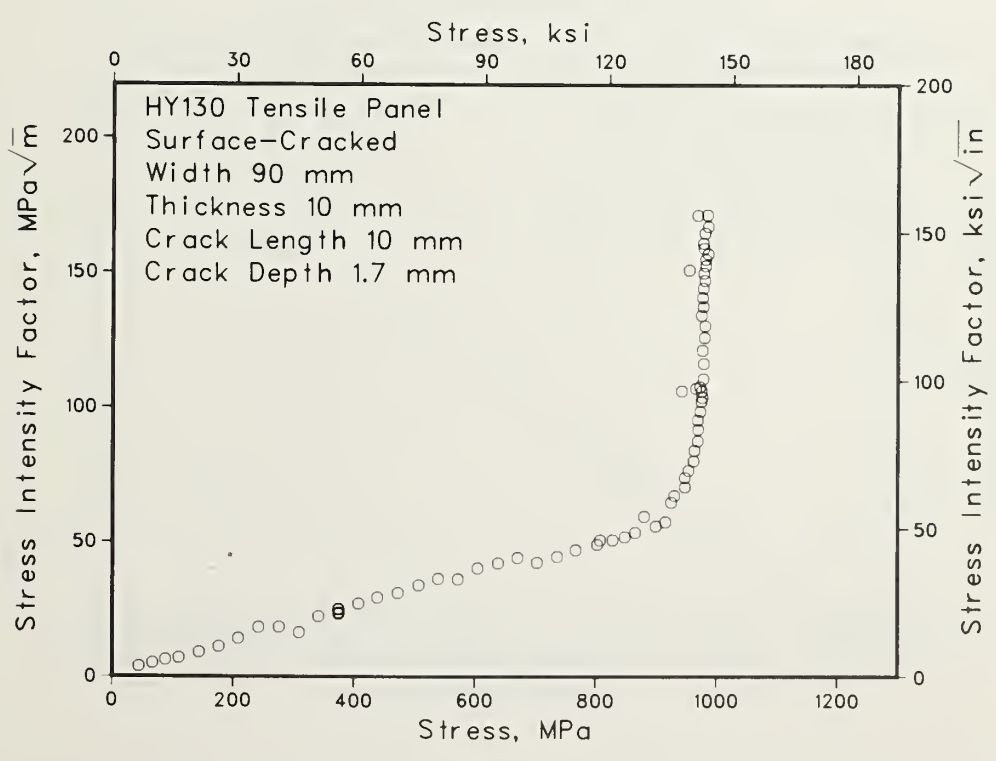


Figure 32d.

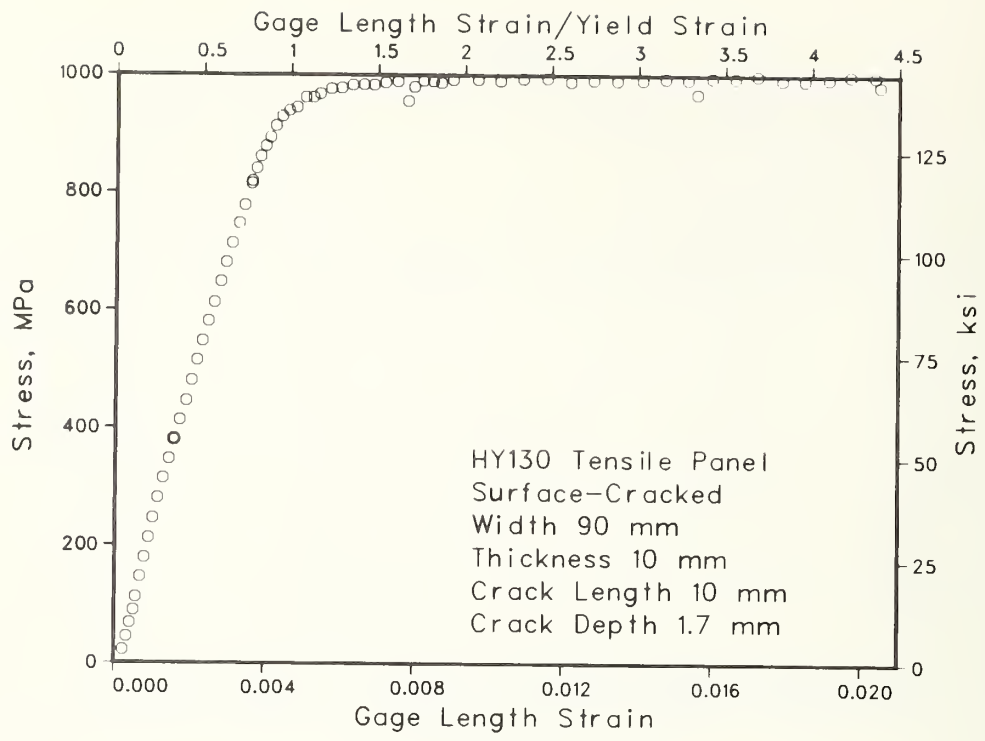


Figure 32e.

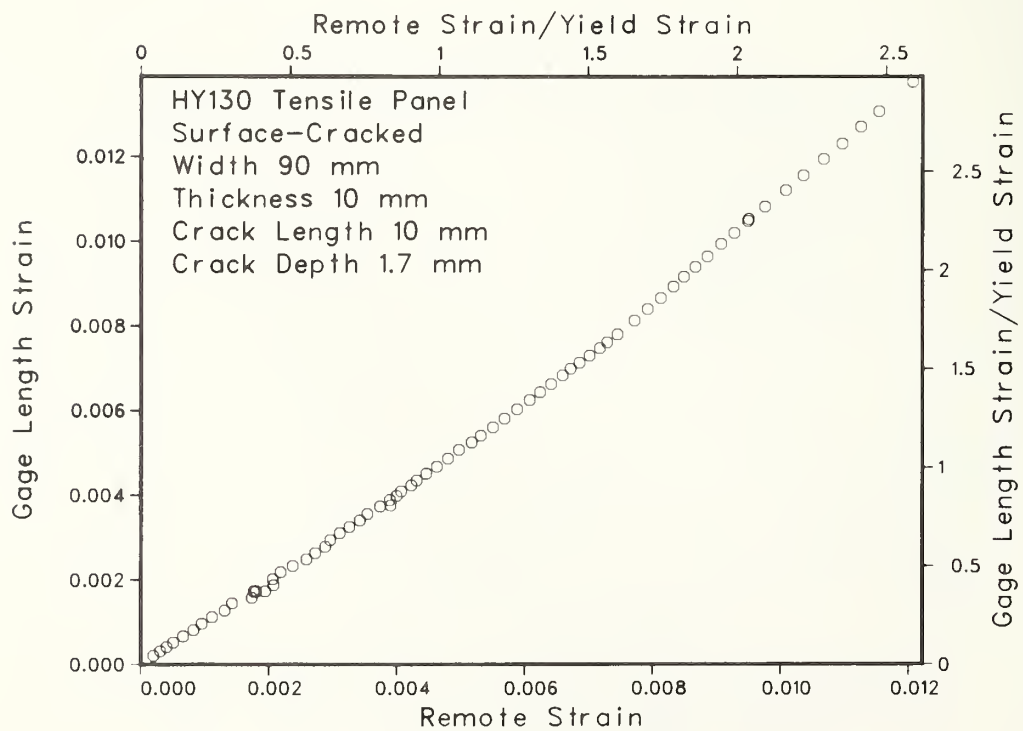


Figure 32f.

Figure 33a-b. Full-length-result plots showing the dependence of crack mouth opening displacement on strain for surface-cracked HY130 base metal tensile panel with crack length 10 mm and crack depth 1.7 mm.

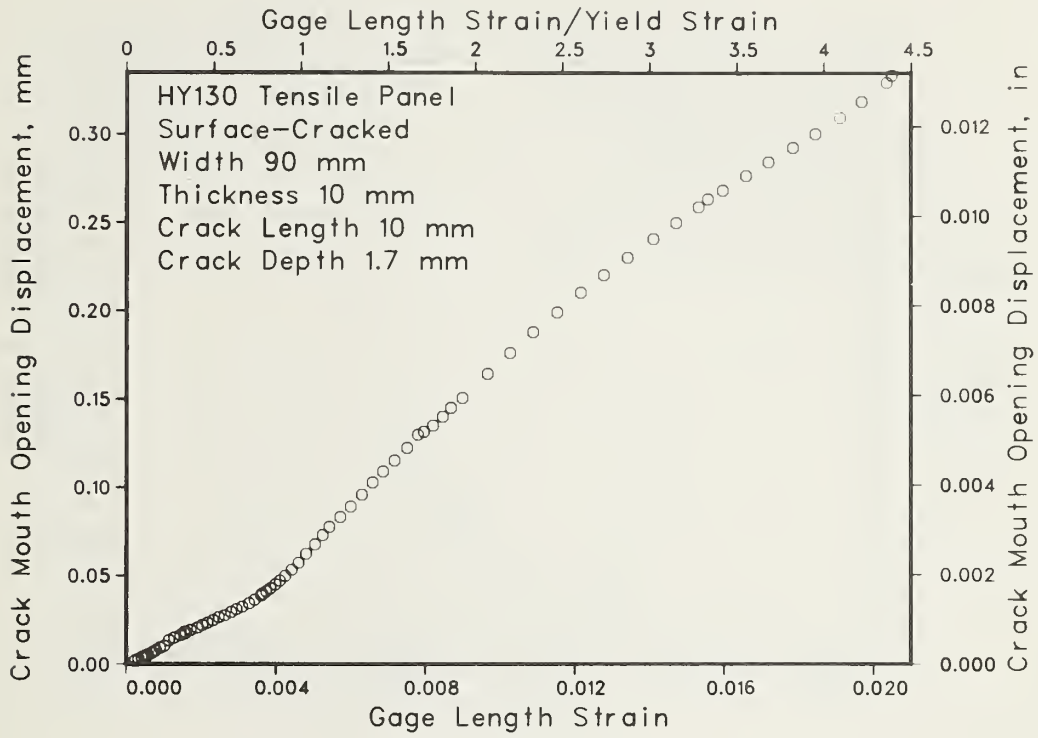


Figure 33a.

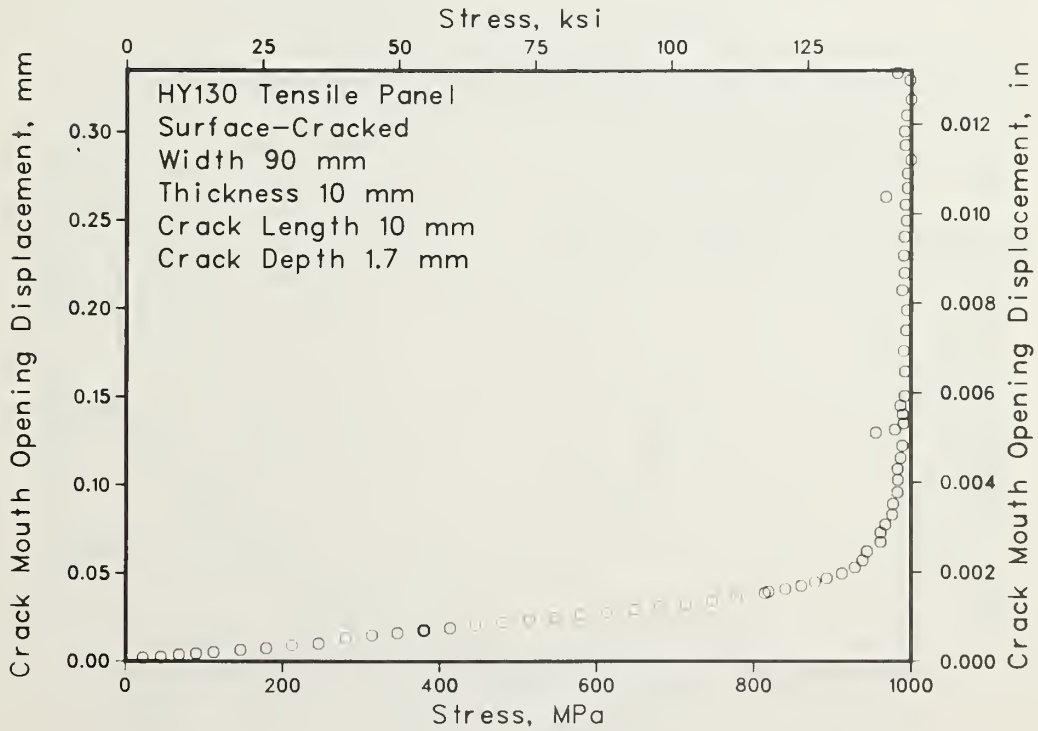


Figure 33b.

Figure 34a-f. Half-length-result plots showing the dependence of J-integral on strain for surface-cracked HY130 base metal tensile panel with crack length 5 mm and crack depth 1.7 mm.

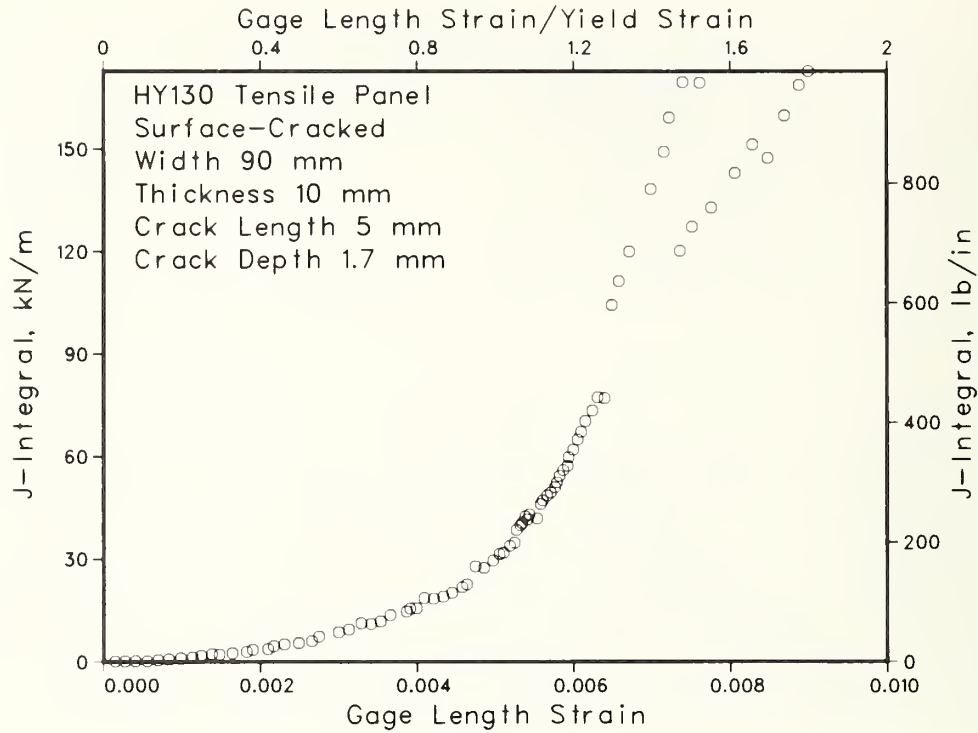


Figure 34a.

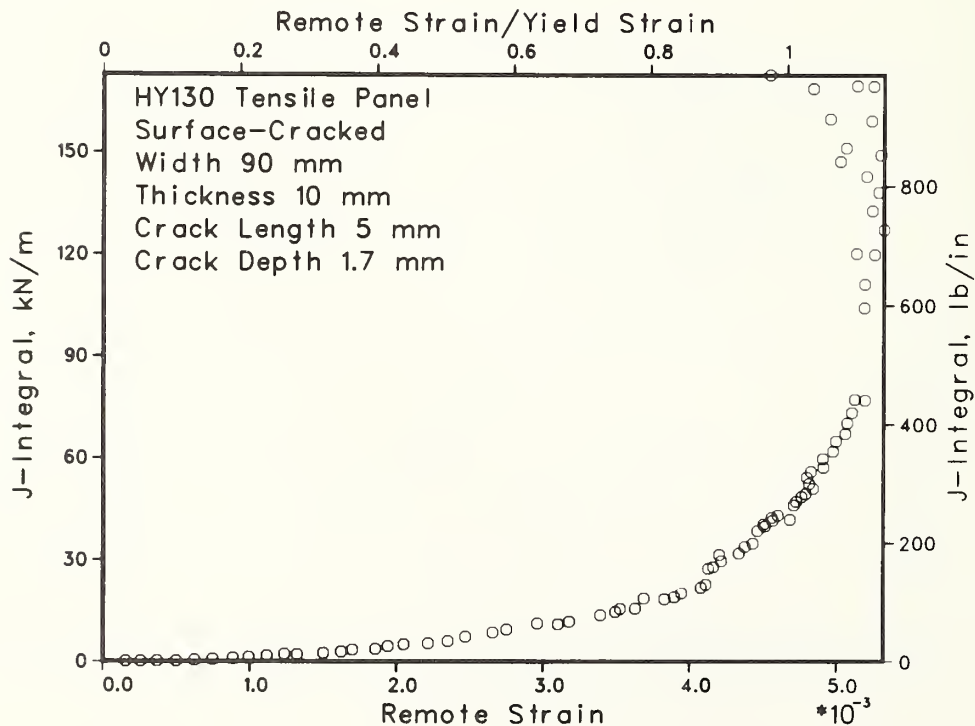


Figure 34b.

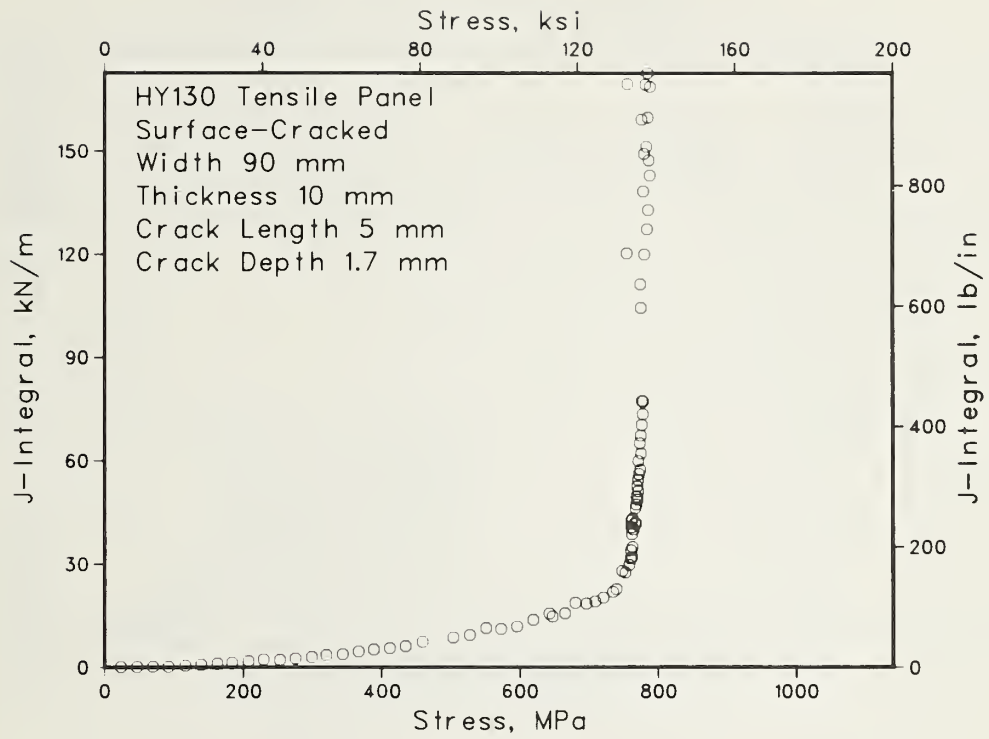


Figure 34c.

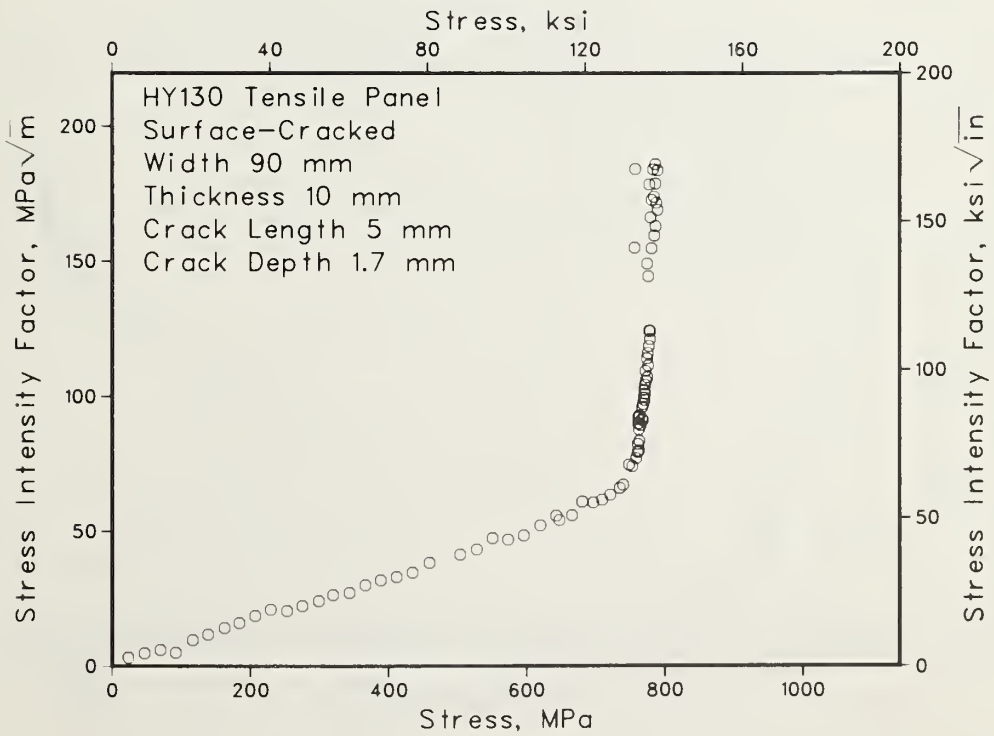


Figure 34d.

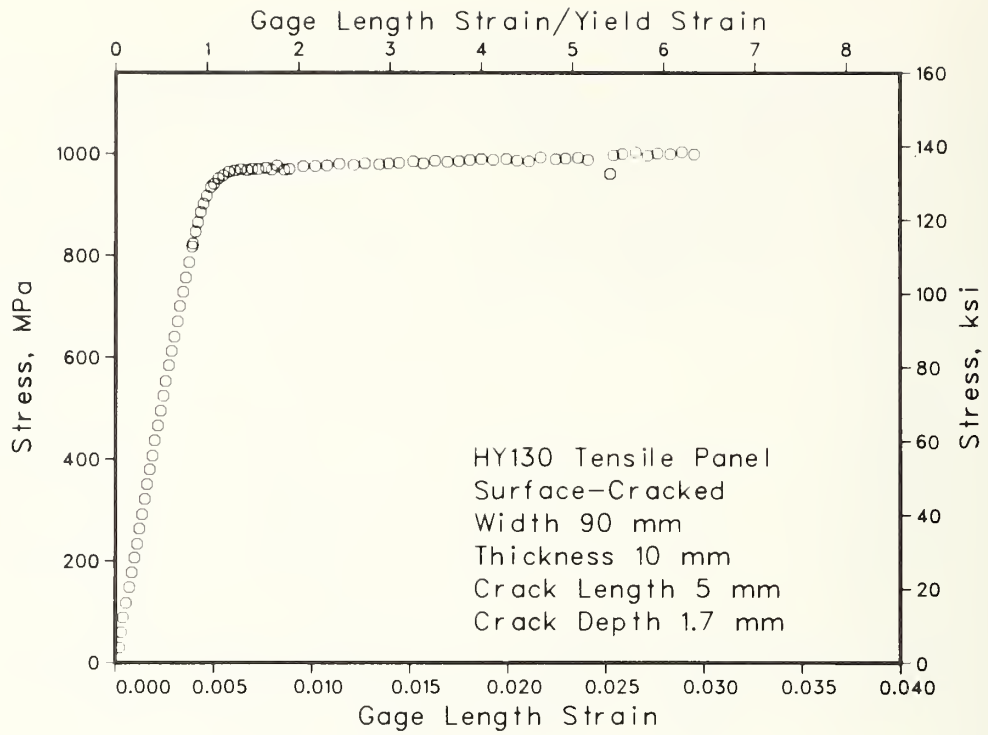


Figure 34e.

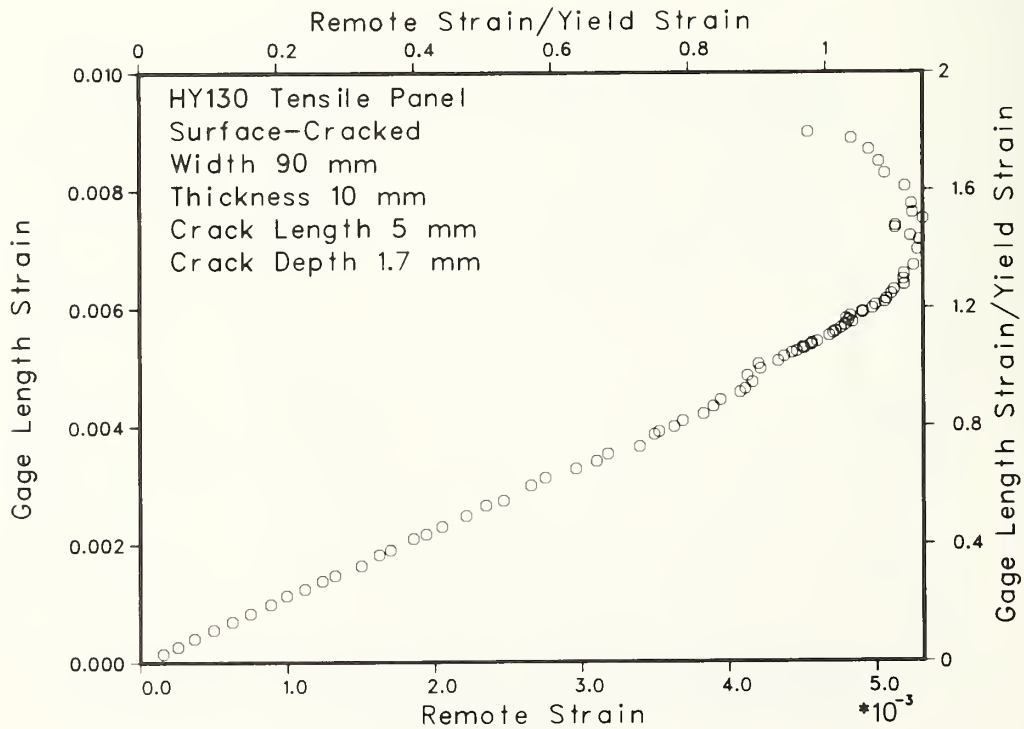


Figure 34f.

Figure 35a-b. Full-length-result plots showing the dependence of crack mouth opening displacement on strain for surface-cracked HY130 base metal tensile panel with crack length 5 mm and crack depth 1.7 mm.

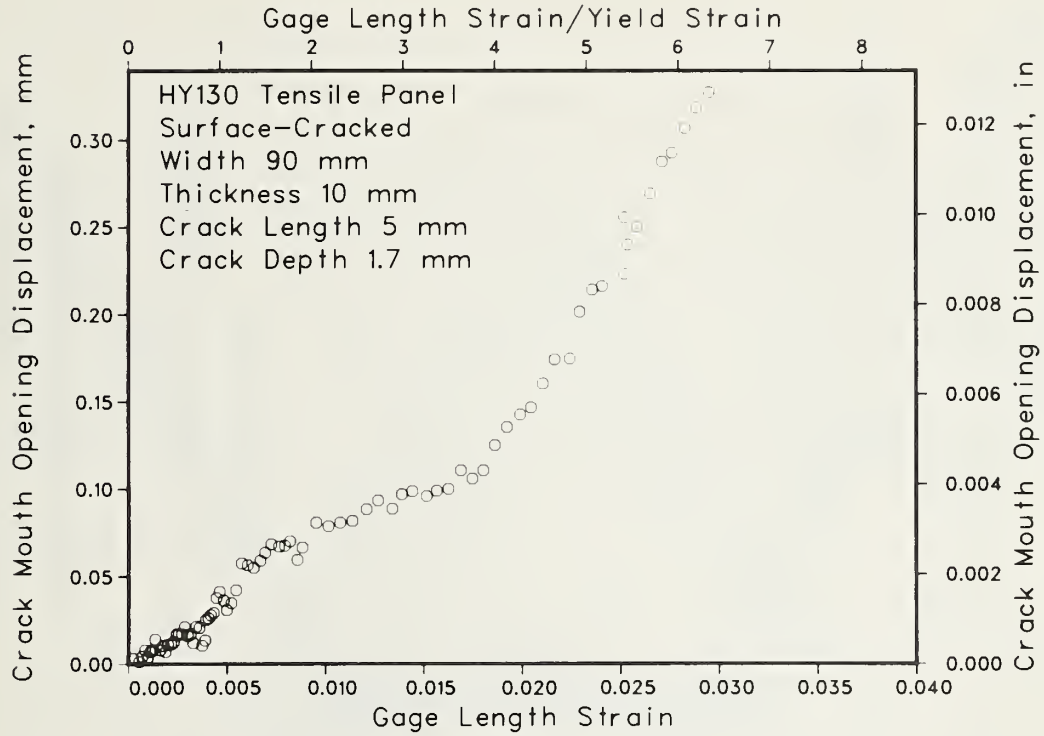


Figure 35a.

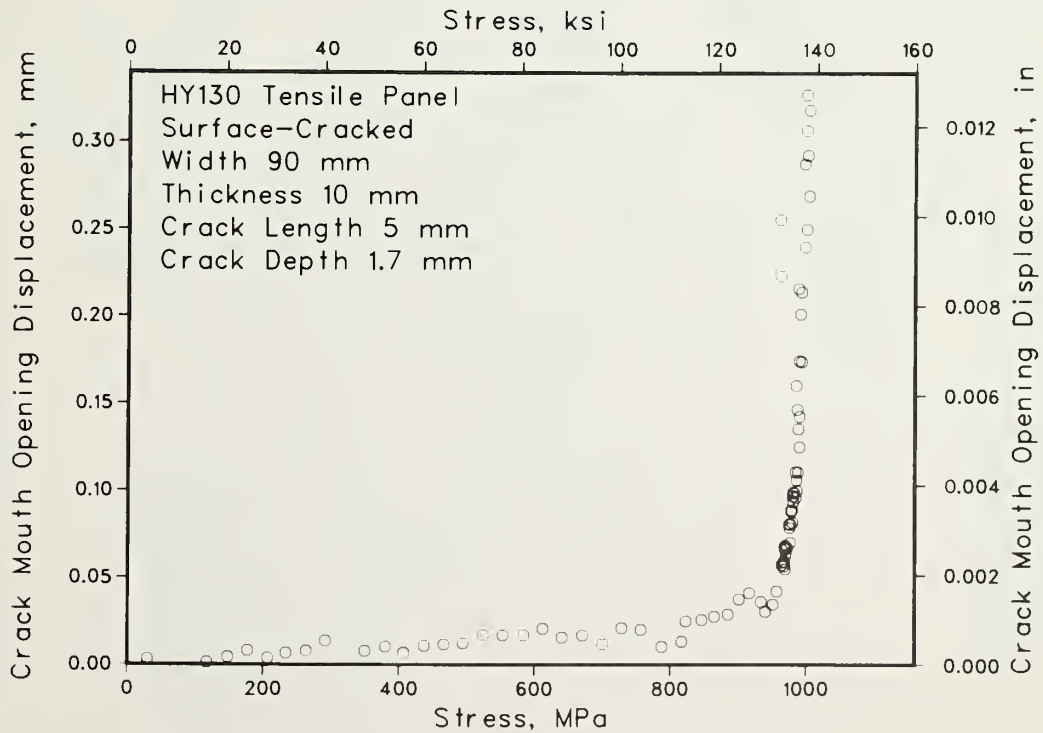


Figure 35b.

HY 130 Welded Tensile Panel

Width = 254 mm

Thickness = 20 mm

Crack Depth = 2.5 mm

Crack Length = 30 mm

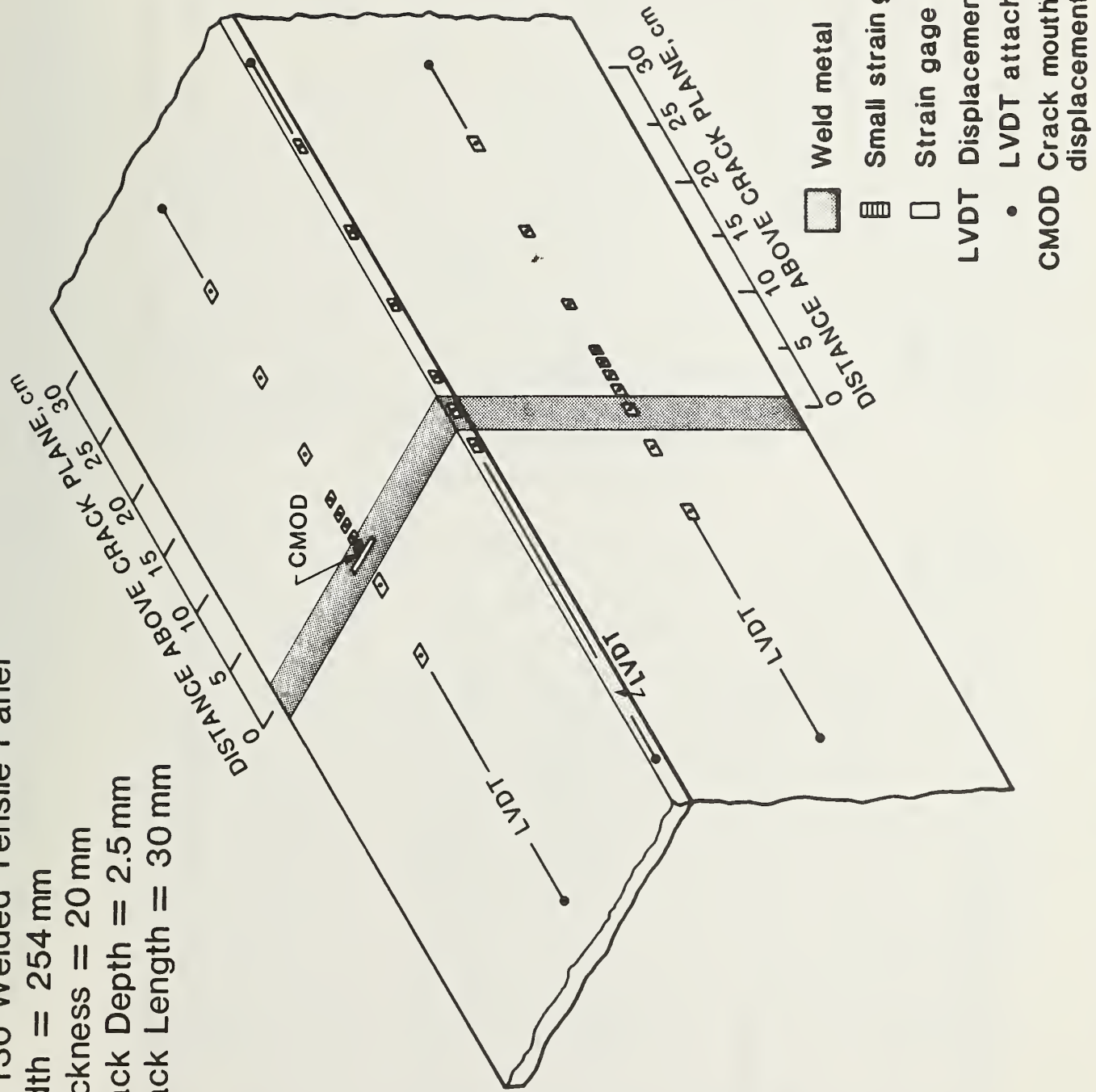


Figure 37. Instrumentation layout for transverse-welded surface-cracked HY130 tensile panel with crack length 30 mm and crack depth 2.5 mm.

HY 130 Welded Tensile Panel Surface-Cracked Width 90 mm
 Thickness 10 mm Crack Length 5 mm Crack Depth 1.7 mm

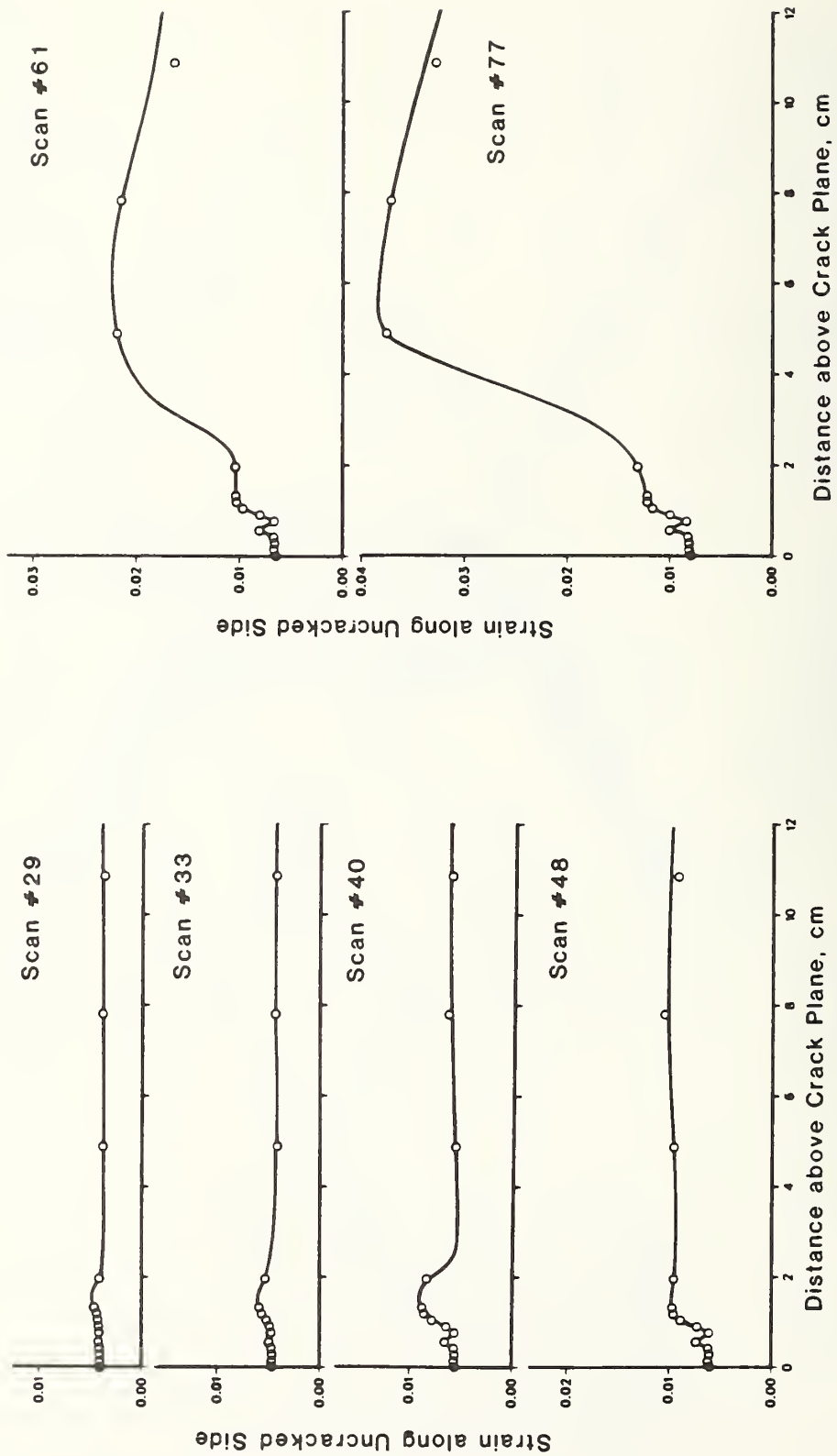


Figure 38. Strain gage strains for transverse-welded surface-cracked HY130 tensile panel with crack length 5 mm and crack depth 1.7 mm.

Scan #	29	33	40	48	61	77
Gage Length Strain	0.0043	0.0049	0.0070	0.0101	0.0178	0.0309
Remote Strain	0.0038	0.0043	0.0062	0.0102	0.0216	0.0370
J-Integral, kN/m *	19	25	36	43	49	69

* 1 kN/m = 5.71 lb/in

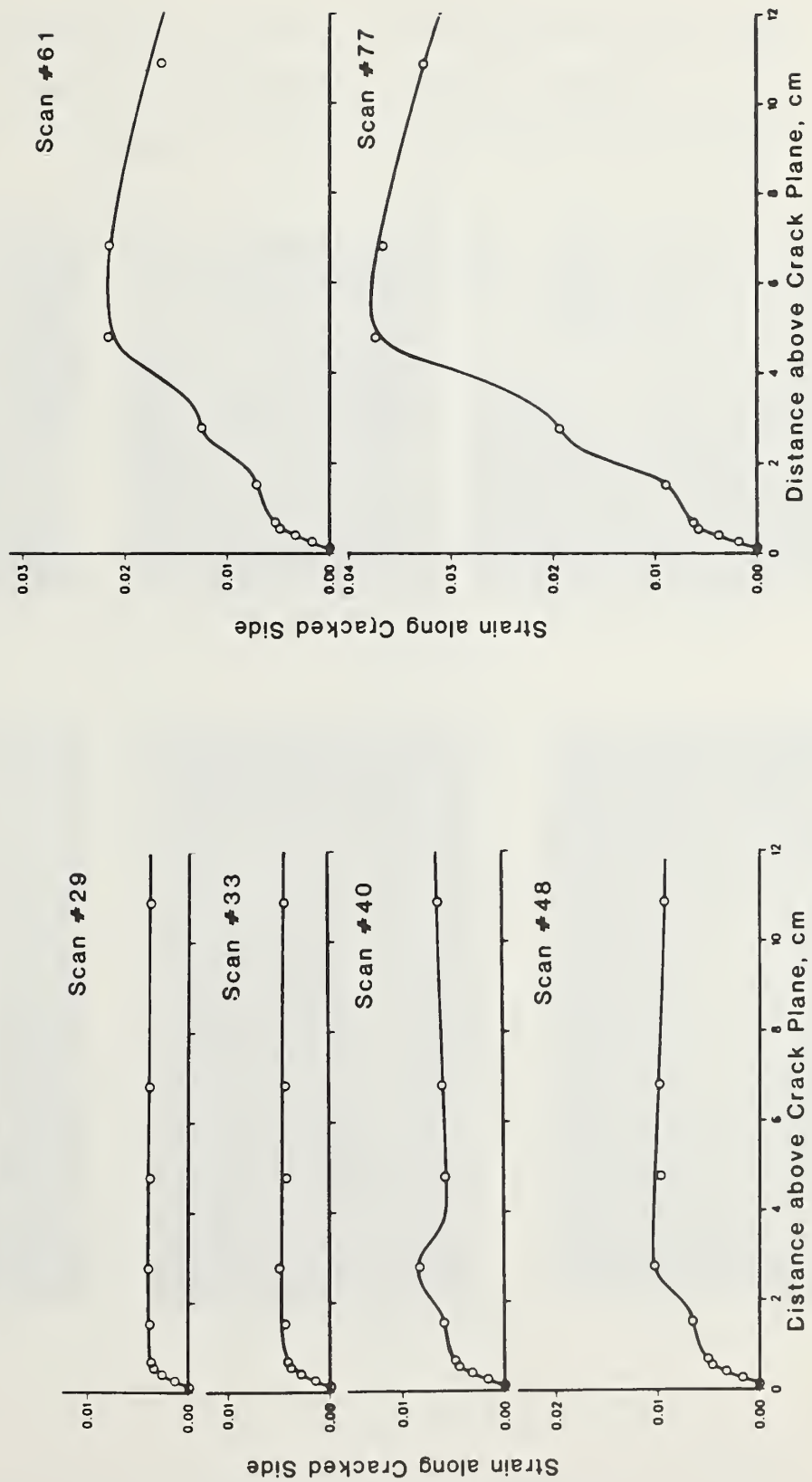
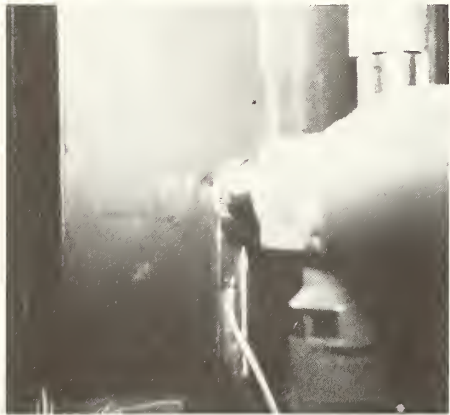


Figure 38, continued.

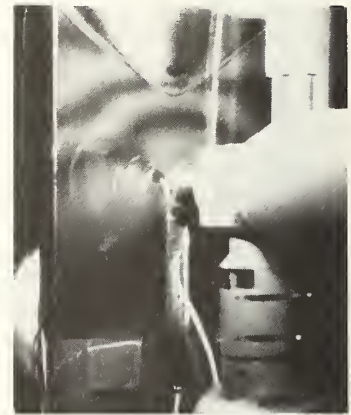
HY 130 Tensile Panel Surface-Cracked
Width 90 mm Thickness 10 mm
Crack Length 5 mm Crack Depth 1.7 mm



Scan #35



Scan #52



Scan #59



Scan #35



Scan #52



Scan #59

Figure 39. Strain pattern as revealed by photoelastic coating on transverse-welded surface-cracked HY130 tensile panel with crack length 5 mm and crack depth 1.7 mm.

HY130 Welded Tensile Panel Surface-Cracked Width 254 mm
 Thickness 20 mm Crack Length 30 mm Crack Depth 2.5 mm

Scan #	Gage Length Strain	Remote Strain	J-Integral, kN/m *
25	0.0038	0.0038	40
32	0.0052	0.0050	65
49	0.0114	0.0133	105

* 1 kN/m = 5.71 lb/in

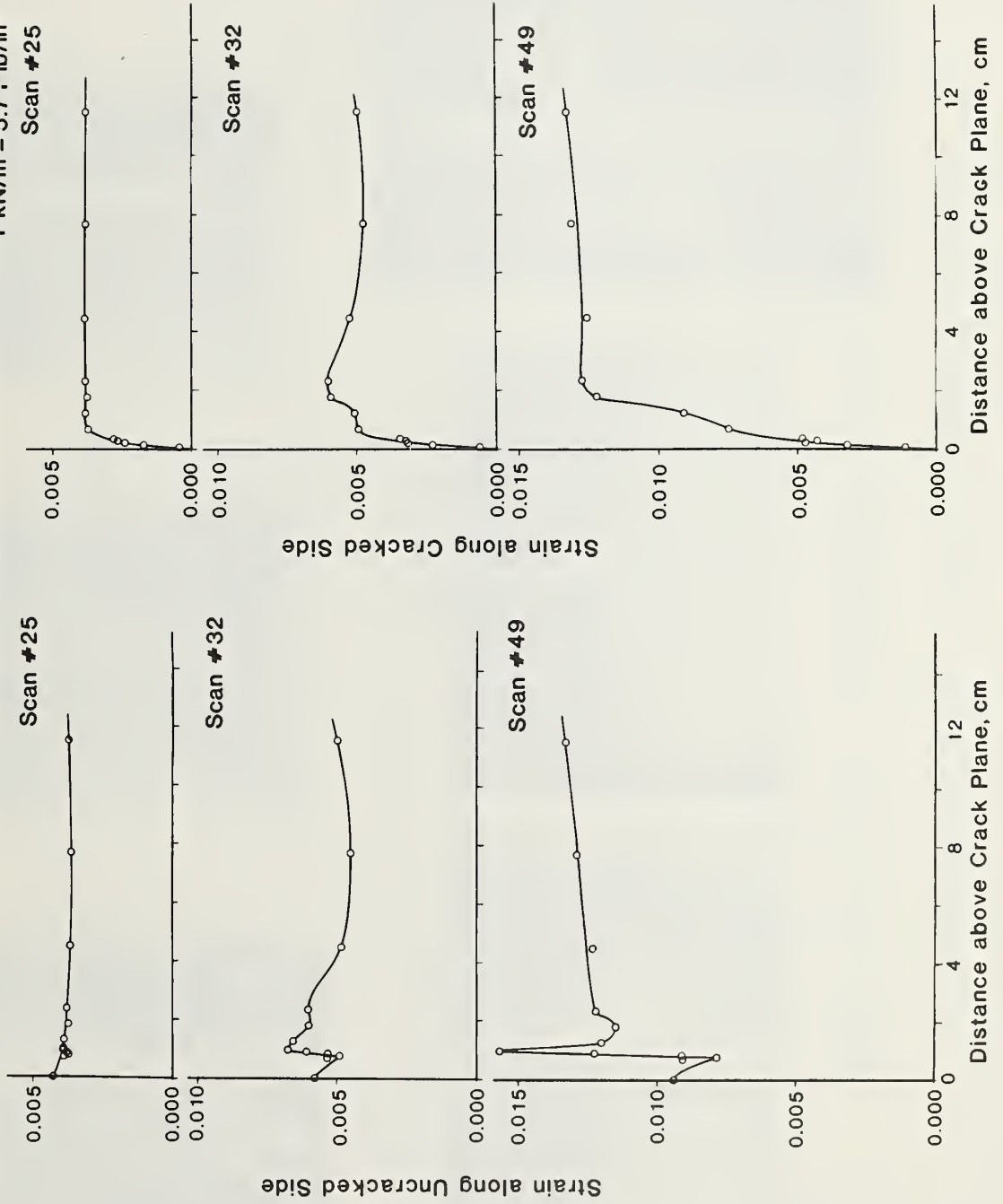


Figure 40. Strain gage strains for transverse-welded surface cracked HY130 tensile panel with crack length 30 mm and crack depth 2.5 mm.

HY130 Welded Tensile Panel Surface-Cracked
Crack Length 30 mm Crack Depth 2.5 mm

Width 254 mm Thickness 20 mm



Scan #25

Scan #32

Scan #49



Scan #25

Scan #32

Scan #49

Figure 41. Strain pattern as revealed by photoelastic coating on transverse-welded surface cracked HY130 tensile panel with crack length 30 mm and crack depth 2.5 mm.

Figure 42a-k. Strain and stress dependences of J-integral and crack mouth opening displacement for transverse-welded surface cracked HY130 tensile panel with crack length 5 mm and crack depth 1.7 mm.

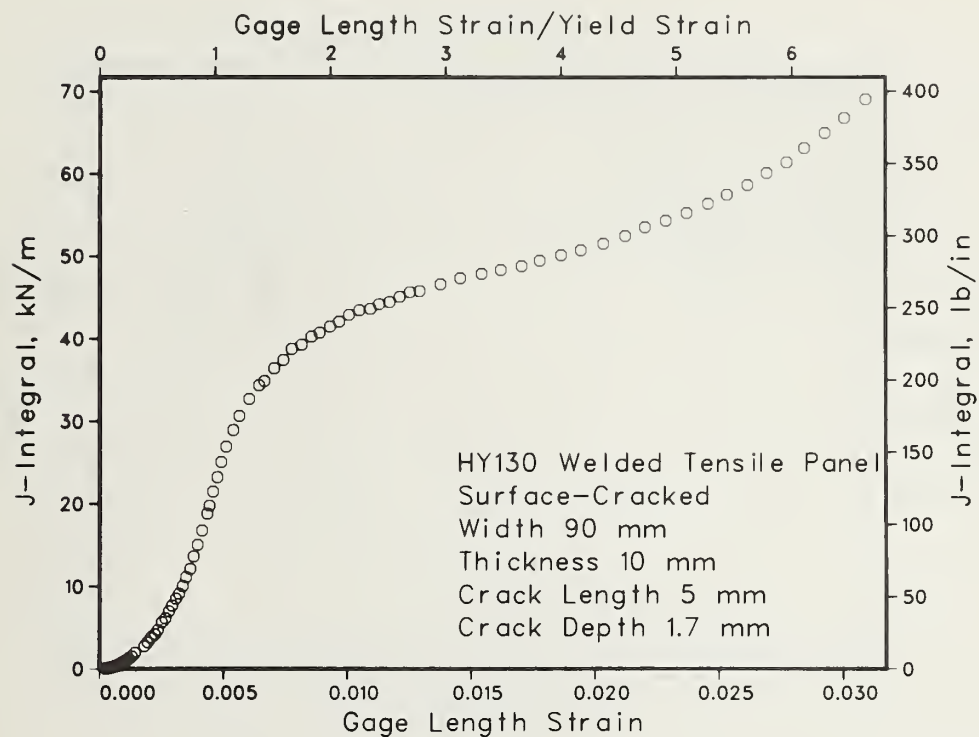


Figure 42a.

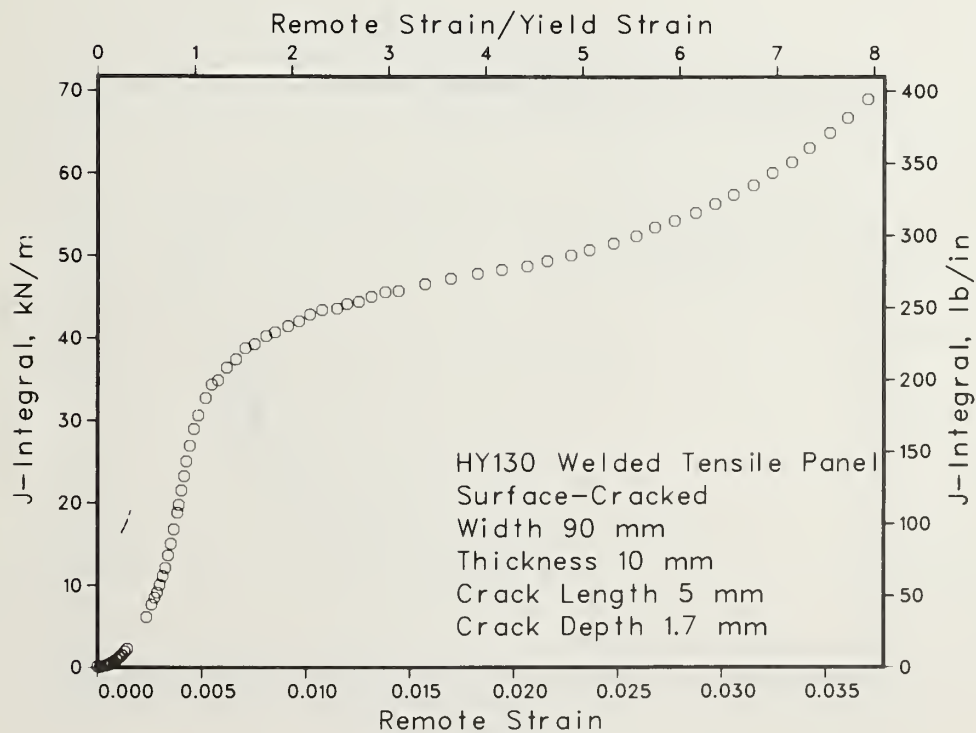


Figure 42b.

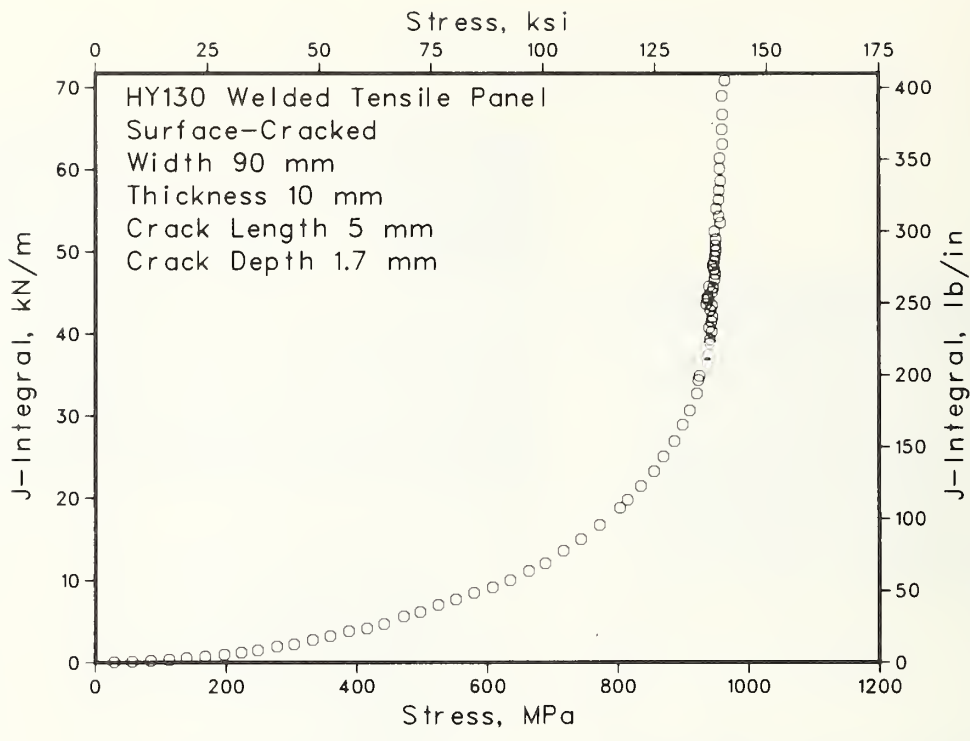


Figure 42c.

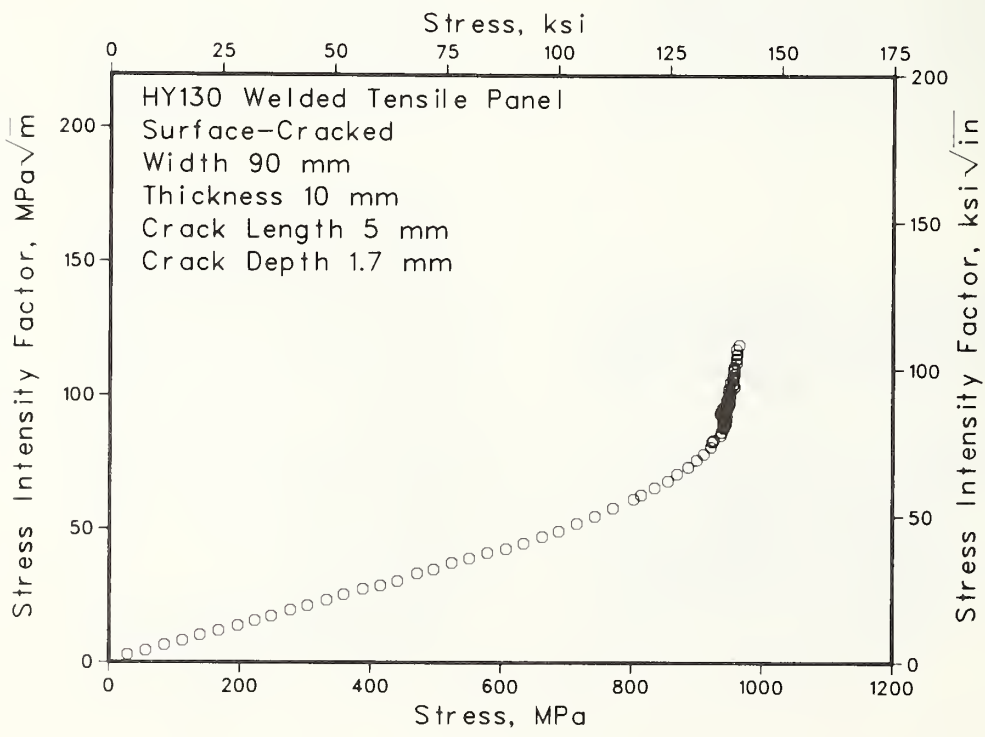


Figure 42d.

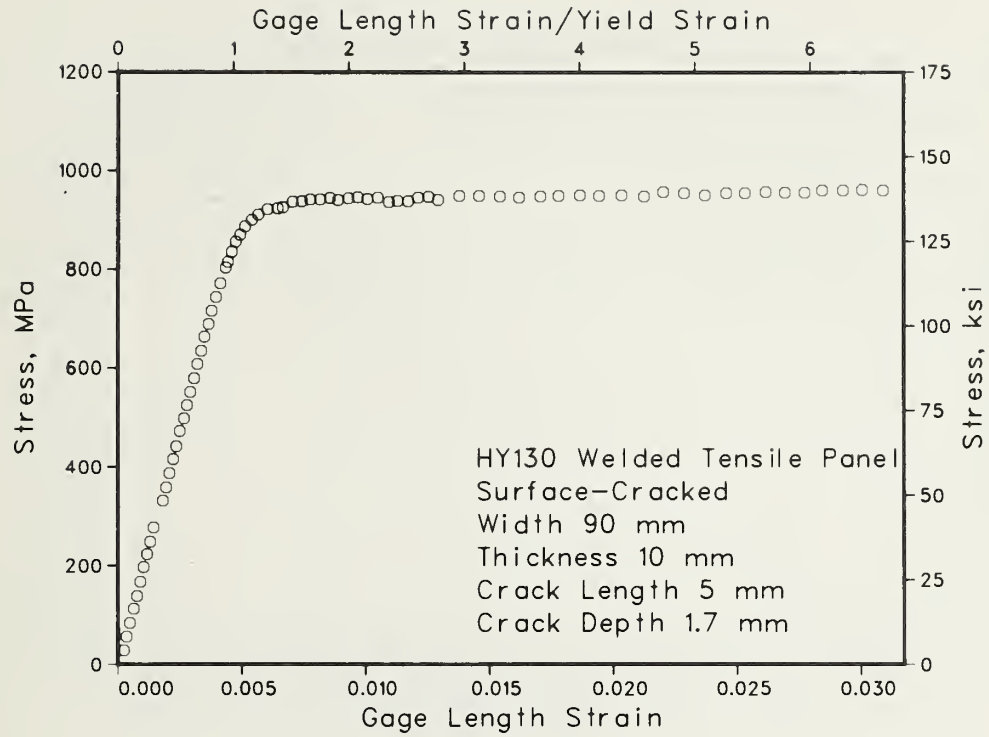


Figure 42e.

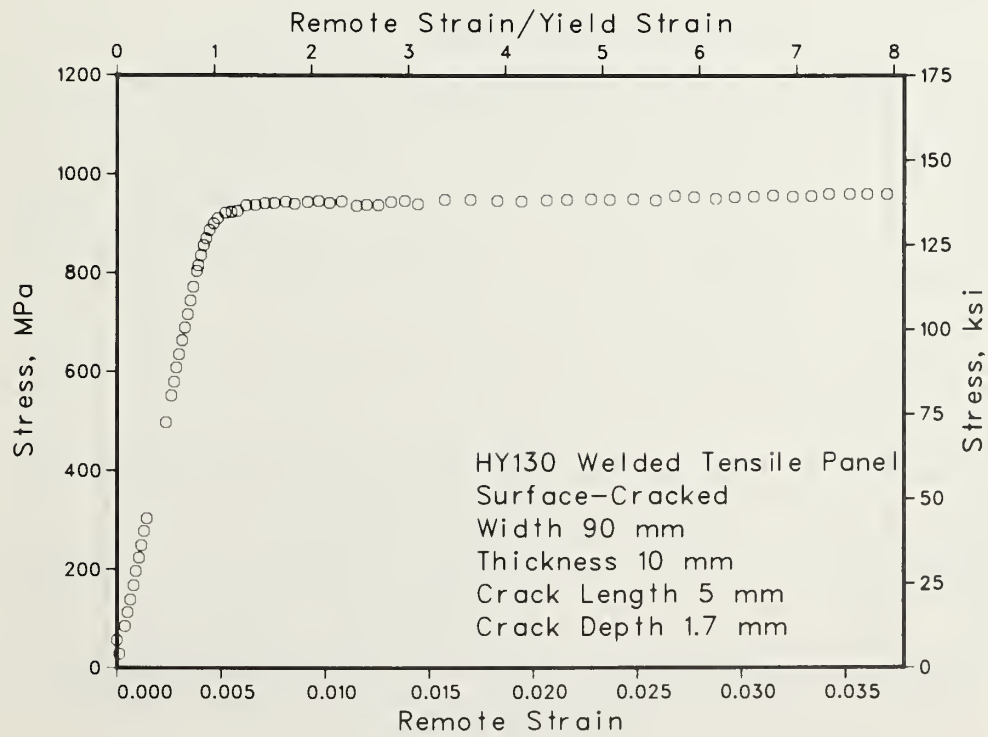


Figure 42f.

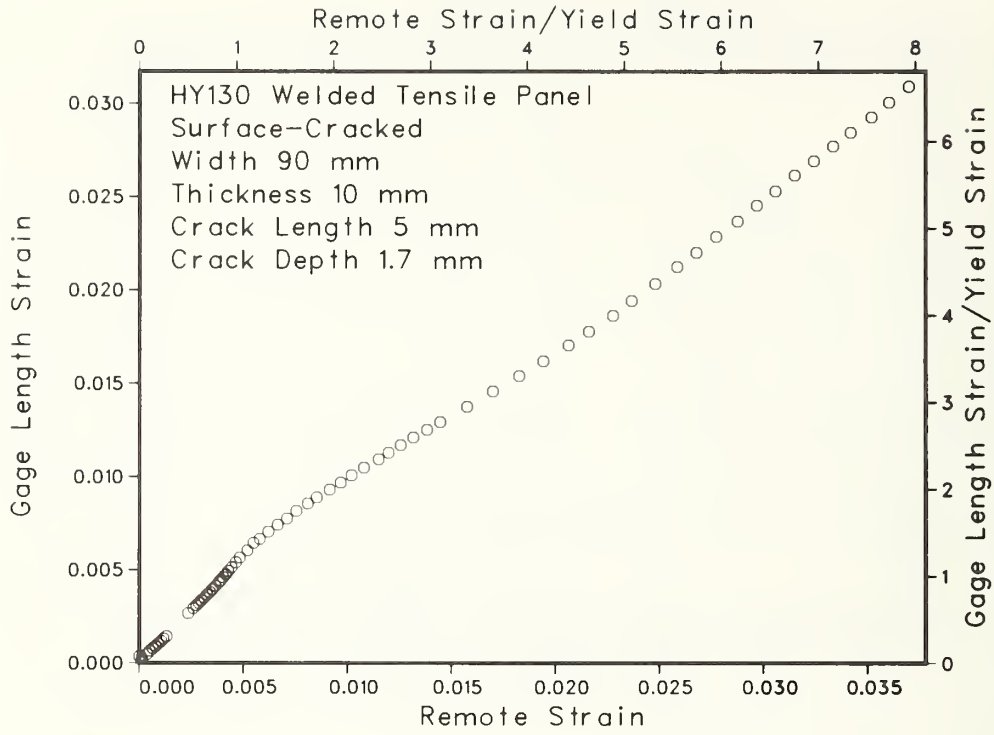


Figure 42g.

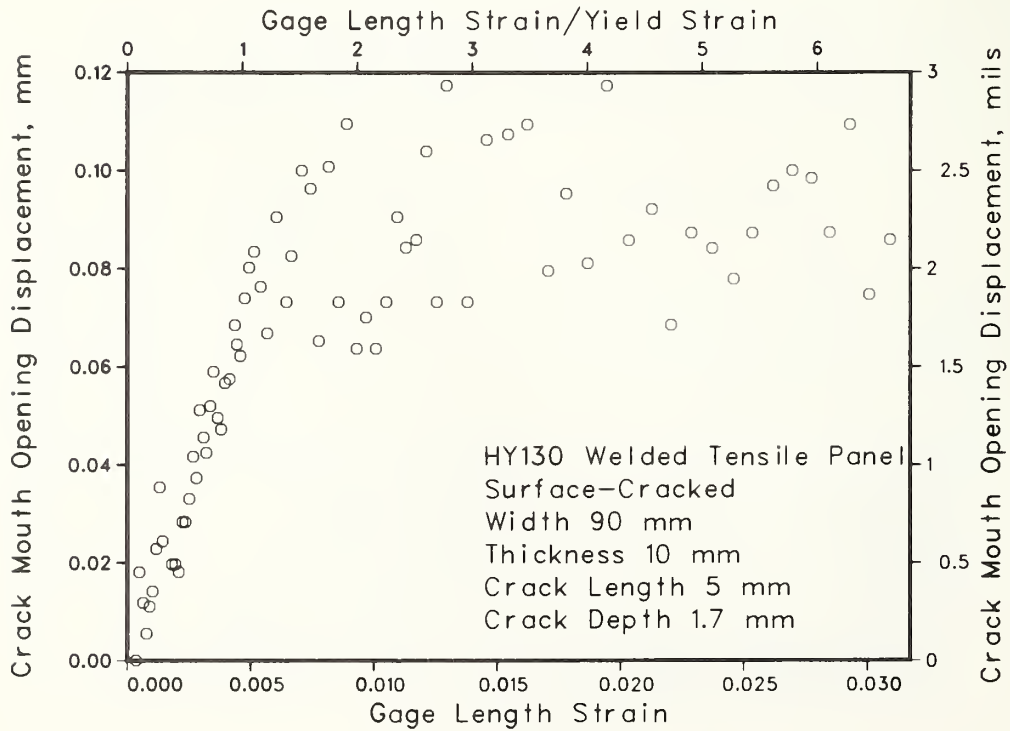


Figure 42h.

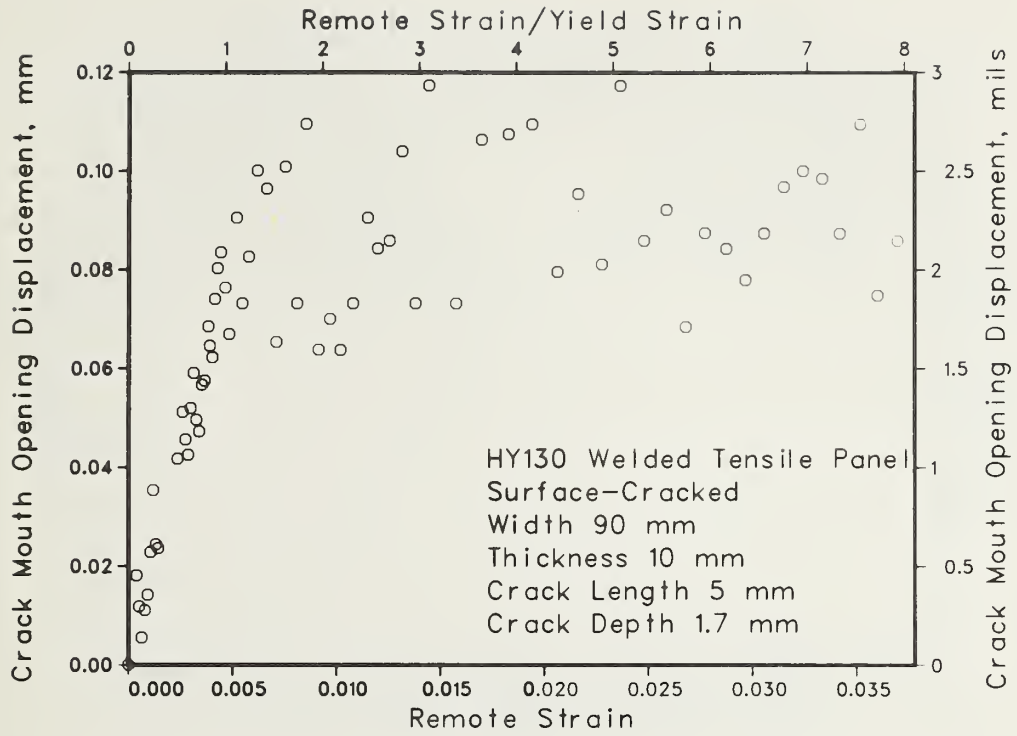


Figure 42i.

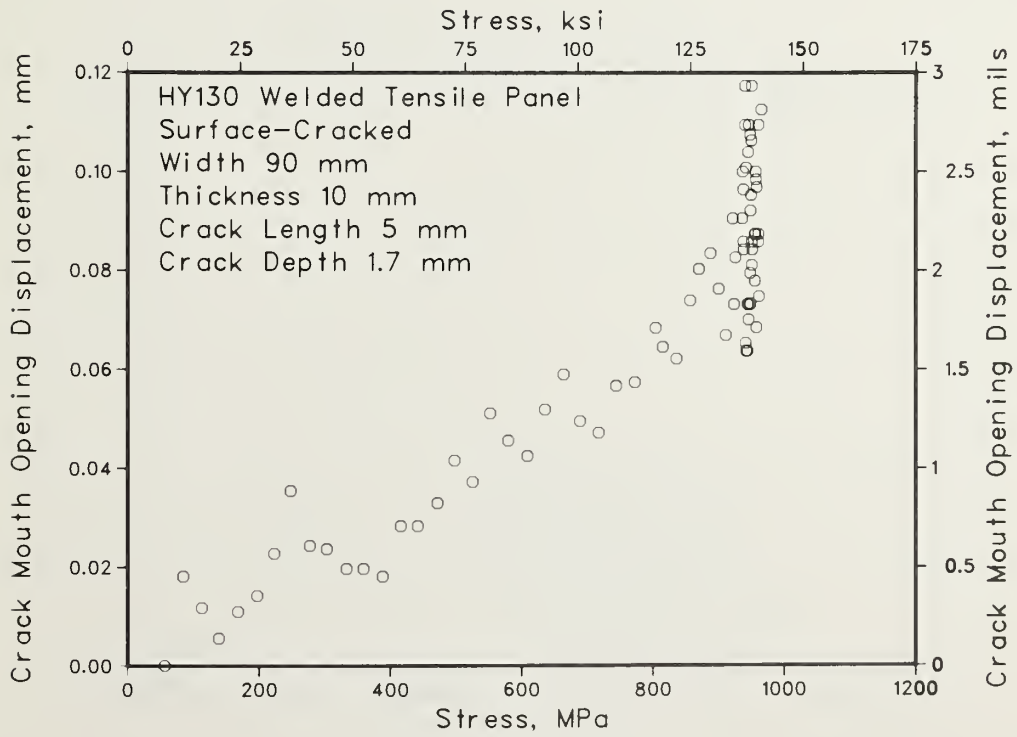


Figure 42j.

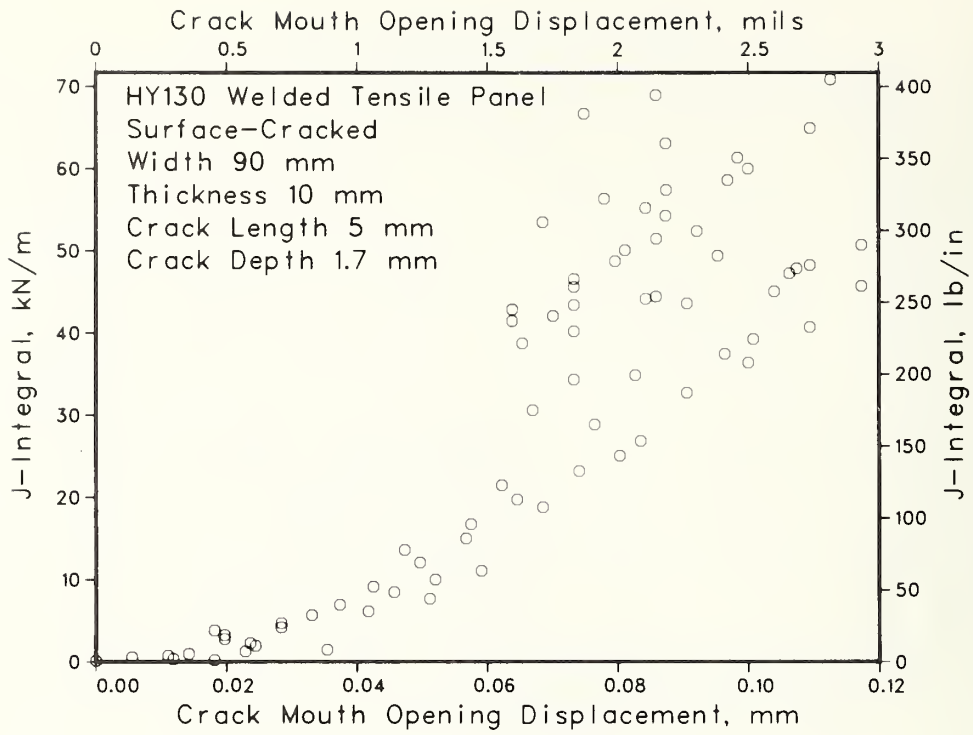


Figure 42k.

Figure 43a-k. Strain and stress dependences of J-integral and crack mouth opening displacement for transverse-welded surface-cracked HY130 tensile panel with crack length 30 mm and crack depth 2.5 mm.

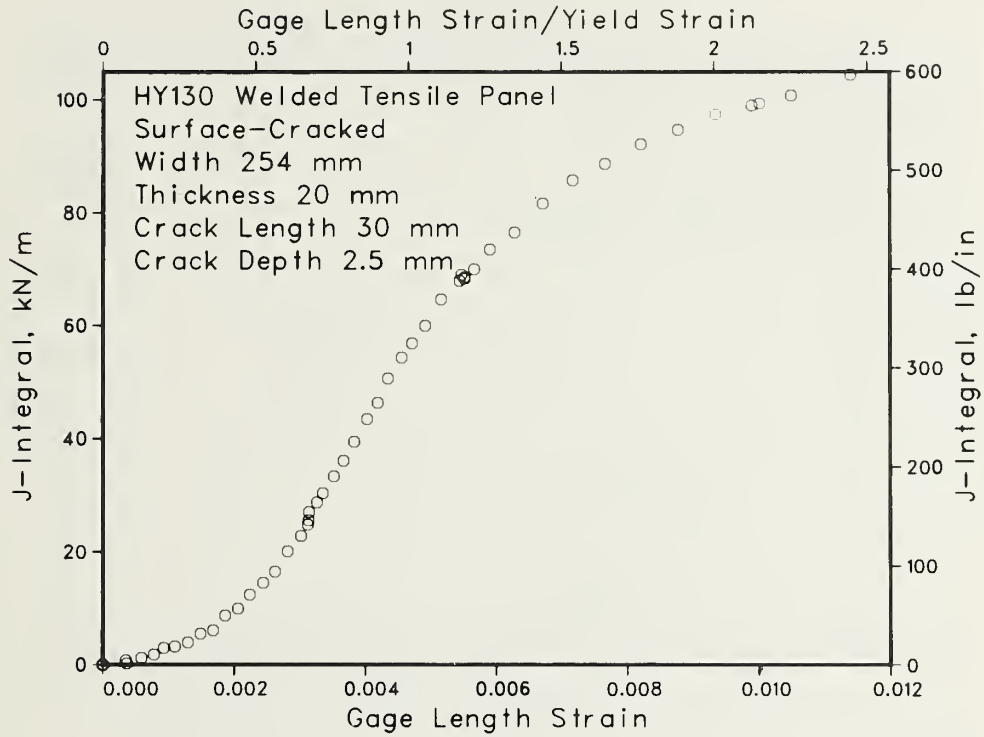


Figure 43a.

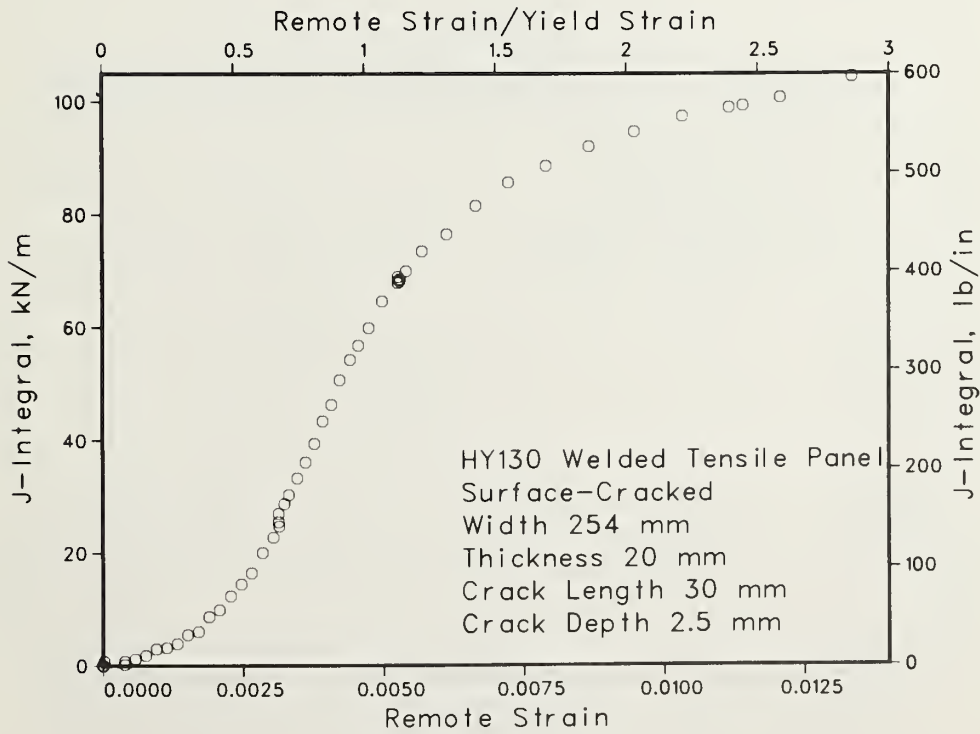


Figure 43b.

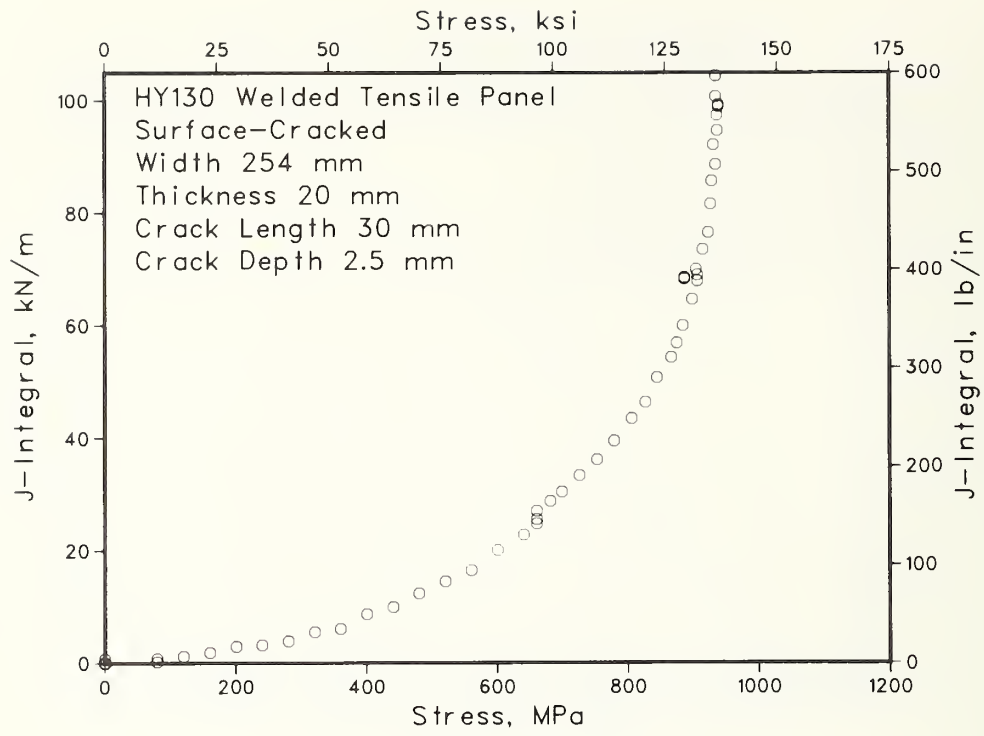


Figure 43c.

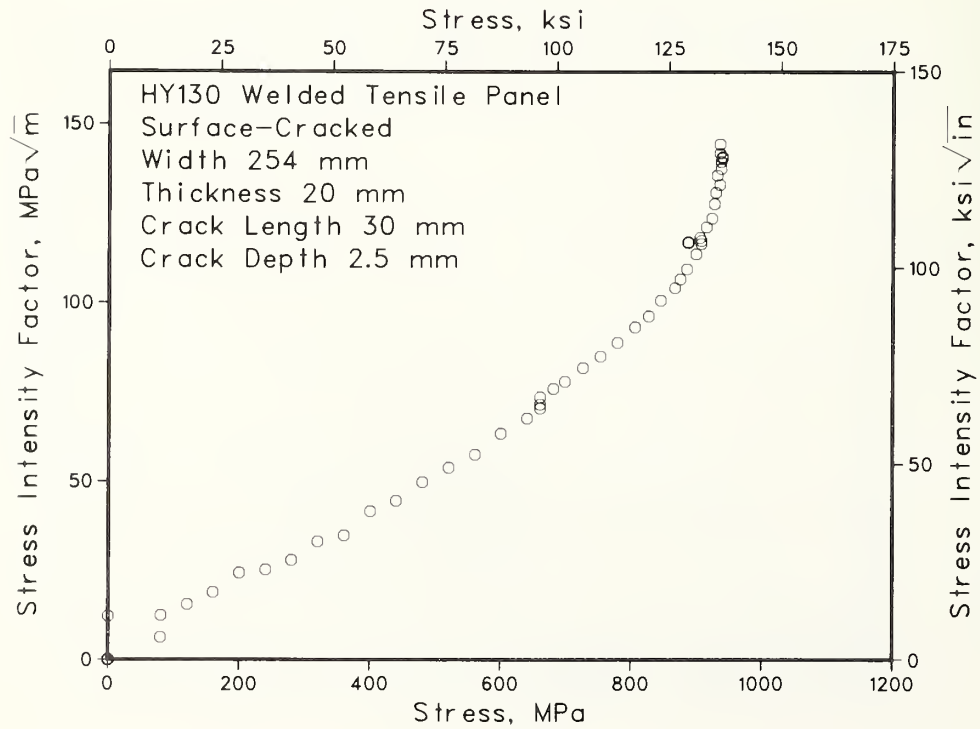


Figure 43d.

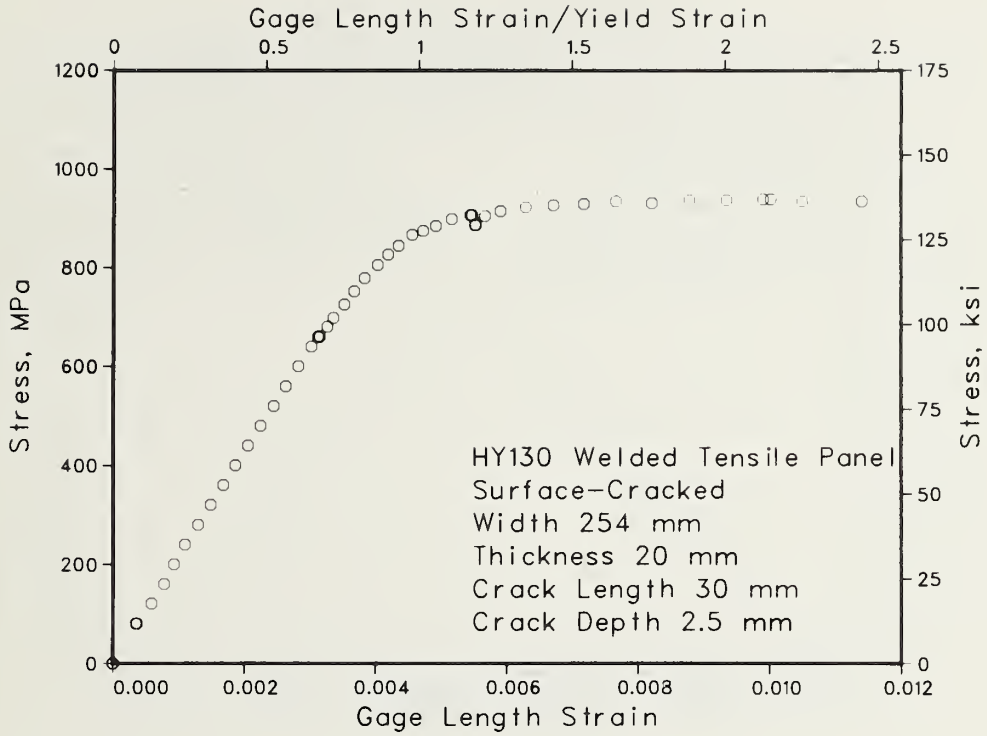


Figure 43e.

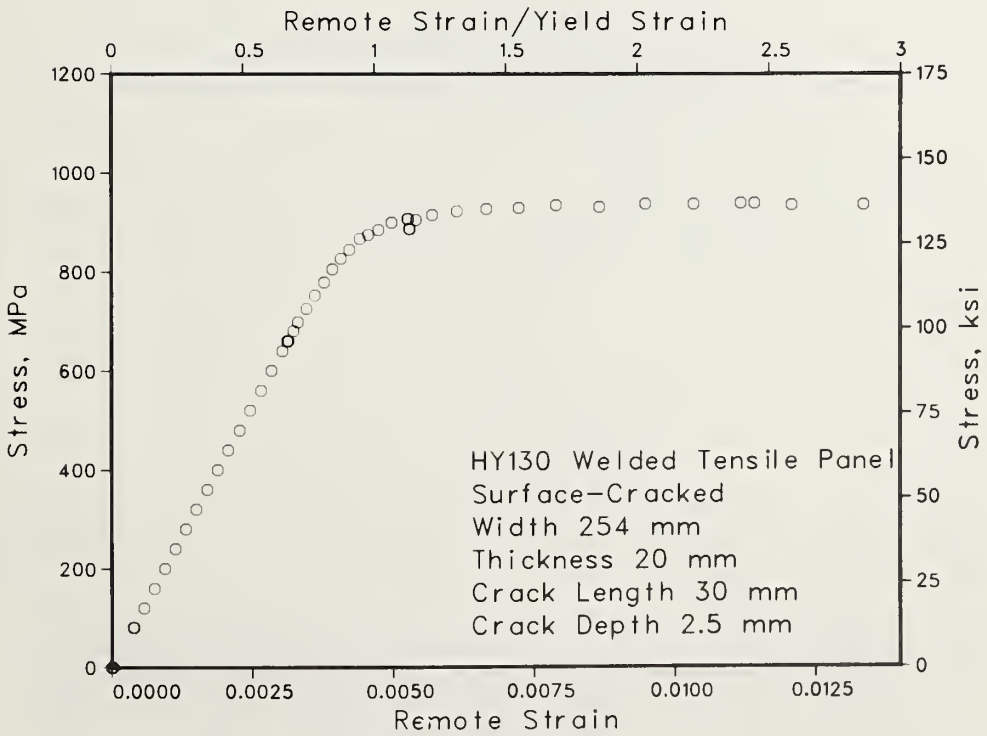


Figure 43f.

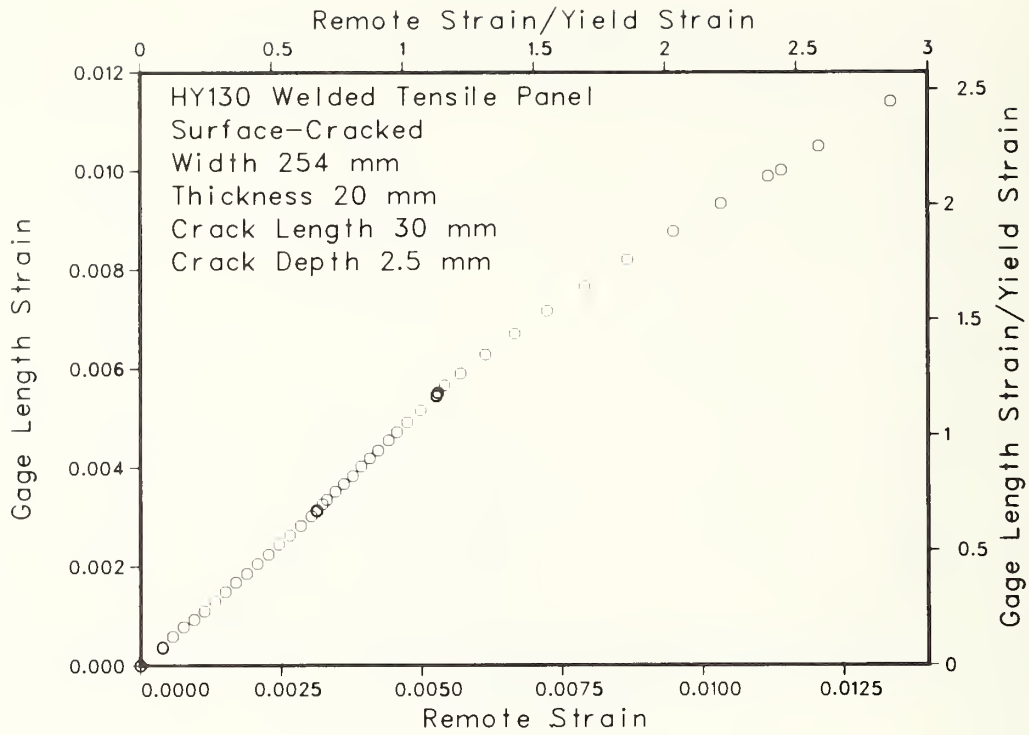


Figure 43g.

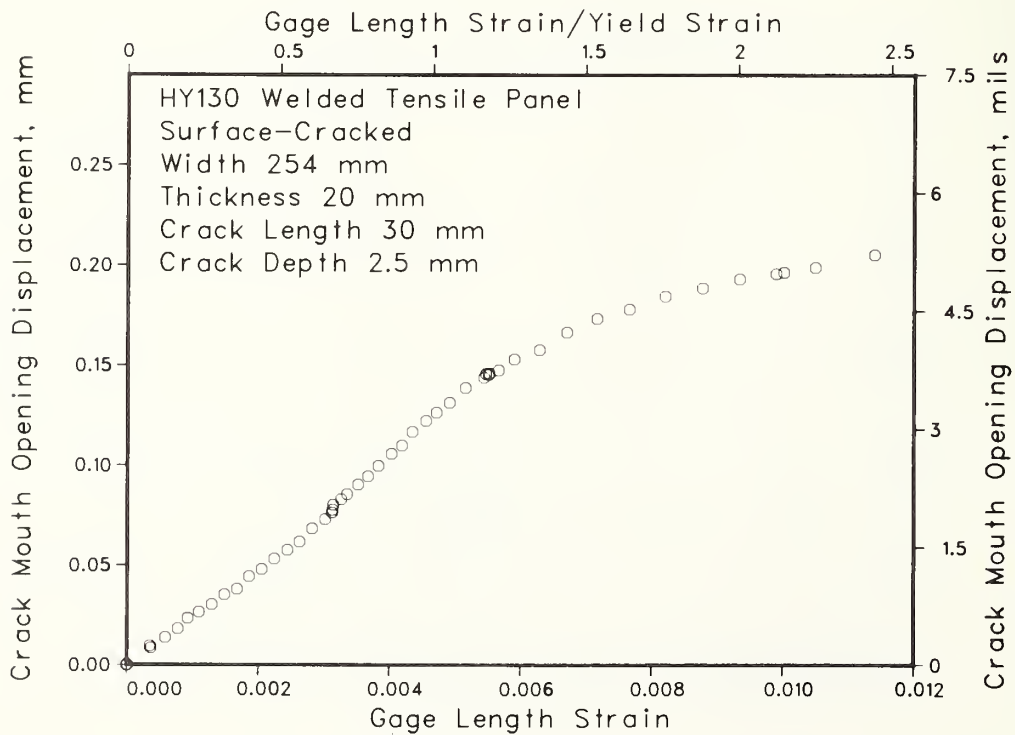


Figure 43h.

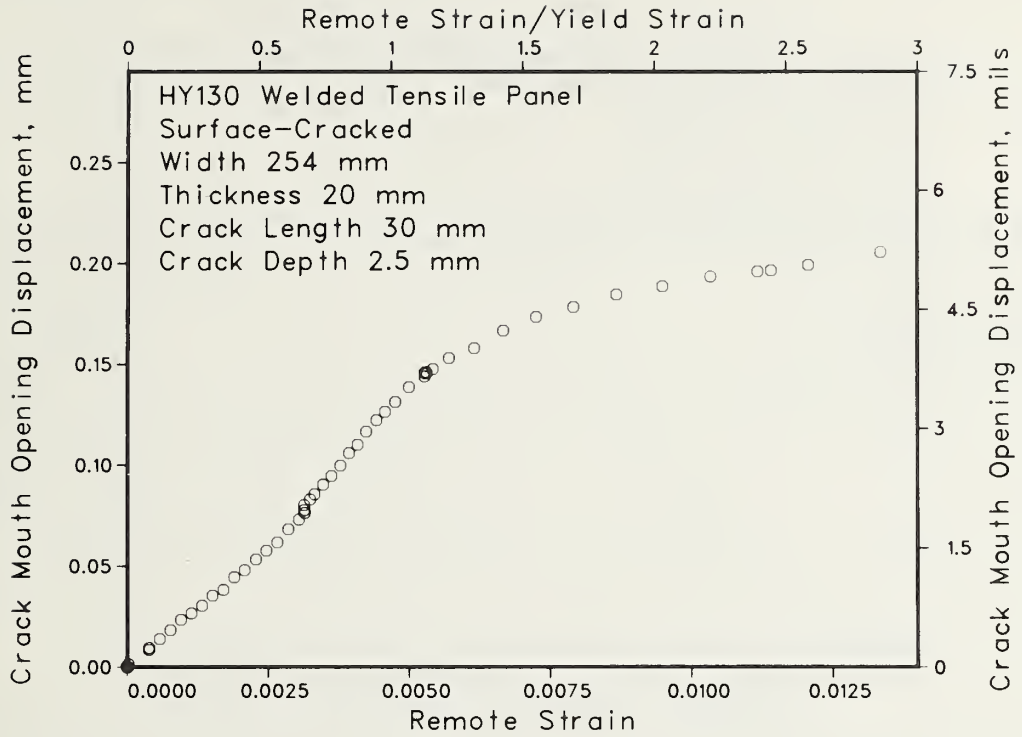


Figure 43i.

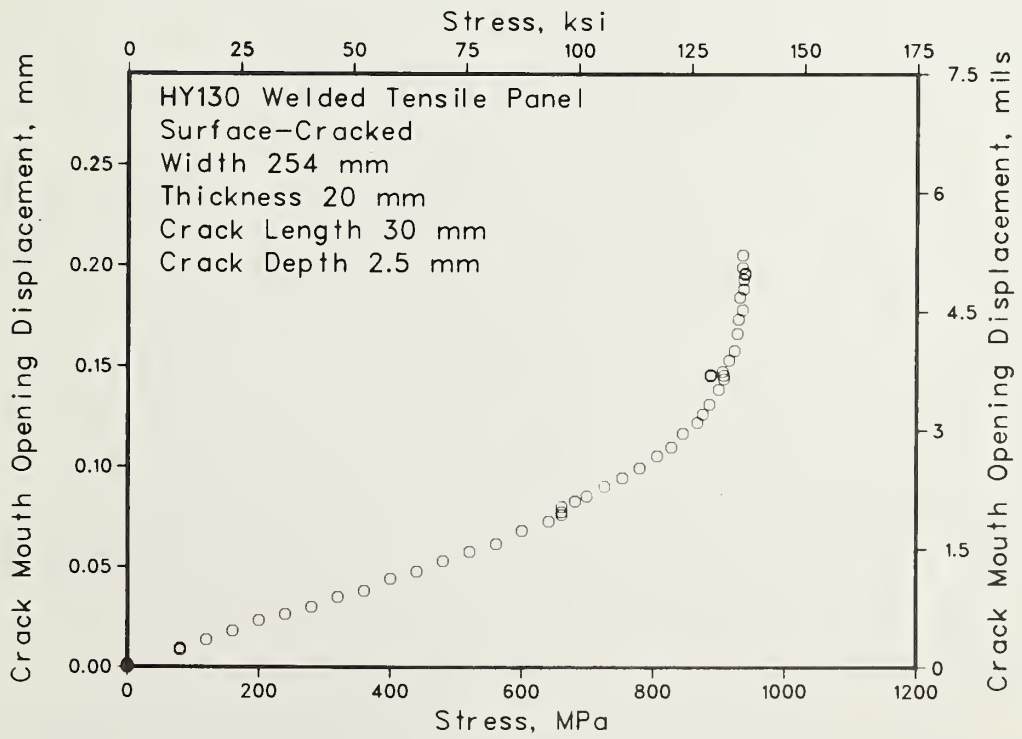


Figure 43j.

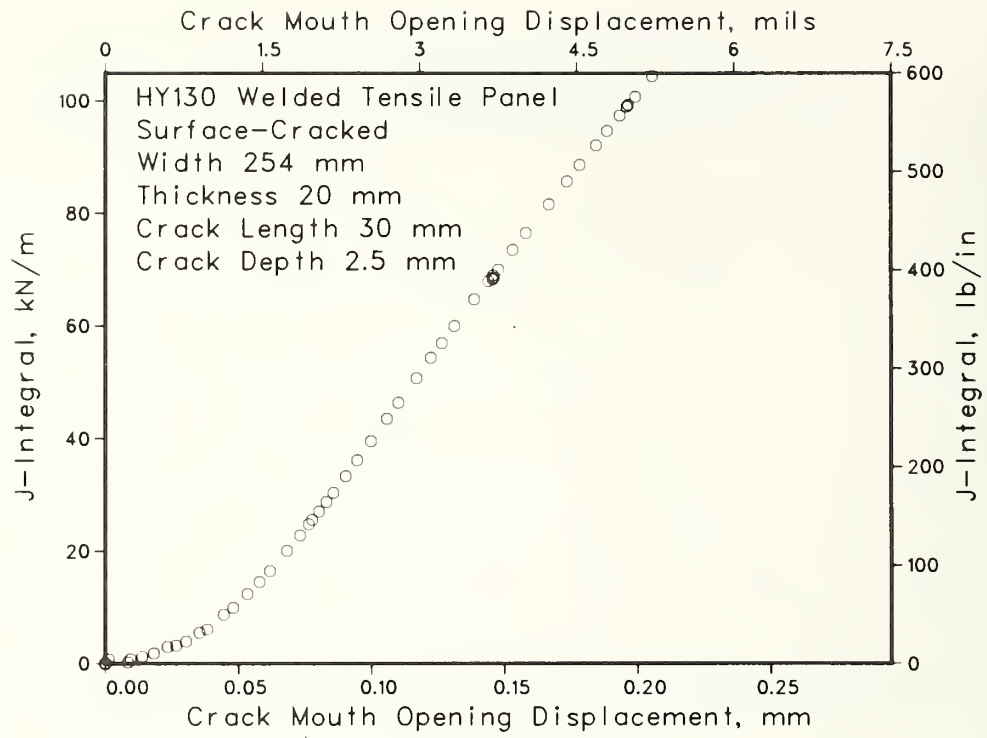


Figure 43k.

U.S. DEPT. OF COMM. BIBLIOGRAPHIC DATA SHEET <i>(See instructions)</i>	1. PUBLICATION OR REPORT NO. NBSIR 84-1699	2. Performing Organ. Report No.	3. Publication Date March 1984
4. TITLE AND SUBTITLE Experimental Results for Fitness-for-Service Assessment of HY130 Weldments			
5. AUTHOR(S) D. T. Read			
6. PERFORMING ORGANIZATION <i>(If joint or other than NBS, see instructions)</i> NATIONAL BUREAU OF STANDARDS DEPARTMENT OF COMMERCE WASHINGTON, D.C. 20234		7. Contract/Grant No.	8. Type of Report & Period Covered Final - 10/81 - 9/82
9. SPONSORING ORGANIZATION NAME AND COMPLETE ADDRESS <i>(Street, City, State, ZIP)</i> Naval Sea Systems Command (SEA 05R25) under direction of: David Taylor Naval Ship R&D Center, Annapolis, MD 21402			
10. SUPPLEMENTARY NOTES <input type="checkbox"/> Document describes a computer program; SF-185, FIPS Software Summary, is attached.			
11. ABSTRACT <i>(A 200-word or less factual summary of most significant information. If document includes a significant bibliography or literature survey, mention it here)</i> <p>Applied J-integral values for through and surface cracks in HY130 weldments and for surface cracks in HY130 base metal have been measured using a previously developed technique. The applied J-integral is taken as a measure of the crack driving force. The results confirmed previous conclusions, namely, the strong effect of deformation pattern on applied J-integral values, the utility of the J-integral estimation curve for fitness-for-service assessment in cases of gross section yielding (crack size less than 1 percent of load-bearing cross-section), and the need to consider ligament yielding behind surface cracks. Additional conclusions for surface cracks and for weldments were: surface-crack depth controls crack driving force; overmatching weld metal strength greatly reduces crack driving force for strains above yield; the relationship between crack length and crack driving force for cases of residual stress is similar to that for applied stress; for a crack in a weld transverse to the tensile axis, gross section yielding occurs if the crack intercepts less than 1.5 percent of the load-bearing cross section; the effective crack size for J-integral estimation is 0.75 of the actual crack depth for crack aspect ratios of 12 or less, and is no larger than the crack depth for any crack length; the line J-integral in the plane perpendicular to the surface crack root at the crack center is sufficiently path independent to allow direct experimental measurement of the J-integral.</p>			
12. KEY WORDS <i>(Six to twelve entries; alphabetical order; capitalize only proper names; and separate key words by semicolons)</i> design curve; elastic-plastic fracture mechanics; gross section yielding; net section yielding; residual stress; surface crack.			
13. AVAILABILITY <input checked="" type="checkbox"/> Unlimited <input type="checkbox"/> For Official Distribution. Do Not Release to NTIS <input type="checkbox"/> Order From Superintendent of Documents, U.S. Government Printing Office, Washington, D.C. 20402. <input checked="" type="checkbox"/> Order From National Technical Information Service (NTIS), Springfield, VA. 22161		14. NO. OF PRINTED PAGES 93 15. Price \$11.50	

